
VYSOKÉ UČENÍ TECHNICKÉ V BRNĚ

BRNO UNIVERSITY OF TECHNOLOGY



FAKULTA STROJNÍHO INŽENÝRSTVÍ

ÚSTAV MECHANIKY TĚLES, MECHATRONIKY A BIOMECHANIKY

FACULTY OF MECHANICAL ENGINEERING

INSTITUTE OF SOLID MECHANICS, MECHATRONICS AND BIOMECHANICS


# VYTVOŘENÍ APLIKACE PRO ZÍSKÁNÍ MODÁLNÍCH PARAMETRŮ PŘI EXPERIMENTÁLNÍ MODÁLNÍ ANALÝZE

CREATION OF MODAL PARAMETER ESTIMATION APPLICATION FOR EXPERIMENTAL MODAL ANALYSIS

DIPLOMOVÁ PRÁCE

MASTER'S THESIS


AUTOR PRÁCE — Bc. VÁCLAV ONDRA

AUTHOR

VEDOUCÍ PRÁCE — Ing. PETR LOŠÁK, Ph.D.

SUPERVISOR



BRNO 2013

Vysoké učení technické v Brně, Fakulta strojního inženýrství

Ústav mechaniky těles, mechatroniky a biomechaniky
Akademický rok: 2013/2014

# ZADÁNÍ DIPLOMOVÉ PRÁCE

student(ka): Bc. Václav Ondra

který/která studuje v **magisterském navazujícím studijním programu**

obor: **Inženýrská mechanika a biomechanika (3901T041)**

Ředitel ústavu Vám v souladu se zákonem č.111/1998 o vysokých školách a se Studijním a zkušebním řádem VUT v Brně určuje následující téma diplomové práce:

**Vytvoření aplikace pro získání modálních parametrů při experimentální modální analýze**

v anglickém jazyce:

**Creation of Modal Parameter Estimation Application for Experimental Modal Analysis**

Stručná charakteristika problematiky úkolu:

Proces získání modálních paramertů z experimentálně měřených dat je důležitá část experimentální modální analýzy (EMA). Výstupem této práce bude aplikace, která z naměřených FRF extrahuje modální parametry pomocí několika metod.

Cíle diplomové práce:

1) Zpracovat teoretické základy výpočtové a experimentální modální analýzy.
2) Popsat vybrané metody pro získání modálních paramterů
3) Vybrané metody zapracovat do aplikace, jejíž vstup bude FRF a výstup bude vlastní frekvence, tlumení a vlastní tvary.

Seznam odborné literatury:

[1] Petruška, J.: Počítačové metody mechaniky I a II, Metoda konečných prvků, VUT FSI v Brně, listopad 2003
[2] Petruška, J.:MKP v inženýrských výpočtech, VUT FSI v Brně,
[3] Zeman V., Hlaváč Z.: Kmitání mechanických soustav, ZČU Plzeň, 2004, 218 s., ISBN 80-7043-377-X

Vedoucí diplomové práce: Ing. Petr Lošák, Ph.D.

Termín odevzdání diplomové práce je stanoven časovým plánem akademického roku 2013/2014.

V Brně, dne 21.11.2013

L.S.

| | |
|---|---|
| prof. Ing. Jindřich Petruška, CSc. | prof. RNDr. Miroslav Doupovec, CSc., dr. h. c. |
| Ředitel ústavu | Děkan fakulty |

## ABSTRACT

The aim of this diploma thesis is a creation of modal parameter estimation application. Modal properties (natural frequencies, damping factors and mode shapes) are used in many dynamics analysis and their accurate determination is very important therefore the modal parameter estimation is one of the most significant part of the experimental modal analysis. Many methods have been developed for modal parameter estimation, each of them with different assumptions and with different accuracy. In the beginning of this thesis, a theory connected with modal analysis and a theory which is necessary for understanding to presented modal parameter methods are given. Then four different modal parameter estimation methods are presented - Peak Picking, Circle Fit, Least Square method and Eigensystem Realization Algorithm. The application for the modal parameter estimation is the output of this diploma thesis. In addition, the application allows performing all experimental modal analysis such as estimation of frequency response functions, animation of the found mode shapes, different kinds of comparison etc. In the conclusion, three structures are shown on which the application and modal parameter estimation methods were tested.

## KEYWORDS

experimental modal analysis, modal properties, modal parameter estimation methods, Peak Picking, Circle Fit, Least Square, Eigensystem Realization Algorithm

## ABSTRAKT

Cílem této práce je tvorba aplikace pro získání modálních parametrů z naměřených dat. Modální parametry (vlastní frekvence, tlumení a vlastní tvary) jsou používané v mnoha další analýzách a jejich přesné určení velmi důležité, proto proces získání modálních parametrů je jedním z nejdůležitějších při experimentální modální analýze. Pro určování těchto parametrů bylo vyvinuto spoustu metod a technik, které stojí na různých předpokladech a jsou různě přesné. Na začátku této práce je zpracována teorie související s modální analýzou a teorie, která je nutná pro pochopení presentovaných metod. Potom jsou popsány čtyři rozdílné metody pro získání modálních parametrů - Peak Picking, Circle Fit method, Least Square methods a Eigensystem Realization Algorithm. Výstupem této práce je aplikace, které kromě popsaných metod umožnuje provádět celou experimentální modální analýzu včetně zpravování naměřených dat do vhodného formátu, animaci výsledných vlastních tvarů, různé druhy porovnání modálních parametrů atd. V závěru práce jsou presentovány tři příklady na kterých byla aplicace a metody otestovány.

## KLÍČOVÁ SLOVA

experimentální modální analýza, modální vlastnosti, metody získání modálních parametrů, Peak Picking, Circle Fit, Least Square, Eigensystem Realization Algorithm

ONDRA, Václav *Creation of modal parameter estimation application for experimental modal analysis*: master's thesis. Brno: Brno University of Technology, Faculty of Mechanical Engineering, Institute of Solid Mechanics, Mechatronics and Biomechanics, 2014. 129 p. Supervised by Ing. Petr Lošák, Ph.D.

# DECLARATION

I declare that I have written my master's thesis on the theme of "Creation of modal parameter estimation application for experimental modal analysis" independently, under the guidance of the master's thesis supervisor and using the technical literature and other sources of information which are all quoted in the thesis and detailed in the list of literature at the end of the thesis.

As the author of the master's thesis I furthermore declare that, as regards the creation of this master's thesis, I have not infringed any copyright. In particular, I have not unlawfully encroached on anyone's personal and/or ownership rights and I am fully aware of the consequences in the case of breaking Regulation § 11 and the following of the Copyright Act No 121/2000 Sb., and of the rights related to intellectual property right and changes in some Acts (Intellectual Property Act) and formulated in later regulations, inclusive of the possible consequences resulting from the provisions of Criminal Act No 40/2009 Sb., Section 2, Head VI, Part 4.

Brno ..... .....

(author's signature)

## ACKNOWLEDGEMENT

I would like to express my gratitude to my supervisor Ing. Petr Lošák, Ph.D. for the professional guidance, consultation, patience and insightful suggestions to this diploma thesis. Also, I would like to thank Ing. Petr Marcián, Ph.D. for the provided facilities and hardware support. Last but not least I would like to thank Lucie for providing a great amount of motivation as she always does.


Brno ..... .....

(author's signature)

# CONTENTS

# LIST OF FIGURES

# LIST OF TABLES

# 1 INTRODUCTION

In this time, when the technology has become a great part of everyday life, when we can't image our lives without cars, airplanes, electricity, we, as engineers, have to deal with many problems connected with all benefits that technology gives us.

One of the often discussed problem is a vibration of the mechanical structures. There is no way how to absolutely avoid vibration in some applications. The airplane wings will always vibrate due to circulation of the air during flight or production machines will vibrate during processing raw materials into final products.

On the other hand, there are machines which use vibration for their main task, for instance compactions are used in civil engineering or the various kinds of shakers are used in the vibration laboratories.

In general, when we can't avoid vibration, we try to avoid at least a resonance or minimize its consequences. Greater displacements, noise and visual effects are usually connected with the resonance. In order to control vibrations we can update the design of the construction, use special damping elements, deal with excitation effect..., but in every case, we have to understand how to describe vibrations, how to predict and measure them. A theory were developed from this reason. This theory use the modal parameters for handle a complex character of the subject. These parameters are natural frequency, damping factor and mode shape. Next to the theoretical approach there is an experimental view on the modal analysis, which brings information about constructions that are already made.

It is convenient today, that we can easy perform a theoretical modal analysis using finite element method (FEM) for every geometry. This method has great advantage but it has some disadvantage as well. We usually don't know exactly the material properties or a history of the loading. This is the point where the experimental approach is needed. We can obtain the modal properties from the existing part using experimental modal analysis and these can be used for a verification of our numerical FEM model or for other applications.

This thesis is not focused on a modal testing, but only on the estimation of the modal parameters, which is one of the main parts of the modal testing. The purpose and main aims of the thesis are summarized in the second chapter.

In the third chapter, we give a theoretical background. At the beginning we will repeat classic modal theory of single-degrees-of-freedom systems and we will continue to multi-degrees-of-freedom systems. A theory that is necessary for understanding principles of modal parameter estimation such as derivation on a frequency response function, its forms of the presentation and basic properties is presented in the next part.

The modal parameter estimation comes right after the theory. Several methods

are discussed. Methods are divided into a few groups. Four methods are described in this chapter, namely Peak Picking method, Circle Fit method, Least Square methods and Eigensystem Realization Algorithm. A brief description of function of a stabilization diagram and some standard version of it are given in the end of the chapter.

The topic of the diploma thesis is creation of the modal parameter estimation application for the experimental modal analysis so in the next section this application is described. However, the description of the creation itself is not included but only the description of the application and only in the range which is needed for this thesis. All main parts of the application are shown together with the description of their functions.

A few test cases are given in the last part of the thesis. First of all, two simulated cases are used - one side fixed beam (6 DOF) and two side fixed plane (15 DOF). The modal parameter estimation was done for these structures based on the theoretical frequency response functions. In next stage the experimental modal analysis was performed on the turbine wheel. The comparison of the experimental results with results of finite element method is given and main differences or features of used modal parameter estimation methods are pointed out.

The most important points which were discussed are summarized in the conclusion of the thesis and a future work possibility is given.

# 2 PROBLEM FORMULATION AND AIMS OF DIPLOMA THESIS

A modal parameter estimation (MPE) is one of the most important part of an experimental modal analysis (EMA) and an operation modal analysis (OMA) because the modal parameters (natural frequencies, damping factors and mode shapes) are obtained in this process. The problem is how to extract these parameters from a measured data, which are usually represented by the frequency response functions in case of EMA and the by time-signals in case of OMA. This thesis is focused on the experimental modal analysis and those modal parameter estimation methods, which are used in EMA. However, some of the presented methods can be applied in the field of the operation modal analysis as well.

A great amount of MPE methods have been presented throughout the literature. The objective of this thesis is to implement some of these techniques into an application, which inputs are the frequency response functions (FRFs) and outputs the modal properties. For the better comprehension, the theoretical foundations connected with a theoretical modal analysis and an experimental modal analysis are given. Description of the chosen MPE techniques is presented as well. Three main aims have been declared:

1. Present a background of the theoretical and the experimental modal analysis
2. Describe the chosen modal parameter estimation methods
3. Implement the chosen MPE methods into an application. The input of the application will be created by FRFs and the output will be natural frequencies, damping factors and mode shapes.

# 3 THEORETICAL BACKGROUND

A theoretical foundations of a modal analysis are necessary for understanding and successful implementation of the experimental modal analysis. The theory is divided into five sections. Firstly, the applications of a modal testing are mentioned. Then, single-degree-of-freedom (SDOF) system theory is presented. It is truth, that we can't find the real SDOF system, but the theory is important, since we can look on the multi-degree-of-freedom (MDOF) system as on the set of the SDOF systems. The theory of the MDOF system is shown in the next section of this chapter. We present the theory according to Fig. 3.1 so we go from *Spatial model* to *Response model*. We will discuss a case of an undamped system and a system with a proportional viscous damping. Other kinds of damping models exist (structural, non-proportional etc.), but they will not be presented here and they can be found in [1] or [2].

Beside to SDOF and MDOF systems theory, a section about the frequency response functions is given in which their mathematical forms and different kinds of a presentation are shown.

The last section of this chapter is focused on a comparison of the modal properties. Strictly speaking, this is not a part of the theory but it is important if we want to compare results obtained by the different modal parameter estimation methods.

## 3.1 Applications of modal testing

The experimental study of the structural vibration, undertaken in order to obtain the modal properties, is called the modal testing. The name, modal testing, encompass the processes involved in a testing of components or structures with the objective of obtaining a mathematical description of their dynamic or vibration behavior [1]. There are two types of modal tests. The first one, where vibration responses are measured during "operation" of the structure, is usually refer as the *operation modal analysis* (OMA) or as the *output-only modal analysis*. The second is a test, where the components are vibrated with a known, measurable excitation. The second test is made under much more controllable conditions and therefore the information about structures obtained by this way are more accurate and contains more details. The second type of the test is called *experimental modal analysis* (EMA).

Even so we don't describe OMA further in the work, the results are used in the same way as the EMA ones. So before we start with the theory, we should answer the question 'why modal tests are undertaken and where can be the results used?'

There are many applications where the results from the modal testing can be put, there are named three of them.

(A) The most often used and one of the simplest application is a comparison of corresponding data from the modal test with data produced by a finite element method or other theoretical technique. This application is often used like a verification of theoretical model, which is used in further analysis such as a prediction of the response of the structure to complex excitations (shock, random excitation, seismic activity...). The information, we require for this application from the modal tests are
   - the accurate estimates of the natural frequencies and
   - description of the mode shapes, in the way, that is usable in the comparison (the experimental grid and finite element mesh have to correspond in the measured points).

   The comparison can be done by a simple tabulation and/or using statistics methods. Some special criterion are also developed just for modal shapes such as Modal Assurance Criterion (MAC).

(B) Previous application simply comparing two sets of results. Next stage can be an attempt to adjust or correct the theoretical model in order to get its modal properties closer to the experimental ones. This can be done using correlation rather than the comparison. Correlation is a process in which two sets of the data are combined in order to identify the causes of the discrepancies. This application is clearly more powerful but the mode shapes have to be measured with much more accuracy.

(C) It is not possible to predict the damping factors from the theoretical analysis and therefore there is nothing we can compare with the measured damping factors. However, the damping factor is used, since it can be incorporated into the theoretical model using any of the damping models.

## 3.2 Theoretical vs. experimental approach of a modal analysis

We should make sure what we mean under the "theoretical" and the "experimental" approach to the modal analysis.

The theoretical approach route is shown Fig. 3.1. This figure illustrates the way, how a typical vibration analysis goes.

We usually start with a description of a structure in terms of its mass, stiffness and damping properties. This description is refereed as a *Spatial model*.

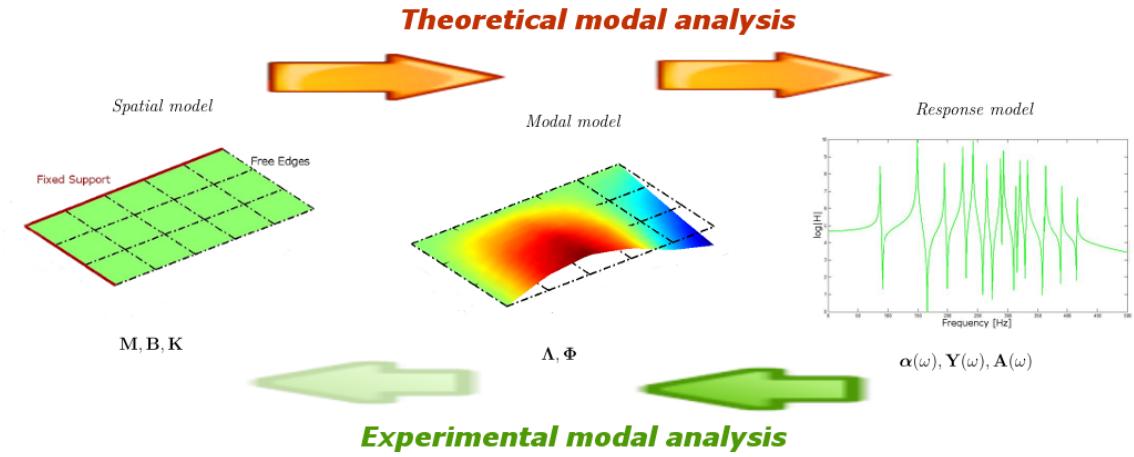


Fig. 3.1: Theoretical vs. experimental approach to modal analysis

On this model, we can perform the analytical modal analysis which leads to a description of the vibration behavior of the structure with a set of the natural frequencies with corresponding vibration mode shapes and the damping factors. All these properties together create the *Modal Model*. The analytical modal analysis assumes that the structure is capable of the vibration naturally (there is no kind of excitation) and therefore the mode shapes are sometimes called "normal" or "natural" modes of the structure [1].

The third stage of the analysis depends along the physical characteristics (mass, stiffness, damping) on a kind and a magnitude of the excitation. The excitation may have a lot of forms (random, impulse, sinusoid...), however, it is convenient to present the analysis of the structure's response to a "standard" excitation, from which the solution of any another case can be derived. The "standard" excitation chosen here is an unit-amplitude sinusoidal force applied to each point on the structure at the specified range of the frequency. The solution of the structure vibrated under "standard" excitation is called the *Response model* and consists of a set of the frequency response functions (FRFs).

As it is possible to proceed from the spatial model to the response, it is also possible to undertaken an analysis in the inverse direction. This means, we can deduce modal properties from the response description (the measured FRFs). This is marked as an experimental route on the Fig. 3.1.

We usually perform the experimental modal analysis only for obtaining the modal properties. The spatial model derivation needs more sophisticated techniques. It is not usually derived since it is not necessary in many applications.

## 3.3 Single-degree-of-freedom system theory

The basic, well known, model of SDOF system is shown in Fig. 3.2. We can see the spatial model in this figure. It consists of mass ($m$), stiffness ($k$) and viscous damper described by constant ($b$) in the case of damped system. The system is excited by a time-varying force $f(t)$. System's displacement response is described by $x(t)$.

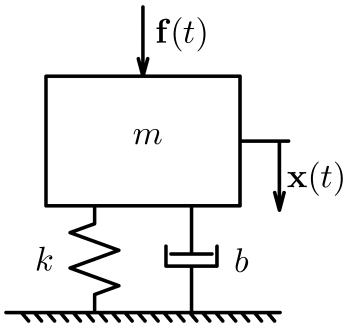


Fig. 3.2: Single-degree-of-freedom system

### 3.3.1 SDOF without damping

The undamped system's *spatial model* consists just mass ($m$) and stiffness ($k$).

#### Modal model derivation

For the derivation of the *modal model*, we assume that there is no excitation i.e. $f(t) = 0$. The equation of motion for this case is given by:

$$m\ddot{x} + kx = 0 \tag{3.1}$$

The solution is being found in the form

$$x(t) = xe^{i\omega t} \tag{3.2}$$

After substituting (3.2) into (3.1) we obtain

$$k - \omega^2 m = 0$$

The *modal model* consists of a single natural frequency $\omega_0$, which can be extract from the last equation thus it is given by:

$$\omega_0 = \sqrt{\frac{k}{m}} \tag{3.3}$$

**Response model derivation**

We have to assume the "standard" excitation in order to extract the *response model*. The excitation has a form

$$f(t) = fe^{i\omega t} \tag{3.4}$$

Hence the equation of motion becomes

$$m\ddot{x} + kx = fe^{i\omega t} \tag{3.5}$$

The solution is being found in the form (3.2) again. After substituting this form into (3.5). We have an equation:

$$(k - \omega^2 m)xe^{i\omega t} = fe^{i\omega t}$$

from which we extract *response model* in the form of a frequency response function (FRF), which is called "Receptance".

$$\alpha(\omega) = \frac{x}{f} = \frac{1}{k - \omega^2 m} \tag{3.6}$$

This particular FRF is a real function, which is independent on the excitation.

### 3.3.2 SDOF with damping

The damped system's *spatial model* is described by the all properties in Fig. 3.2 i.e. mass ($m$), viscous damper constant ($b$) and stiffness ($k$).

**Modal model derivation**

An equation of motion becomes (for no excitation again):

$$m\ddot{x} + b\dot{x} + kx = 0 \tag{3.7}$$

We have to use more general form of the solution for finding of modal properties:

$$x(t) = xe^{st} \tag{3.8}$$

in which $s$ is a complex number with a real and an imaginary part (only the imaginary part is in (3.2)). Substituting (3.8) into (3.7) leads to

$$ms^2 + bs + k = 0$$

The roots can be found as

$$s_{1,2} = -\frac{b}{2m} \pm \frac{\sqrt{b^2 - 4km}}{2m} = -\omega_0 b_r \pm i\omega_0\sqrt{1 - b_r^2} \tag{3.9}$$

where the new marks means: $\omega_0$ is an undamped natural frequency from (3.3) and $b_r$ (somewhere marked as $\zeta_r$) is marking a damping factor (or a damping ratio) which is given by:

$$b_r = \frac{b}{2\sqrt{km}}$$

Equation (3.9) contents the natural frequency and thus gives us the *modal model*. This natural frequency has two parts:

- the imaginary part: damped frequency - $\omega_r = \omega_0\sqrt{1-b_r^2}$
- the real part: damping rate - $\omega_0 b_r$

The physical significance of these two parts is shown in a free response plot of the SDOF structure in Fig. 3.3 in which $T$ marks a period of the vibration.

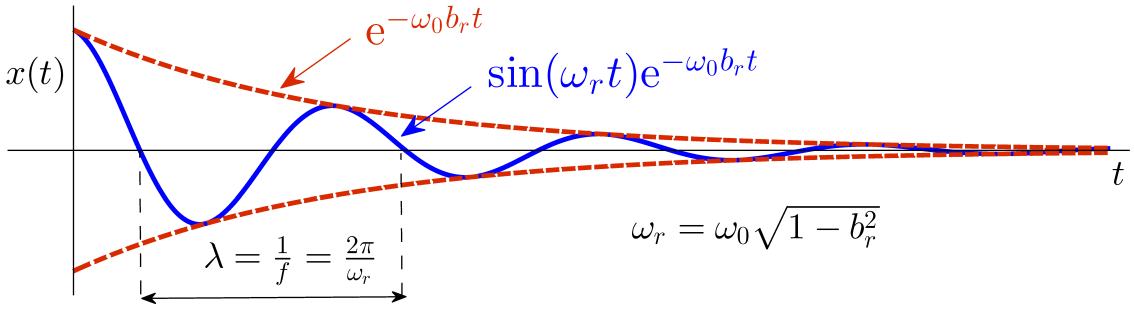


Fig. 3.3: Free vibration response of SDOF system

### Response model derivation

We assume again the excitation in form of (3.4) and the response in form of (3.2) for derivation of a response model of the damped structure. Here, the equation of motion becomes:

$$m\ddot{x} + b\dot{x} + kx = fe^{i\omega t} \tag{3.10}$$

After substituting (3.2) into (3.10) we obtain

$$(k + i\omega b - \omega^2 m)x\mathrm{e}^{i\omega t} = f\mathrm{e}^{i\omega t}$$

from which we extract system receptance FRF in the form

$$\alpha(\omega) = \frac{x}{f} = \frac{1}{(k-\omega^2 m) + i\omega b} \tag{3.11}$$

This FRF is complex now, but still is independent on the excitation.

## 3.4 Multi-degree-of-freedom system theory

We discuss more general case than SDOF system in this section. The MDOF system may have 2 or 100 DOF, but a mathematical description of its dynamics behaviour remains the same. Matrices and vectors are presented in the analysis instead of the scalar quantities.

### 3.4.1 MDOF without damping

#### Modal model derivation

When we consider MDOF system with $n$ DOF and no excitation, the equation of motion looks

$$\mathbf{M}\ddot{\mathbf{x}}(t) + \mathbf{K}\mathbf{x}(t) = 0 \tag{3.12}$$

where $\mathbf{M}$ is $n$ x $n$ mass matrix, $\mathbf{K}$ is $n$ x $n$ stiffness matrix and $\mathbf{x}(t)$ is $n$ x 1 vector of time-varying displacements. For this case (the free vibration), the solution exists in a form:

$$\mathbf{x}(t) = \mathbf{x}\mathrm{e}^{i\omega t} \tag{3.13}$$

where $\mathbf{x}$ is $n$ x 1 vector of the time-independent amplitudes. Substitution of (3.13) into (3.12) leads to

$$(\mathbf{K} - \omega^2\mathbf{M})\mathbf{x} = 0 \tag{3.14}$$

In order to avoid a trivial solution ($\mathbf{x} = 0$), so-called frequency determinant has to be equal zero:

$$\det\left|\mathbf{K} - \omega^2\mathbf{M}\right| = 0 \tag{3.15}$$

this determinant can be spread into the polynomial form for $\omega^2$ as the variable

$$a_n\omega^{2n} + a_{n-1}\omega^{2(n-1)} + \cdots + a_1\omega^2 + a_0 = 0$$

where $a_n, \ldots, a_1$ are real constants. The roots of the polynomial create $n$ undamped system's natural frequencies $(\omega_1^2, \omega_2^2, \ldots, \omega_n^2)$. After substituting any of the natural frequencies back into (3.14), we obtain a corresponding set of values for $\mathbf{x}$. We call these eigenvectors or mode shape vectors and mark them $\boldsymbol{\psi}$. The values in the eigenvectors are not unique, but relative. It means that they don't content an information about absolute displacement, but just about the mode shape. If the eigenvectors are scaled according to mass matrix, they are usually marked $\boldsymbol{\phi}$ and we call them mass-normalized mode shapes. More information about the mode shapes, their scaling and properties is given for example in [1],[2],[3],[4] or [5].

**Response model derivation**

Turning now to a response analysis, we assume the system is excited by sinusoidal force. The equation of motion becomes

$$\mathbf{M}\ddot{\mathbf{x}}(t) + \mathbf{K}\mathbf{x}(t) = \mathbf{f}\mathrm{e}^{i\omega t} \tag{3.16}$$

where $\mathbf{f}$ is $n$ x 1 vector of time-independent complex amplitudes. The solution is being found in the form of (3.13) again. Substitution this form into (3.16) leads to

$$(\mathbf{K} - \omega^2\mathbf{M})\mathbf{x}\mathrm{e}^{i\omega t} = \mathbf{f}\mathrm{e}^{i\omega t}$$

or

$$\mathbf{x} = (\mathbf{K} - \omega^2\mathbf{M})^{-1}\mathbf{f} \tag{3.17}$$

which can be written as

$$\mathbf{x} = (\boldsymbol{\alpha}(\omega))\mathbf{f}$$

where $\boldsymbol{\alpha}(\omega)$ is $n$ x $n$ receptance matrix. Previous expressions are the definition of the receptance of MDOF system, however, it contents an inverse of matrix, which can be an inefficient operation for big systems (large $n$) thus some mathematical operation can be done in order to obtain the receptance in more friendly form [1].

Any individual FRF parameter $\alpha_{jk}(\omega)$ can be compute using one of the following ways

$$\alpha_{jk}(\omega) = \sum_{r=1}^{n} \frac{({}_r\phi_j)({}_r\phi_k)}{\omega_r^2 - \omega^2} \tag{3.18}$$

or

$$\alpha_{jk}(\omega) = \sum_{r=1}^{n} \frac{{}_rA_{jk}}{\omega_r^2 - \omega^2} \tag{3.19}$$

where $r$ indicates the number of the mode shape. And ${}_rA_{jk}$ is refer as a *modal constant*[1]. The relation (3.18) shows the fact, that one can see MDOF system as a superposition of SDOF systems.

### 3.4.2 MDOF with proportional viscous damping

As it was pointed above, there exist more types of the damping model, which are well described in [6]. The proportional damping model is chosen here because it is special type of damping which has the advantages of being particularly easy to analyse and it is used often in FEA software. More about viscous damping identification can be found in [7].

[1]The modal constant is referred as *residue* and the natural frequency as *pole* in some system identification publications

The damping matrix $\mathbf{B}$ is derived from mass and stiffness matrix (There can be found more possible form of the proportional damping model in [1] or [8]).

$$\mathbf{B} = \alpha\mathbf{M} + \beta\mathbf{K} \tag{3.20}$$

where $\alpha$ and $\beta$ are real scalars. The values of the constants depend on the units of matrices $\mathbf{M}$ and $\mathbf{K}$ but if we use basic SI units i.e. $kg$ for $\mathbf{M}$ and $Nm^{-1}$ for $\mathbf{K}$ the value of $\alpha$ different between 0 and 10 and $\beta$ is between 0 and $10^{-4}$ [5]. Coefficient $\alpha$ models a structural damping, $\beta$ represents a material damping.

### Modal model derivation

The equation of motion for no excitation case in matrix form looks

$$\mathbf{M}\ddot{\mathbf{x}} + \mathbf{B}\dot{\mathbf{x}} + \mathbf{K}\mathbf{x} = 0 \tag{3.21}$$

In order to determine damped natural frequencies and the mode shapes, it is convenient to transform equation (3.21) into so-called *state space*. This yields, in fact, into the reduction of the equation order. The state space is defined by the state vector $\bar{\mathbf{x}}$:

$$\bar{\mathbf{x}} = \begin{bmatrix} \dot{\mathbf{x}} \\ \mathbf{x} \end{bmatrix}$$

Then, the transformation of the equations of motion looks

$$\begin{bmatrix} \mathbf{0} & \mathbf{M} \\ \mathbf{M} & \mathbf{B} \end{bmatrix} \begin{bmatrix} \ddot{\mathbf{x}} \\ \dot{\mathbf{x}} \end{bmatrix} + \begin{bmatrix} -\mathbf{M} & \mathbf{0} \\ \mathbf{0} & \mathbf{K} \end{bmatrix} \begin{bmatrix} \dot{\mathbf{x}} \\ \mathbf{x} \end{bmatrix} = \begin{bmatrix} \mathbf{0} \\ \mathbf{0} \end{bmatrix} \tag{3.22}$$

which is written in a short form as

$$\bar{\mathbf{M}}\dot{\bar{\mathbf{x}}} + \bar{\mathbf{K}}\bar{\mathbf{x}} = \mathbf{0} \tag{3.23}$$

The solution of the equation of motion is being found in the similar way as (3.8)

$$\mathbf{x}(t) = \mathbf{x}\mathrm{e}^{st} \tag{3.24}$$

Substituting (3.24) into (3.23) leads to

$$(\bar{\mathbf{K}} - \omega^2\bar{\mathbf{M}})\mathbf{x}\mathrm{e}^{st} = 0 \tag{3.25}$$

from which the damped natural frequencies can be found using the process described above (under (3.15)). The natural frequencies have two parts again, the real (damping) and the imaginary (frequency). The mode shapes are exactly the same for the proportional damped system and the undamped one [1].

It is useful to note that the modal properties of the MDOF can be found as the eigenvalues and the eigenvectors of the matrix $\mathbf{A}$. The matrix looks for a undamped system as

$$\mathbf{A} = -\mathbf{M}^{-1}\mathbf{K} \tag{3.26}$$

and for a damped system

$$\mathbf{A} = -\bar{\mathbf{M}}^{-1}\bar{\mathbf{K}} \tag{3.27}$$

The very previous equation is the main reason why is the state space taken into analysis. Solving the eigenvalue problem is more effective than go thought the frequency determinant.

Results of the eigenvalue problem or from solution thought the frequency determinant can be expressed into two $n_x n$ matrices [4],[5]. First one is so-called *spectral matrix*, marked as $\mathbf{\Lambda}$, containing complex eigenvalues (poles, complex natural frequencies) $\lambda_r = -\lambda_r^{\mathrm{re}} + \mathrm{i}\lambda_r^{\mathrm{im}}$ on its diagonal.

$$\mathbf{\Lambda} = \begin{bmatrix} \lambda_1 & 0 & \dots & 0 \\ 0 & \lambda_2 & \dots & 0 \\ \vdots & \vdots & \ddots & \vdots \\ 0 & 0 & \dots & \lambda_n \end{bmatrix} \tag{3.28}$$

Second one is referred as *modal matrix* (marked $\mathbf{\Psi}$ for unscaled mode shapes or $\mathbf{\Phi}$ for mass-normalized mode shapes), which contents all eigenvectors (mode shape vectors). The $r$-th column in the modal matrix corresponds with one eigenvector ${}_r\boldsymbol{\psi}$.

$$\mathbf{\Psi} = \begin{bmatrix} {}_1\psi_1 & {}_2\psi_1 & \dots & {}_n\psi_1 \\ {}_1\psi_2 & {}_2\psi_2 & \dots & {}_n\psi_2 \\ \vdots & \vdots & \ddots & \vdots \\ {}_1\psi_n & {}_2\psi_n & \dots & {}_n\psi_n \end{bmatrix} \tag{3.29}$$

Our modal properties (natural frequency $f_r$ and damping factor $b_r$) can be calculated from the complex eigenvalues as [9],[10]:

$$f_r = \frac{\Im(\lambda_r)}{2\pi}, \qquad b_r = -\frac{\Re(\lambda_r)}{|\lambda_r|} \tag{3.30}$$

### Response model derivation

Now, in order to find the *response model*, we add the "standard" excitation into the equations of motion

$$\mathbf{M}\ddot{\mathbf{x}} + \mathbf{B}\dot{\mathbf{x}} + \mathbf{K}\mathbf{x} = \mathbf{f}\mathrm{e}^{i\omega t} \tag{3.31}$$

the solution is being found in the form (3.13) again. Substituting it into (3.31) leads to

$$(\mathbf{K} + i\omega\mathbf{B} - \omega^2\mathbf{M})\mathbf{x}\mathrm{e}^{i\omega t} = \mathbf{f}\mathrm{e}^{i\omega t}$$

or

$$\mathbf{x} = (\mathbf{K} + i\omega\mathbf{B} - \omega^2\mathbf{M})^{-1}\mathbf{f} \tag{3.32}$$

which can be written as

$$\mathbf{x} = (\boldsymbol{\alpha}(\omega))\mathbf{f}$$

where $\boldsymbol{\alpha}(\omega)$ is the general receptance FRF. It can be derived also as [1]

$$\alpha_{jk}(\omega) = \sum_{r=1}^{n} \frac{({}_r\phi_j)({}_r\phi_k)}{\omega_r^2 - \omega^2 + i2b_r\omega_r\omega} \tag{3.33}$$

A usage of the equations (3.32) and (3.33) is discussed in section 3.5.2.

### 3.4.3 Example of 6-DOF system

A numerical example of the proportional viscous damped system with six degrees of freedom is given in this section for better understanding of the presented theory.

#### Description of the structure

The system structure is drawn in the Fig. 3.4, it can be considered as an approximation of the one-side fixed beam. The structure is created by 6 participles (has 6 degrees-of-freedom ($n = 6$)), which are numbered $1, 2, \ldots, 6$. Mass of the every element is $m_i = m = 1$kg, elements are connected by the linear springs with stiffness $k_i = k = 10^6$ N/m. The damping is added into system by the viscous proportional model according to equation (3.20), where the constants are chosen in the common bounds ([5]) as $\alpha = 2$ and $\beta = 10^{-8}$.

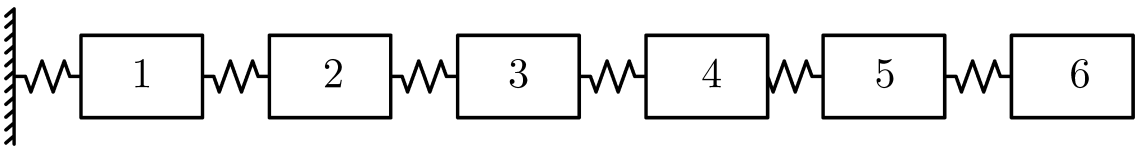


Fig. 3.4: Multi-degrees-of-freedom system

All elements of the structure are capable to vibrate in the vertical direction only, displacements of the elements are marked as $x_i$. For the case of the free vibration, in order to derive modal model, we assume, the structure is not excited. For the forced vibration, in order to derive response model, the structure is excited by a sinusoid force ($f(t) = f\mathrm{e}^{i\omega t}$) in every participle in the vertical direction.

**Equations of motion**

First, we have to formulate the equations of motion for the structure and derive the mass, stiffness and damping matrix from them. The equations of motion for MDOF system can be assembled by more ways [4]. We use well-known Lagrange equations of second kind.

$$\frac{\mathrm{d}}{\mathrm{d}t}\left(\frac{\partial E_k}{\partial \dot{x}_i}\right) - \frac{\partial E_k}{\partial x_i} + \frac{\partial E_p}{\partial x_i} = 0 \quad \text{for} \quad i = 1, 2, \ldots, n \tag{3.34}$$

in which the kinetic energy of the participles is given by

$$E_k = \frac{1}{2}m_1\dot{x}_1^2 + \frac{1}{2}m_2\dot{x}_2^2 + \cdots + \frac{1}{2}m_n\dot{x}_n^2 \tag{3.35}$$

and the potential energy of the springs is described by the following term

$$E_p = \frac{1}{2}kx_1^2 + \frac{1}{2}k(x_2 - x_1)^2 + \frac{1}{2}k(x_3 - x_2)^2 + \cdots + \frac{1}{2}k(x_{n-1} - x_n)^2 \tag{3.36}$$

after substituting (3.35) and (3.36) into (3.34) we obtain $n$ equations of motion in the form

$$\begin{gathered}
m_1\ddot{x}_1 + 2kx_1 - kx_2 = 0 \\
m_2\ddot{x}_2 - kx_1 + 2kx_2 - kx_3 = 0 \\
\vdots \\
m_{n-1}\ddot{x}_{n-1} - kx_{n-2} + 2kx_{n-1} - kx_n = 0 \\
m_n\ddot{x}_n - kx_{n-1} + kx_n = 0
\end{gathered}$$

They can be grouped into matrix form (3.21) where mass matrix $\mathbf{M}$, stiffness matrix $\mathbf{K}$ and vector of participles' displacements $\mathbf{x}$ are given by

$$\mathbf{M} = m\begin{bmatrix} 1 & 0 & 0 & 0 & 0 & 0 \\ 0 & 1 & 0 & 0 & 0 & 0 \\ 0 & 0 & 1 & 0 & 0 & 0 \\ 0 & 0 & 0 & 1 & 0 & 0 \\ 0 & 0 & 0 & 0 & 1 & 0 \\ 0 & 0 & 0 & 0 & 0 & 1 \end{bmatrix} \quad \mathbf{K} = k\begin{bmatrix} 2 & -1 & 0 & 0 & 0 & 0 \\ -1 & 2 & -1 & 0 & 0 & 0 \\ 0 & -1 & 2 & -1 & 0 & 0 \\ 0 & 0 & -1 & 2 & -1 & 0 \\ 0 & 0 & 0 & -1 & 2 & -1 \\ 0 & 0 & 0 & 0 & -1 & 1 \end{bmatrix} \quad \mathbf{x} = \begin{bmatrix} x_1 \\ x_2 \\ x_3 \\ x_4 \\ x_5 \\ x_6 \end{bmatrix}$$

Damping matrix $\mathbf{B}$ is assembled according to (3.20) as

$$\mathbf{B} = \alpha\mathbf{M} + \beta\mathbf{K} = (\alpha m + \beta k)\begin{bmatrix} 3 & -1 & 0 & 0 & 0 & 0 \\ -1 & 3 & -1 & 0 & 0 & 0 \\ 0 & -1 & 3 & -1 & 0 & 0 \\ 0 & 0 & -1 & 3 & -1 & 0 \\ 0 & 0 & 0 & -1 & 3 & -1 \\ 0 & 0 & 0 & 0 & -1 & 2 \end{bmatrix}$$

### Modal analysis of the structure

For free vibration solution (alias modal analysis) and thus derivation of modal model, we follow the process given in section 3.4.2. After introducing a state space (equation (3.22) resp. (3.23)), we perform the eigenvalue problem solution (based on the equation (3.27)) and obtain the spectral matrix (3.28) and the modal matrix scaled to unity modal vector length[2] (3.29). The natural frequencies and the damping factors can be extracted from spectral matrix according to (3.30). The process is computed in Matlab. Code listing, together with comments, is given in appendix A.1.

Found natural frequencies and the damping factors are summarized in the table 3.1. The modal matrix is written into table 3.2 and mode shapes are also visualized in the Fig. 3.5a - 3.5f.

| $r$ | $\lambda_r$ | $f_r$ [Hz] | $b_r$[%] |
|---|---|---|---|
| 1 | $-0.1 + 241.1\text{i}$ | 38.37 | 0.41 |
| 2 | $-0.1 + 709.2\text{i}$ | 112.87 | 0.14 |
| 3 | $-0.1 + 1136.1\text{i}$ | 180.82 | 0.09 |
| 4 | $-0.1 + 1497.0\text{i}$ | 238.26 | 0.07 |
| 5 | $-0.1 + 1770.9\text{i}$ | 281.85 | 0.06 |
| 6 | $-0.1 + 1941.9\text{i}$ | 309.06 | 0.05 |

Tab. 3.1: Natural frequencies and damping factors of example structure

| ${}_r\psi_k$ | ${}_1\psi_k$ | ${}_2\psi_k$ | ${}_3\psi_k$ | ${}_4\psi_k$ | ${}_5\psi_k$ | ${}_6\psi_k$ |
|---|---|---|---|---|---|---|
| ${}_r\psi_1$ | 0.1327 | 0.3678 | -0.5187 | 0.5507 | -0.4565 | 0.2578 |
| ${}_r\psi_2$ | 0.2578 | 0.5507 | -0.3678 | -0.1327 | 0.5187 | -0.4565 |
| ${}_r\psi_3$ | 0.3678 | 0.4565 | 0.2578 | -0.5187 | -0.1327 | 0.5507 |
| ${}_r\psi_4$ | 0.4565 | 0.1327 | 0.5507 | 0.2578 | -0.3678 | -0.5187 |
| ${}_r\psi_5$ | 0.5186 | -0.2578 | 0.1327 | 0.4565 | 0.5507 | 0.3678 |
| ${}_r\psi_6$ | 0.5507 | -0.5187 | -0.4565 | -0.3678 | -0.2578 | -0.1327 |

Tab. 3.2: Modal matrix of example structure

[2]Scaling formula is shown in equation (4.5)

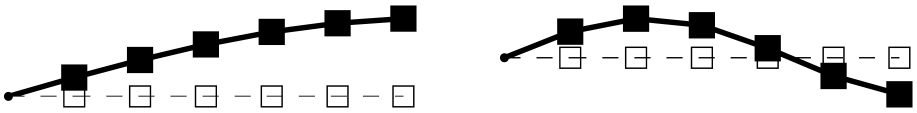

(a) Mode 1 - 38.37 Hz



(b) Mode 2 - 112.87 Hz

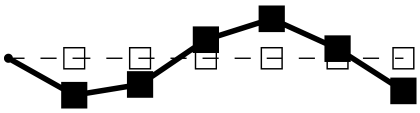

(c) Mode 3 - 180.82 Hz

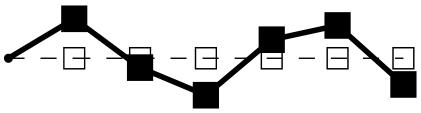

(d) Mode 4 - 238.26 Hz

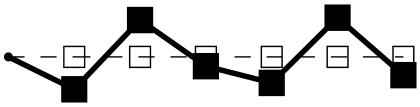

(e) Mode 5 - 281.85 Hz

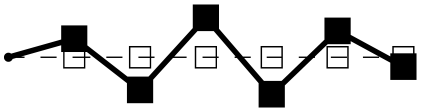

(f) Mode 6 - 309.06 Hz

Fig. 3.5: Mode shape visualization

### Harmonic analysis of the structure

We perform a harmonic analysis described in section 3.4.2 in order to derive the response model of the structure. We can use equation (3.32) for a computation of the complete FRF matrix or, since we already know the modal properties, equation (3.33), from which we can extract only some parts of FRF matrix we need.

It is convenient and sufficient to measure only one row or one column of FRF matrix during the experimental measurement of the modal properties (explanation of the fact is given e.g. in [3]), therefore we calculate just one row as well. We assume that the driving point[3] is point 1 from the Fig. 3.4.

Harmonic analysis is computed in Matlab. Code listing is given in appendix A.2. There are used both methods of the computation of FRF ((3.32) and (3.33)). Elapsed time for every method is measured and it is written into table 3.3, from which the difference between elapsed times is clearly seen. The direct inversion of the system matrix is much slower than mode superposition calculation. The direct inversion has more disadvantages. These are discussed in the section 3.5.2. Independent on the used method, the result of the harmonic analysis is first row of FRF matrix. It means 6 frequency response functions between given point and the driving point. These functions are complex. This fact brings several problems connected with presentation of FRFs. The methods of the visualization of FRFs are

[3]Driving point is a point of the structure in which an accelerometer is stuck during the hammer impact measurement in case of SISO measurements. Position of the driving point specify row number from FRF matrix, which is measured. More information about driving point and hammer impact measurement can be found in [1],[2] or [11].

| method | elapsed time [s] |
|---|---|
| direct inverse (3.32) | 2.161 |
| mode superposition (3.33) | 0.070 (0.092 include modal analysis) |

Tab. 3.3: Time of FRF computation

discussed in section 3.5.3, where are used results from this example. Here is given probably the most common form of FRF visualization in the Fig. 3.6 - magnitude in logarithmic scale vs. frequency.

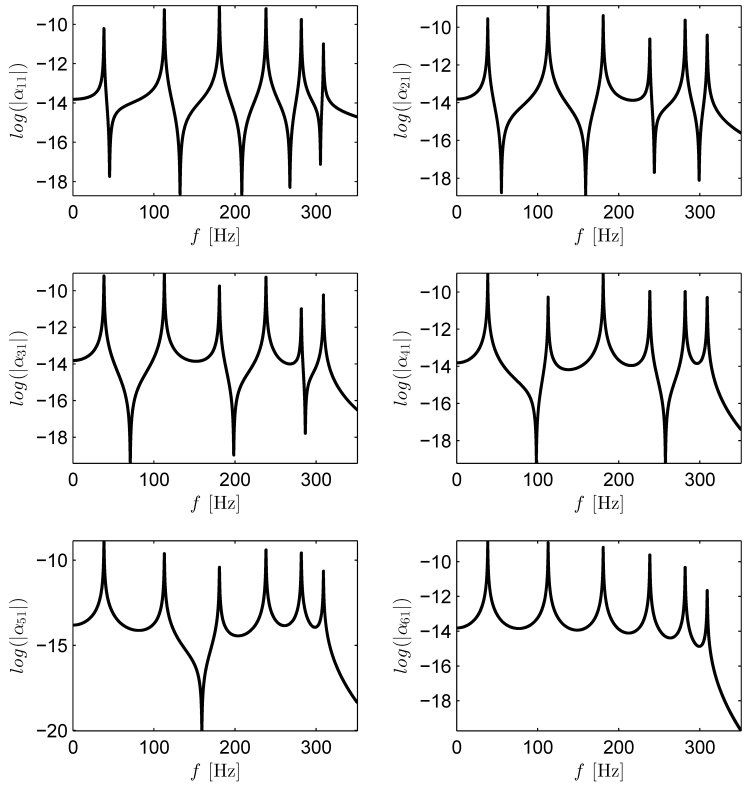


Fig. 3.6: Frequency response functions for example structure

## 3.5 Frequency response function

Frequency response function (FRF) is a complex function, which is always independent on the excitation [1]. We derived its basic forms in the previous sections, but an alternative form of FRF can be used, the function can be described by many mathematical expressions and because of complex domain, there are different ways of its presentation in a graphical form.

### 3.5.1 Alternative definitions of FRF

So far, we have defined *receptance* frequency response function as the ratio between output and input

$$\boldsymbol{\alpha}(\omega) = \frac{\mathbf{x}}{\mathbf{f}}$$

which is the ratio of the displacement response and the force excitation. But we could also select the response velocity as the output parameter and define first alternative form of FRF as

$$\mathbf{Y}(\omega) = \frac{\mathbf{v}}{\mathbf{f}}$$

this form of FRF is called *mobility*. There exists a relation between response displacement and velocity (in case of "standard" excitation), therefore there exists a relation between the receptance and the mobility as well. Displacement and velocity are related by

$$\mathbf{v}(t) = \dot{\mathbf{x}}(t) = i\omega\mathbf{x}\mathrm{e}^{i\omega t}$$

thus the relation between receptance and mobility

$$\mathbf{Y}(\omega) = \frac{\mathbf{v}}{\mathbf{f}} = i\omega\frac{\mathbf{x}}{\mathbf{f}} = i\omega\boldsymbol{\alpha}(\omega)$$

We can use an acceleration as the output parameter in similar way we used velocity. Then, we define next form of FRF as

$$\mathbf{A}(\omega) = \frac{\mathbf{a}}{\mathbf{f}} = -\omega^2\boldsymbol{\alpha}(\omega)$$

This form is called *accelerance* and it is used most often, since it is customary to measure the acceleration in the experiments. Three more forms of FRF can be found. They are defined as inverse expressions to receptance, mobility and accelerance, however they are seldom used. An overview of all FRF forms with their symbols and names is given in table 3.4.

| Definition | Symbol | Name |
|---|---|---|
| $\mathbf{x}/\mathbf{f}$ | $\boldsymbol{\alpha}(\omega)$ | Receptance, Dynamic flexibility |
| $\mathbf{v}/\mathbf{f}$ | $\mathbf{Y}(\omega)$ | Mobility |
| $\mathbf{a}/\mathbf{f}$ | $\mathbf{A}(\omega)$ | Accelerance, Inertance |
| $\mathbf{f}/\mathbf{x}$ | $\boldsymbol{\alpha}^{-1}(\omega)$ | Dynamic stiffness |
| $\mathbf{f}/\mathbf{v}$ | $\boldsymbol{Y}^{-1}(\omega)$ | Mechanical impedance |
| $\mathbf{f}/\mathbf{a}$ | $\boldsymbol{A}^{-1}(\omega)$ | Apparent mass |

Tab. 3.4: Alternative definitions of frequency response function

### 3.5.2 Mathematical forms of FRF

A receptance matrix $\boldsymbol{\alpha}(\omega)$ was derived from the undamped MDOF system in (3.17) as

$$\boldsymbol{\alpha}(\omega) = (\mathbf{K} - \omega^2\mathbf{M})^{-1} \tag{3.37}$$

It is possible to determine the receptance matrix at any frequency of interest simply from the previous equation. However, this involves an inversion of the matrix at each frequency. This process has several disadvantages from a point of view of the numerical mathematics and even from a practical implementation, namely [1],[12]:

- it becomes costly for large-order systems (a lot of DOF) and thus computing is time inefficient
- it is inefficient if only a few of the individual FRF expressions in the specific locations are required
- the inversion of the system matrix does not provide insight into the FRF properties
- it is impossible to calculate the FRF from the modal properties by this way

Due to these reasons, the alternative means of deriving of FRF can be used. This process takes into account the modal properties of the system. Its description can be found in [1] or [12], the main results are summarized below.

The receptance matrix $\boldsymbol{\alpha}(\omega)$ is symmetric, which reflect the principle of the reciprocity. Then, an element in the FRF can be defined as

$$\alpha_{jk} = \frac{x_j}{f_k} = \alpha_{kj} = \frac{x_k}{f_j}$$

We can compute any individual FRF parameter $\alpha_{jk}(\omega)$ using the following formula

$$\alpha_{jk}(\omega) = \sum_{r=1}^{n} \frac{({}_r\phi_j)({}_r\phi_k)}{\omega_r^2 - \omega^2} = \sum_{r=1}^{n} \frac{{}_rA_{jk}}{\omega_r^2 - \omega^2} \tag{3.38}$$

which in very simpler and more informative than the direct inverse of the system matrix. The parameter, ${}_rA_{jk}$, is referred as *modal constant* for the $r$-th mode and for the specific coordinates $j$ and $k$. This relation often creates a base of the modal parameters estimation techniques, however it can be rewritten and used in another forms. One of the possible formulations is, so-called numerator-denominator transfer function form

$$\alpha_{jk}(\omega) = \frac{B_0 + B_1\omega^2 + B_2\omega^4 + \cdots + B_{n-1}\omega^{2(n-2)}}{A_0 + A_1\omega^2 + A_2\omega^4 + \cdots + A_n\omega^{2n}} \tag{3.39}$$

where $B_i$ and $A_i$ can be complex or real constants ([9], [10]). The denominator is formed by the frequency determinant (3.15) thus its roots are the natural frequencies of the system. Clearly, equation (3.39) could be written as

$$\alpha_{jk}(\omega) = C * \frac{(D_1 - \omega^2)(D_2 - \omega^2)\cdots(D_{n-1} - \omega^2)}{(\omega_1^2 - \omega^2)(\omega_2^2 - \omega^2)\cdots(\omega_n^2 - \omega^2)} \tag{3.40}$$

in which $C$ and $D_i$ are other complex or real constants. This form is also referred as *pole-residue* notation of FRF in the signal processing publications ([1],[13]). The residue is related to our modal constant and poles are the natural frequencies $\omega_r$, which are seen in the denominator again. The equation (3.40) can be spread out into the partial fractions series form, such as

$$\alpha_{jk}(\omega) = \sum_{r=1}^{n} \frac{{}_rA_{jk}}{\omega_r^2 - \omega^2}$$

which is the same expression as (3.38). This shows that it doesn't matter which expression is used in order to find the modal properties. They are used according to the used modal parameter estimation method.

The characteristics and mathematical forms of the response models were presented for the undamped MDOF system, but they can be generalized for the damped systems. The expressions (3.39) and (3.40) remain the same for all damping models, but (3.38) and (3.33) are changed in the case of the proportional viscous damping. More information about FRF and its properties can be found in [1],[2],[12] or [3].

### 3.5.3 Visualization of FRF

Since the frequency response function is complex in general, we have to deal with three variables - frequency, real part and imaginary part. This brings a complication how to plot FRF data. Of course, all these variables can be plot in one 3D graph, but this kind of the visualization doesn't bring useful information. It is convenient and more useful to plot specific pairs rather then 3D graph. Several combination of these pairs are possible. The most common forms of presentation of FRFs are [1]:

1. Magnitude[4] vs Frequency and Phase vs Frequency - there can be earmarked two sub-types:
   - Magnitude in a linear scale - Fig. 3.7a - we can see absolute, real values of the magnitude with the physical significance - it reflects a measured displacement (resp. velocity or acceleration)
   - Magnitude in a logarithmic scale - Fig. 3.7b - when we use logarithmic scale for the magnitude on the y-axis, we lose the direct physical significance, but *anti-resonances* are emphasized. They can be used for the first, visual check of the measured FRFs [1].
2. Real part vs Frequency and Imaginary part vs Frequency - Fig. 3.8 - there cannot be used logarithmic scale for the real or the imaginary part, since we need to know the sign of the values as well.
3. Nyquist plot (Imaginary vs Real part - plot in Gauss plane) - Fig. 3.9 - Nyquist plot creates a base of Circle Fit estimation method

[4]Magnitude is somewhere called Modulus

The frequency response function of the structure from the Fig. 3.4 is chosen as an example for different types of the visualization. This FRF is obtained by the harmonic analysis described in section 3.4.3. The element of FRF receptence $\alpha_{31}$ is drawn in the following graphs.

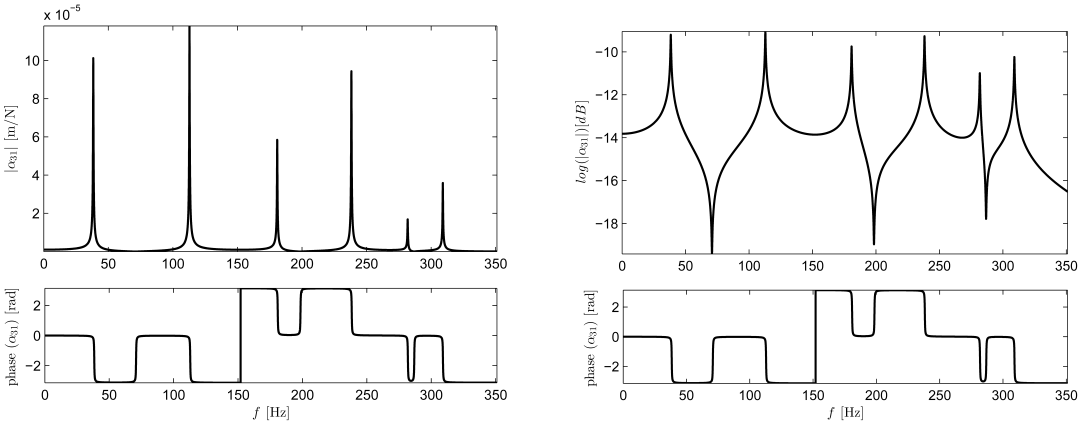


(a) Magnitude in linear scale

(b) Magnitude in logarithmic scale

Fig. 3.7: Magnitude vs. frequency and phase vs. frequency

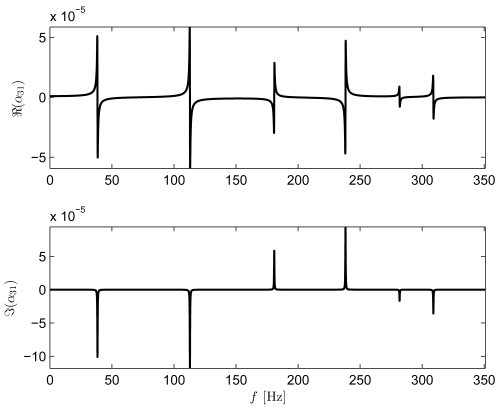


Fig. 3.8: Real part vs frequency and imaginary part vs frequency

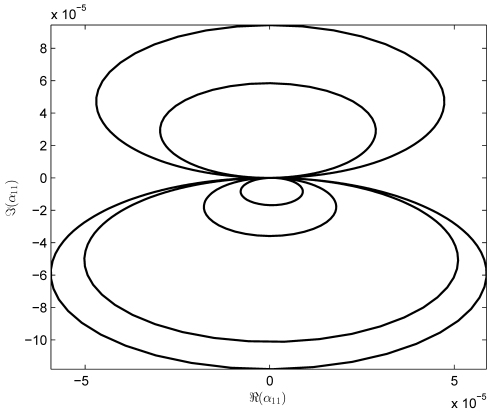


Fig. 3.9: Nyquist plot

The graphs of FRF from the Fig. 3.7 - 3.9 can look different on the first look, but they all illustrate the same element of the frequency response function. It can't be said which type of the visualization is the best or which brings the most useful information. All types are used in the different analysis from time to time.

## 3.6 Comparison of prediction and experiment

The comparison techniques aren't part of a theoretical or an experimental modal analysis itself, however, they are very important for a verification of the theoretical results. We can compare the experimental results with FEM results or we can compare results obtained by different modal parameter estimation techniques. Some simple errors can be seen from these comparisons. Basically, we can used graphical or numerical comparison. Graphical comparison is more illustrative, numerical one brings more exact results. Generally, it is recommended to use as much comparison techniques as possible, not just to rely on one [1].

### 3.6.1 Comparison of frequency response functions

First, most natural, comparison lies in the comparison of the experimental response model with the predicted one. The predicted model can be extracted from known spatial model ($\mathbf{M}$, $\mathbf{B}$, $\mathbf{K}$) using expression (3.32). If we do not know system matrices we can still use this comparison technique but instead of the predicted FRF we can use "regenerated" response model. This FRF can be calculated directly from the estimated modal parameters using (3.33) and comparison perform (Fig. 3.10).

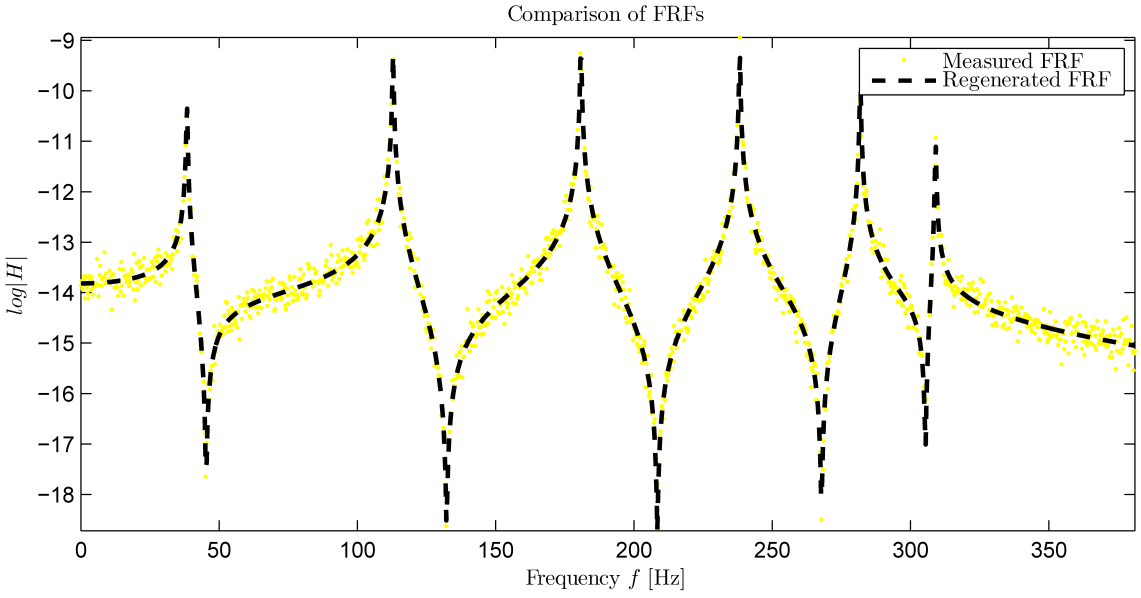


Fig. 3.10: Comparison of FRF

### 3.6.2 Comparison of modal properties

Comparison of the modal properties is one of the most common, because of a simple fact, that the modal properties can be predicted faster and in easier way than the frequency response function. This type of the comparison has greater illustrative signs and is more meaningful for possible following analysis. There can be found great number of the techniques for the modal parameter comparison [1].

#### Comparison of natural frequencies

Direct comparison of the predicted and the measured natural frequencies is one of the most obvious. It can be done by a simple tabulation of these two sets. The table can content a few statistical information such as absolute error, relative error, correlation coefficient between two sets and so on.

Numerical comparison isn't bad, however, graphical interpretation is more useful and more illustrative format. We can plot the experimental values against the predicted ones (Fig. 3.11). It is possible to see the degree of correlation between two sets of results directly and even more from this plot. We can identify the nature and therefore possible cause of any discrepancies which can be included in the results sets. All plotted frequencies should lie close to a straight line of the first

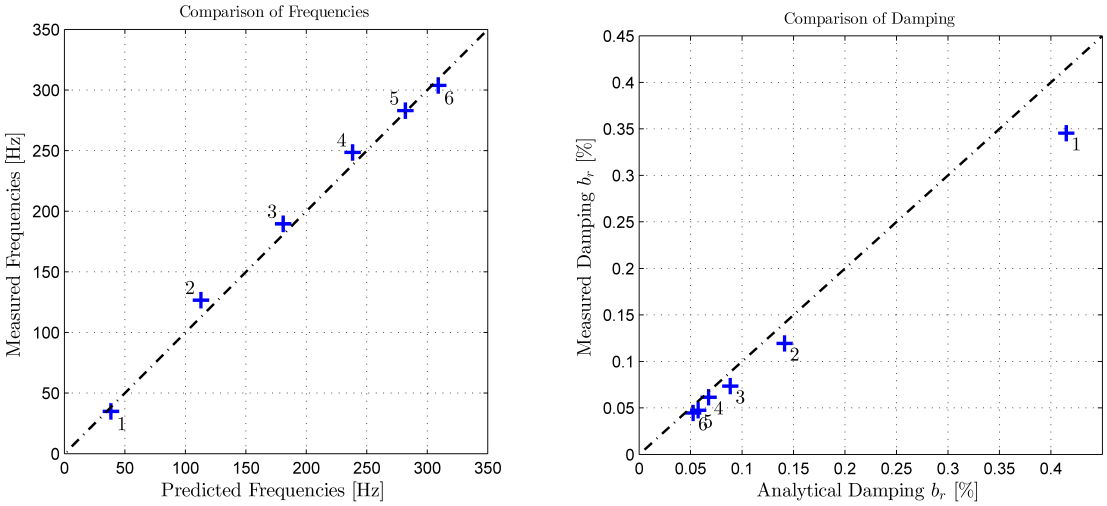


(a) natural frequencies ($f_r$) (b) damping factors ($b_r$)

Fig. 3.11: Comparison of natural frequencies and damping

slope. From the deviation of the points from the straight line we can assume about possible causes of errors. If the points lie scattered widely around the straight line then there probably exist a serious failure of the theoretical or the experimental approach. If the scatter is small and distributed randomly around the straight line then this may be from the normal modeling and the measurement process errors [1].

However, if the deviates aren't random but systematic (e.g. one-side distribution around the straight line) then this situation suggests that a specific character of errors could exist and attention should be paid to re-calculate the theoretical results and/or re-measure the experimental values in order to make sure that the systematic error is caused by the standard experimental errors or if there really exist systematic problem in a material data, used geometrical model, used methodology or somewhere else.

### Comparison of damping factors

Strictly speaking, we cannot compare predicted and measured damping factors, since there is not possibility how to predict damping. However, it is possible to compare the damping factors obtained from two different modal parameter estimation techniques. The ways of the comparison and following judgment are exactly the same as in case of the natural frequencies.

### Graphical comparisons of mode shapes

In this case, we have much more data to deal with for every mode in the frequency range of interest. The most straightforward way of the comparison of two mode shapes would be just to plot them both into one picture and/or animate them (Fig. 3.12). This way has a great disadvantage. Although differences are shown it is difficult to interpret them, even more the final plots become very confusing because so much information is included on them [1].

A more convenient approach is available by plotting a pair of the mode shapes in a similar way as the natural frequencies, along the straight line under 45°. The individual points are related to the specific coordinates on the measured structure and they should also lie close to the straight line. We may formulate the similar conclusions about the distribution of the points around the straight line as in the case of the natural frequencies. We have to keep in mind that the mode shapes have to be normalized in the exactly same way. In another case, straight line wouldn't be under 45° passing thought origin, but under general angle. This kind of the comparison of the mode shapes is more useful when we compare more pairs of the mode shapes plotted in separated pictures. From these pictures, we can identify systematic errors in the same measured points, however, we are not able to identify which set of mode shapes is incorrect. It should be observed that the above method assumes that both mode shapes are real. The comparison of real and complex mode shapes together is very difficult in this way.

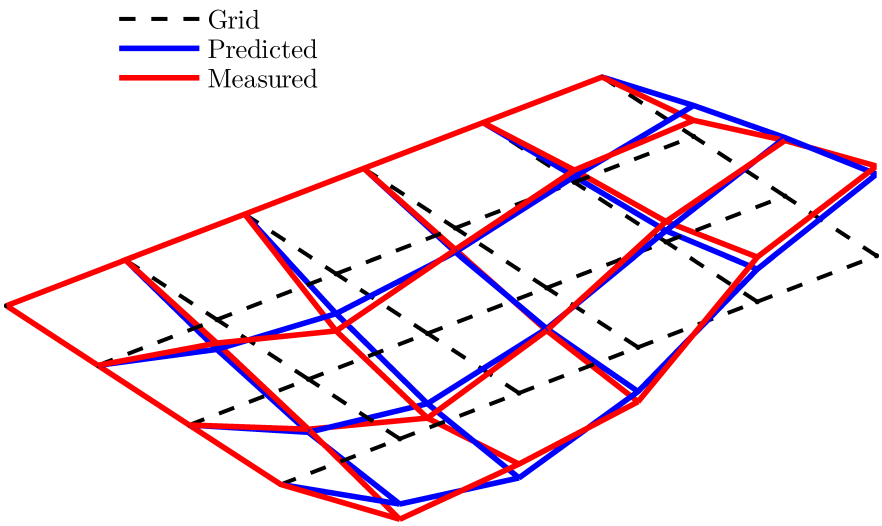


Fig. 3.12: Graphical comparison of mode shapes

### Numerical comparisons of mode shapes

As an alternative to the above graphical comparison we can calculate some simple statistical properties for a pair of the mode shapes (predicted and measured, or both measured by different techniques). The relations don't assume that mode shapes are real but they may be complex as well.

The first formula, which tells us about quantity [1], is sometimes referred as the *Modal Scale Factor* - MSF. It represents the slope of the best straight line. MSF is defined by:

$$MSF(p,e) = \frac{\sum_{j=1}^{n} (\Phi_p)_j (\Phi_e)_j^*}{\sum_{j=1}^{n} (\Phi_e)_j (\Phi_e)_j^*} \tag{3.41}$$

where indexes $p$ and $e$ means the predicted and the experimental set of the mode shapes, respectively, and the predicted mode shape are considered as the reference one. MSF gives no indication of the quality of the fit of the points to the straight line, just its slope.

The second parameter can be found as a Mode Shape Correlation Coefficient (MSCC) or more often a *Modal Assurance Criterion* (MAC). This parameter gives us an estimate of the least squares deviation of the points from the straight line.

This is defined by:

$$MAC(p,e) = \frac{\left|\sum_{j=1}^{n} (\Phi_e)_j (\Phi_p)_j^*\right|^2}{\sum_{j=1}^{n} (\Phi_e)_j (\Phi_e)_j^* \sum_{j=1}^{n} (\Phi_p)_j (\Phi_p)_j^*} \tag{3.42}$$

MAC has always a scalar character, independent of complexity or reality of the mode shapes. Neither Modal Assurance Criterion can described all random effect which can occur in the mode shapes, therefore MAC and MSF are recommended to use together with graphical ways of comparison (Fig. 3.12).

Now, we can consider a case where the mode shape are identical i.e. $\boldsymbol{\Phi_e} = \boldsymbol{\Phi_p}$. It can be shown that

$$MSF(p,e) = 1;$$

and also

$$MAC(p,e) = 1;$$

On the other hand, if the mode shapes are uncorrelated, MAC and MSF are equal to zero. In the reality, of course, the MAC values aren't perfectly equal to unity. If the MAC value is greater than 0.95 it is convenient to assume the mode shapes correspond very well. If we calculate MAC for all possible sets the of mode shapes we can group the results into a matrix and subsequently plot them. The different kinds of the presentation of MAC can be seen in Fig. 3.13. In ideal case, the modal assurance criterion matrix contents only ones on its diagonal and zeros elsewhere.

Values of MAC being less then unity can be caused by [1]:

- uncorrelated mode due to incorrect model
- nonlinear behaviors of the test structure
- noise in the measured data

| | | | | | |
|---|---|---|---|---|---|
| 0.95 | 0.02 | 0.01 | 0.02 | 0.01 | 0.01 |
| 0.04 | 0.97 | 0.03 | 0.03 | 0.01 | 0.01 |
| 0.01 | 0.02 | 0.98 | 0.01 | 0.01 | 0.01 |
| 0.00 | 0.00 | 0.01 | 1.00 | 0.02 | 0.01 |
| 0.01 | 0.02 | 0.01 | 0.02 | 0.95 | 0.01 |
| 0.01 | 0.01 | 0.02 | 0.01 | 0.01 | 0.98 |

(a) MAC matrix

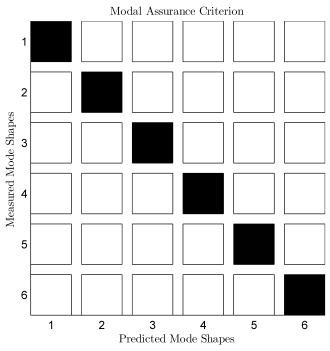


(b) MAC 2D

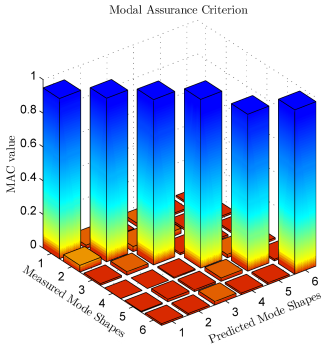


(c) MAC 3D

Fig. 3.13: MAC - different kind of presentation

# 4 MODAL PARAMETER ESTIMATION

The modal parameter estimation is one of the most important part of the experimental modal analysis since this is the part when we will finally get the modal properties. "Parameter estimation" means to take data from the measurement and use one of the many existing methods to find the natural frequencies, the damping factors and the mode shapes.

There is great amount of methods for the parameter estimation, but none of those is perfect and none is suitable for all cases. According to in what domain method works, we can divide methods into time-domain and frequency domain methods. In addition, there can be found methods which works on SDOF only and more complex algorithms operate on MDOF systems.

The SDOF modal analysis techniques are the oldest one developed in objective to describe the modal properties of the structure. All of the methods from this category have one common, important feature. They all use up the following relation

$$\alpha_{jk}(\omega) = \sum_{r=1}^{n} \frac{{}_rA_{jk}}{\omega - \lambda_r} \tag{4.1}$$

which says that we can look at MDOF system as on the superposition of the SDOF systems. Therefore it is possible to analyse every single peak of FRF as it would describe SDOF system, but this is also the biggest limitation of all SDOF methods. If the two or more modes are heavily coupled, we should be very careful in using the SDOF modal analysis techniques in order to avoid great fails in the obtained modal parameters [14]. Three different methods can be found in [1]:

- *Peak-Picking method* - we focus on this method below.
- *Circle-fit method* - we focus on this method below.
- *Inverse method* - this method uses the fact, that the same FRF which generate a circle in the Nyquist plot, trace out a straight line when it is plotted as a reciprocal value. Then, it is fitted by a line instead of a circle.

The more complex methods, sometimes called MDOF methods, do not use the assumption of SDOF system (4.1), but operate on the whole FRF at once. This means they are able to find the modal properties of the all modes in the frequency range in one step. Some of these methods are also referred as a curve fitting (This name reflects a nature of the methods). The list of the most common MDOF modal estimation methods together with their domain and acronym is given in the following table (based on [3]).

We will discuss a few methods in detail in the next parts of this chapter. Namely Peak Picking, Circle Fit method, Least Square estimation (LSCE, OP, RFP,...) and Eigensystem Realization Algorithm.

| Algorithm | Domain | Acronym |
|---|---|---|
| Complex Exponential Algorithm | time | CEA |
| Polyreference Time Domain | time | PTD |
| Ibrahim Time Domain | time | ITD |
| Multi-Reference Ibrahim Time Domain | time | MRITD |
| Subspace stochastic identification | time | SSI |
| Eigensystem Realization Algorithm | time | ERA |
| Polyreference Frequency Domain | frequency | PFD |
| Simultaneous Frequency Domain | frequency | SFD |
| Multi-Reference Frequency Domain | frequency | MRFD |
| Rational Fraction Polynomial | frequency | RFP |
| Orthogonal Polynomial | frequency | OP |
| Maximum likelihood estimation | frequency | MLE |
| Complex Mode Indicator Function | frequency | CMIF |

Tab. 4.1: Summary of modal parameter estimation methods

## 4.1 SDOF methods

As it was said above SDOF modal parameter estimation methods operate on the single peak (mode).

### 4.1.1 Peak-Picking method

This method is sometimes referred also as a peak-amplitude method and it is the simplest of the modal parameter estimation methods. However, this method has some great limitations. First of all, it works well just for structures with the well-separated modes and second for the structures with a "good" damping. For heavily damped systems, the response at a resonance is influenced by more than one mode and on the other hand the accurate measurements at the resonances are difficult to obtain for light damped structures.

The method is divided into four steps described below and these steps can be illustrated by Fig. 4.1

1. An individual resonance peak is found on the FRF plot and its frequency is taken as the natural frequency $\omega_r$
2. Maximum value of the FRF is taken ($|\tilde{\alpha}|$) and the frequency bandwidth for a response level of $|\tilde{\alpha}|/\sqrt{2}$ is determined. Two, so-called half-power points, are

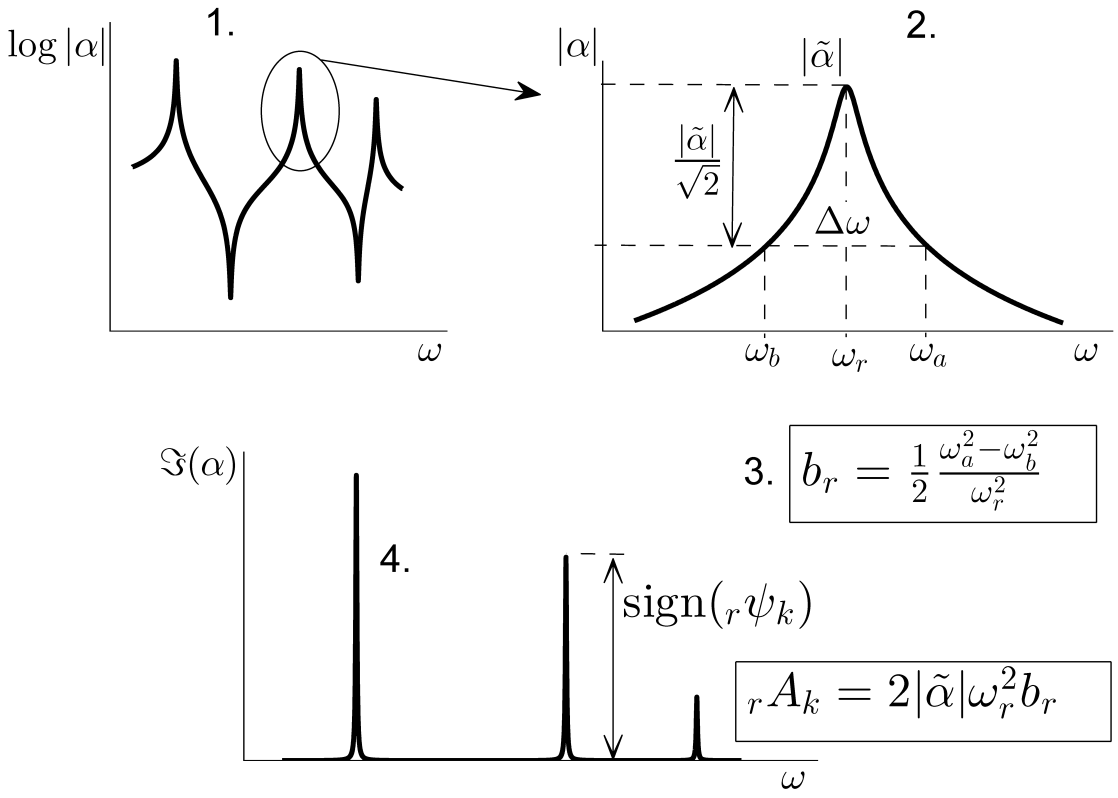


Fig. 4.1: Peak Picking method

identified and marked as $\omega_a$ and $\omega_b$. Their difference gives us the frequency bandwidth ($\Delta\omega = \omega_a - \omega_b$).

3. The damping factor $b_r$ is estimated from the following formula[1]

$$b_r = \frac{1}{2}\frac{\omega_a^2 - \omega_b^2}{\omega_r^2} \cong \frac{1}{2}\frac{\Delta\omega}{\omega_r} \tag{4.2}$$

4. The sign of the mode shape value is directly given by the imaginary part of the FRF but its value has to be computed from a modal constant. The real modal constant, for the given mode (index $r$) and FRF (index $k$), is estimated by

$$_rA_k = |\tilde{\alpha}|\omega_r^2 b_r \tag{4.3}$$

These four steps are repeated for every FRFs we measured. It means, for $N_k$ measured points, $N_k$ times and for every mode we are interested in.

We obtain one value into a matrix of the modal constants. The mode shapes can be computed from the matrix of the modal constants as

$$_r\boldsymbol{\Psi} = \frac{_r\boldsymbol{A}}{_rA_j} \tag{4.4}$$

[1]The explicit derivation can be found in [1]

where $j$ is index of the driving point and $r$ is index of the column (the mode shape). The mode shapes in this form are unscaled so it is appropriate to scale them. There are several method of the scaling possible [3], e.g. to unity modal mass, to unity modal coefficient. Scaling to the unity modal vector length is used in this thesis:

$$ {}_r\mathbf{\Psi} = \frac{1}{||{}_r\mathbf{\Psi}||_2} {}_r\mathbf{\Psi} \tag{4.5} $$

Where $||{}_r\mathbf{\Psi}||_2 = \sqrt{\sum_{k=1}^{N_k} {}_r\psi_k^2}$ is so-called second vector norm or Euclid's norm.

The natural frequencies and the damping factors of the given mode should be the same for every analysed FRFs, but it is understandable they are not because of the influence of the noise during a measurement. Therefore modal parameters have to be averaged. These averaged values of the natural frequencies and the damping factors are taken as the final estimation.

### 4.1.2 Circle Fit method

This method uses a fact, that the FRF is close to a circle in the Nyquist plot[2]. The method fits a circle on the experimental data and derive the modal properties from the properties of the fitted circle (from its position and radius). According to [1], the algorithm of the circle fit method can be described by following sequence:

1. selection of points from FRF close to resonance
2. fitting the circle through these points
3. estimation of a natural frequency
4. calculation of multiple damping estimates and their mean and scatter
5. determination of a modal constant

The step 1 can be perform automatically by selecting the given number of the points around the maximums of FRF in the frequency range of interest, however, better results can be achieved if the selection of the points is made by user, so the points which are not influence by the measured noise and neighbour modes can be selected. In general, more points available for the circle fit should produce better results. In any case, fewer than 6 points should not be used.

In the second step the fitting of the circle is made. This can be done by various number of the numerical techniques, usually based on the least square curve fitting method ([15],[16]). The results of this step are coordinates of the circle centre, its diameter and in a optimal case the information about the quality of the circle fit itself.

The meaning of step 3 is to estimate the natural frequency of the fitted mode. This is done by a construction of the radial lines from the circle centre to the

[2]Nyquits plot contents real part of FRF on the $x$-axis and imaginary part on the $y$-axis

frequency points around the resonance and by calculation the angles they subtend with each other. The frequency at which this angle reaches its maximum can be taken as the natural frequency. All process is performed numerically, but it can be illustrated by Fig. 4.2. The alternative ways of the estimation of the natural

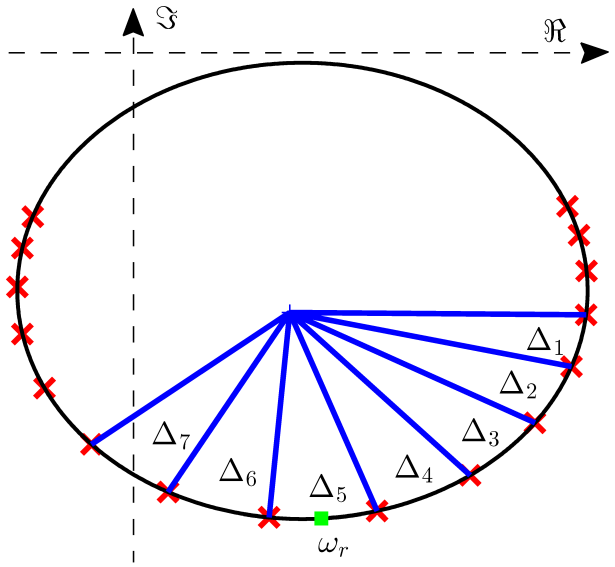


Fig. 4.2: Circle Fit - natural frequency

frequency can be found in [1]. The natural frequency can be the frequency of

- maximum magnitude (modulus) of the response
- maximum imaginary part of the response
- zero real part of the response

The option of the estimation of the natural frequency seldom makes a significant difference on the frequency itself. On the other hand, it can have a great impact on the estimation of the damping factor and subsequently on the determination of the mode shape.

Next, in step 4, we are capable to compute a set of damping estimates when we use every possible combination from the selected data points from below and above the resonance. We calculate the damping factors from the relation (4.6) (its derivation can be found in [1])

$$b_r = \frac{2(\omega_a^2 - \omega_b^2)}{\omega_r^2(\tan(\theta_a/2) + \tan(\theta_b/2))} \tag{4.6}$$

The meaning of the symbols from the previous expression is shown in Fig. 4.3. From this process we can estimate a great amount of the damping factors. It is convenient to plot them into 3D graph where on the $x$-axis are frequencies below the resonance on the $y$-axis frequencies above the resonance and the $z$-axis is for the damping factors. The example of this graph can be seen in Fig. 4.4.

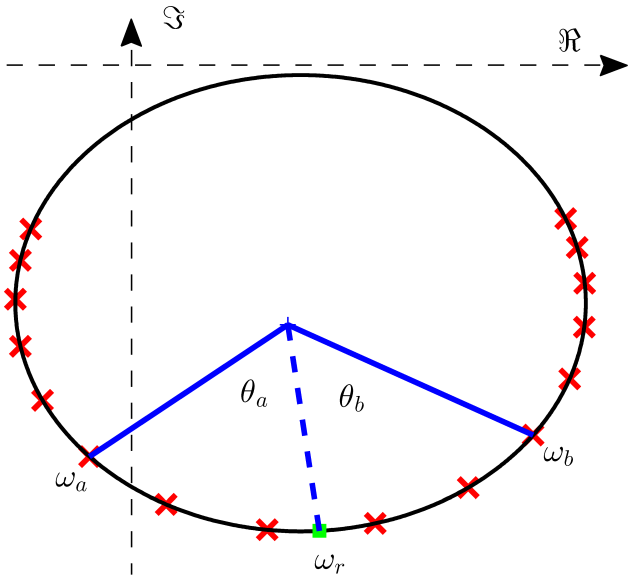


Fig. 4.3: Circle Fit - damping determination

This graph can be obtained for every measured FRF. Trends indicating a non-linear behaviour of the damping can be observed from these graphs. More about these practices is written in [1]. As the final estimate of the damping factor the mean of all values is taken, together with its deviation. If the deviation is less than 5% then we can say we performed the good analysis. However, the scatter around 20% or more can indicate a serious error in the measured data or in the analysing process itself therefore special caution should be paid in these cases.

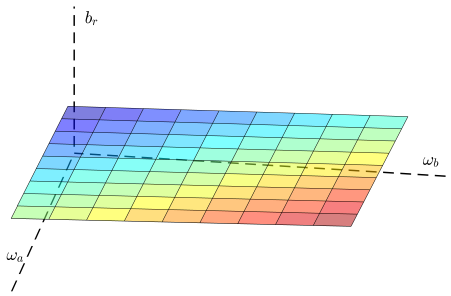


Fig. 4.4: Circle Fit - damping linearity

Finally, step 5 involves a determination of the modal constant. This is done in two sub-steps. Firstly, the magnitude of the modal constant is calculated from

$$_rA = R_r\omega_r^2 b_r \tag{4.7}$$

where $R_r$ is the diameter of the circle for $r$-th resonance. Next sub-step is about the determination of the sign of the modal constant. This sign in given by an orientation of the circle relative to the real and imaginary axes. In the case that receptence data is used for the estimation then when the imaginary part of the circle centre point is positive, the sign of the modal constant is positive as well.

This procedure is repeated for every resonance in the frequency range of interest. The mode shapes are related to the modal constant matrix as in Peak Picking method. It is just matter of a normalization.

## 4.2 Frequency-domain estimation techniques

Frequency domain estimation techniques are methods which operate in the frequency domain. It means that frequency response functions are used for the identification of the modal properties.

### 4.2.1 Least Square estimation

The relation between an output and an input, in the system with $N_k$ points, can be formulated in the frequency domain by means of a numerator-denominator transfer function

$$\hat{H}_k(\omega) = \frac{N_k(\omega)}{d(\omega)} \tag{4.8}$$

where $k = 1, \cdots, N_k$. The numerator is in the form

$$N_k(\omega) = \sum_{j=0}^{n} \Omega_j(\omega) B_{kj} \tag{4.9}$$

and the denominator looks

$$d_k(\omega) = \sum_{j=0}^{n} \Omega_j(\omega) A_j \tag{4.10}$$

The element $\Omega_j(\omega)$ is a polynomial basic function and $n$ is an order of the polynomials. The order of the polynomials, thus the order of the system, isn't known. This problem has to be solved by using of stabilization diagrams which are described in the section 4.4. There are several choices for the polynomial basic function[3], which is evaluate in the discrete frequency $f = 1, \cdots, N_f$ with $T_s$ as the sampling period

[3]The bad numerical stability of the continuous-time domain can be improved by using orthogonal polynomials, e.g. Forsythe, Chebyshev [9].

[10].

$$\Omega_j = \begin{cases} \mathrm{e}^{-i\omega_f T_s j} & \text{frequency domain (Z-domain)} \\ (i\omega_f)^j & \text{lumped continuous-time domain (Laplace domain)} \\ (\sqrt{i\omega_f})^j & \text{diffusion phenomena} \\ (\tanh(i\omega_f))^j & \text{microwaves (Richardson domain)} \end{cases}$$

The real coefficients $A_j$ and $B_{kj}$ are the parameters to be estimated. These coefficients are grouped together as follow

$$\Theta = \begin{Bmatrix} \beta_1 \\ \vdots \\ \beta_{N_p} \\ \alpha \end{Bmatrix}, \quad \beta_k = \begin{Bmatrix} B_{k0} \\ B_{k1} \\ \vdots \\ B_{kn} \end{Bmatrix}, \quad \alpha = \begin{Bmatrix} A_0 \\ A_1 \\ \vdots \\ A_n \end{Bmatrix} \tag{4.11}$$

The error, we want to minimize, between the theoretical ($\hat{H}_k(\Omega_f, \Theta)$) and the measured ($H_k(\omega_f)$) FRF can be written for every frequency in the frequency range $\omega_1, \cdots, \omega_{N_f}$ as

$$\epsilon_k(\omega_f, \Theta) = \hat{H}_k(\Omega_f, \Theta) - H_k(\omega_f) = \frac{N_k(\omega_f, \beta_k)}{d(\omega_f, \alpha)} - H_k(\omega_f) \tag{4.12}$$

This is the nonlinear problem, but it can approximated by a linear form. When we assume that $\epsilon_k(\omega_f, \Theta)$ is close to zero, we can multiply (4.12) with $d(\omega_f, \alpha)$ then the linear form looks

$$\epsilon_k(\omega_f, \Theta) = N_k(\omega_f, \beta_k) - d(\omega_f, \alpha) H_k(\omega_f) \tag{4.13}$$

The last equation can be rewritten in the matrix form since it is linear in the parameters

$$\epsilon_k(\Theta) = \begin{Bmatrix} \epsilon_k(\omega_1, \Theta) \\ \epsilon_k(\omega_2, \Theta) \\ \vdots \\ \epsilon_k(\omega_{N_f}, \Theta) \end{Bmatrix} = [\mathbf{\Gamma}_k \quad \mathbf{\Phi}_k] \ \Theta \tag{4.14}$$

where the new matrices $\mathbf{\Gamma}_k$, $\mathbf{\Phi}_k$ are

$$\mathbf{\Gamma}_k = \begin{bmatrix} \Omega_0(\omega_1) & \Omega_1(\omega_1) & \cdots & \Omega_n(\omega_1) \\ \Omega_0(\omega_2) & \Omega_1(\omega_2) & \cdots & \Omega_n(\omega_2) \\ \vdots & \vdots & & \vdots \\ \Omega_0(\omega_{N_f}) & \Omega_1(\omega_{N_f}) & \cdots & \Omega_n(\omega_{N_f}) \end{bmatrix} \tag{4.15}$$

$$\boldsymbol{\Phi}_k = \begin{bmatrix} -H_k(\omega_1)[\Omega_0(\omega_1) & \Omega_1(\omega_1) & \cdots & \Omega_n(\omega_1)] \\ -H_k(\omega_2)[\Omega_0(\omega_2) & \Omega_1(\omega_2) & \cdots & \Omega_n(\omega_2)] \\ \vdots & \vdots & & \vdots \\ -H_k(\omega_{N_f})[\Omega_0(\omega_{N_f}) & \Omega_1(\omega_{N_f}) & \cdots & \Omega_(\omega_{N_f})] \end{bmatrix} \tag{4.16}$$

The solution of the least square problem can be found by minimizing a total square error. This error is given by a double summation. The first sum is along all frequencies and second one along all the measured FRFs. When we take into account the matrices form described above the error becomes

$$l(\Theta) = \sum_{f=1}^{N_f} \sum_{k=1}^{N_k} |\epsilon_k(\omega_f, \Theta)|^2 = \sum_{f=1}^{N_f} \sum_{k=1}^{N_k} \Theta^H \begin{bmatrix} \boldsymbol{\Gamma}_k^H \boldsymbol{\Gamma}_k & \boldsymbol{\Gamma}_k^H \boldsymbol{\Phi}_k \\ \boldsymbol{\Gamma}_k \boldsymbol{\Phi}_k^H & \boldsymbol{\Phi}_k^H \boldsymbol{\Phi}_k \end{bmatrix} \Theta \tag{4.17}$$

which may be written in a more general form as

$$l(\Theta) = \Theta^H (\boldsymbol{J}^H \boldsymbol{J}) \Theta \tag{4.18}$$

where $\boldsymbol{J}$ is so-called Jacobian matrix given by

$$\boldsymbol{J} = \begin{bmatrix} \boldsymbol{\Gamma}_1 & 0 & \cdots & 0 & \boldsymbol{\Phi}_1 \\ 0 & \boldsymbol{\Gamma}_2 & \cdots & 0 & \boldsymbol{\Phi}_2 \\ \vdots & \vdots & \ddots & \vdots & \vdots \\ 0 & 0 & \cdots & \boldsymbol{\Gamma}_{N_k} & \boldsymbol{\Phi}_{Nk} \end{bmatrix}$$

The Jacobian matrix $\boldsymbol{J}$ has $N_f N_k$ rows and $(n+1)(N_k+1)$ columns (for $N_f \gg n$) [9]. The operator $(*)^H$ symbols Hermitian transposition which is only defined for the complex numbers. Therefore the coefficients $\alpha$ and $\beta_k$ would be complex as well, but we assumed that the coefficients are real thus we take into account just the real parts of the matrices, in addition, we mark new variables as follow

$$\boldsymbol{R}_k = \Re(\boldsymbol{\Gamma}_k^H \boldsymbol{\Gamma}_k)$$

$$\boldsymbol{S}_k = \Re(\boldsymbol{\Gamma}_k^H \boldsymbol{\Phi}_k)$$

$$\boldsymbol{T}_k = \Re(\boldsymbol{\Phi}_k^H \boldsymbol{\Phi}_k)$$

Now, the cost function (4.17) may be rewritten to the following expression

$$l(\Theta) = \sum_{f=1}^{N_f} \sum_{k=1}^{N_k} \Theta^T \begin{bmatrix} \boldsymbol{R}_k & \boldsymbol{S}_k \\ \boldsymbol{S}_k^T & \boldsymbol{T}_k \end{bmatrix} \Theta \tag{4.19}$$

In order to find the minimum of the cost function the derivatives have to be zero

$$\frac{\partial l(\Theta)}{\partial \beta_k} = (\boldsymbol{R}_k \beta_k + \boldsymbol{S}_k \alpha) = 0 \tag{4.20}$$

$$\frac{\partial l(\Theta)}{\partial \alpha} = \sum_{k=1}^{N_k} \boldsymbol{S}_k^T \beta_k + \boldsymbol{T}_k \alpha = 0 \tag{4.21}$$

These two equations are the so-called normal equations and they are usually formulated as

$$\begin{bmatrix} \boldsymbol{R}_1 & 0 & \cdots & \boldsymbol{S}_1 \\ 0 & \boldsymbol{R}_2 & \cdots & \boldsymbol{S}_2 \\ \vdots & \vdots & \ddots & \vdots \\ \boldsymbol{S}_1^T & \boldsymbol{S}_2^T & \cdots & \sum_{k=1}^{N_k} \boldsymbol{T}_k \end{bmatrix} \begin{bmatrix} \beta_1 \\ \vdots \\ \beta_{N_k} \\ \alpha \end{bmatrix} = \Re(\boldsymbol{J}^H \boldsymbol{J})\Theta = 0 \tag{4.22}$$

We could calculate unknown parameters from this system already, but the system matrix is very large, with an atypical structure, so the calculation would not be time efficient. Therefore when we substitute (4.20) ($\beta_k = -\boldsymbol{R}_k^{-1}\boldsymbol{S}_k\alpha$ ) into (4.21) we obtain

$$\sum_{k=1}^{N_k} (\boldsymbol{T}_k - \boldsymbol{S}_k^T \boldsymbol{R}_k^{-1} \boldsymbol{S}_k)\alpha = \boldsymbol{M}\alpha = 0 \tag{4.23}$$

The size of system matrix $\boldsymbol{M}$ is only $(n+1)$ so it is much smaller than the size of $\Re(\boldsymbol{J}^H\boldsymbol{J})$. Moreover, more effective algorithm can be achieved by using the properties of $\boldsymbol{R}_k, \boldsymbol{S}_k, \boldsymbol{T}_k$ matrices. When we examine the matrices in more details we find out the formula for each element. ($r$ is a row index, $s$ stands for a column one)

$$\boldsymbol{R}_{k_{[r,s]}} = \Re \sum_{f=1}^{N_f} \Omega_{r-1}^H(\omega_f)\, \Omega_{s-1}(\omega_f) \tag{4.24}$$

$$\boldsymbol{S}_{k_{[r,s]}} = -\Re \sum_{f=1}^{N_f} H_k(\omega_f)\, \Omega_{r-1}^H(\omega_f)\, \Omega_{s-1}(\omega_f) \tag{4.25}$$

$$\boldsymbol{T}_{k_{[r,s]}} = \Re \sum_{f=1}^{N_f} |H_k(\omega_f)|^2\, \Omega_{r-1}^H(\omega_f)\, \Omega_{s-1}(\omega_f) \tag{4.26}$$

These matrices have a Toeplitz structure[4]. In addition, $\boldsymbol{R}_k$ and $\boldsymbol{T}_k$ are Hermitian matrices[5]. These properties of the matrices are very useful, because of assembling $\boldsymbol{R}_k$ and $\boldsymbol{T}_k$ we have to compute the first row and for $\boldsymbol{S}_k$ the first row and the first column only. Thus, the process of the assembling system matrix becomes high time-effective.

The system of equations (4.23) cannot be solved in this form since we have to avoid a trivial solution ($\alpha = 0$) and therefore we need choose one of the element of

[4] A Toeplitz matrix or diagonal-constant matrix is a matrix in which constant values are on each diagonal, it means $A(i,j) = A(i+1, j+1)$ for all indexes $i$, $j$

[5] A Hermitian matrix or self-adjoint matrix is a square matrix with complex entries in which the element in the $i$-th row and $j$-th column is equal to the complex conjugate of the element in the $j$-th row and $i$-th column, for all indexes $i$ and $j$

$\alpha$ to be equal to non-zero constant. It is convenient that the last element of $\alpha$ is equal to unity [9]. Then, the reduced normal equations (4.23) become

$$\boldsymbol{A}\boldsymbol{c} = \boldsymbol{b} \tag{4.27}$$

in which

$$\boldsymbol{A} = \boldsymbol{M}_{[1:n,1:n]} \quad \text{and} \quad \boldsymbol{b} = -\boldsymbol{M}_{[1:n,n+1]} \tag{4.28}$$

The solution of this system $\boldsymbol{c}$ is related to $\alpha$ as

$$\alpha = \begin{Bmatrix} \boldsymbol{c} \\ 1 \end{Bmatrix} \tag{4.29}$$

Subsequently, all $\beta_k$ coefficients can be found from (4.20) ($\beta_k = -\boldsymbol{R}_k^{-1}\boldsymbol{S}_k\alpha$). Now, we fully know the numerator-denominator transfer function (4.8), but for finding the modal properties we have to transfer this numerator-denominator form into a pole-residue parametrization

$$H(\omega) = \sum_{r=1}^{n} \frac{R_r}{\omega - \lambda_r} + \frac{R_r^*}{\omega - \lambda_r^*} \tag{4.30}$$

where the so-called *poles* ($\lambda_r$) are found as the roots of the denominator (4.9) with $\alpha$ coefficients. The *residue* matrix $R_r$ can be computed as

$$R_r = \lim_{\omega \to \lambda_r} \hat{H}(\omega, \Theta)(\omega - \lambda_r) \tag{4.31}$$

The residuals $R_r$ are directly related to the mode shapes. The damped natural frequencies $\omega_r$ and the damping factors $b_r$ are obtained from the poles as

$$\omega_r = \Im(\lambda_r) \quad \text{and} \quad b_r = -\frac{\Re(\lambda_r)}{|\lambda_r|} \tag{4.32}$$

Note, if Z-domain ($\Omega_j = \mathrm{e}^{-i\omega_f T_s j}$) is used, the poles $\lambda_r$ and the residues $R_r$ have to be transformed to the Laplace domain by means of the impulse invariant transformation ($z = \mathrm{e}^{sT_s}$) [10]. It should be acknowledged that there is no unique least-square solution.

## 4.3 Time-domain estimation techniques

Time domain methods operate in the time-domain which means that as an input for an identification of the modal properties measured time-signals or impulse response functions (IRF) can be used.

### 4.3.1 Eigensystem Realization Algorithm

The Eigensystem Realization Algorithm (ERA) is the time-domain method which was publicated by Juang and Pappa in 1985 [17]. This method can be used for EMA and also for OMA. Only difference lies in the data that are used as method's input. An impulse response function (IRF) is calculated from FRF using fast fourier transform in case of EMA and this IRF is used for the modal parameter estimation. In case of OMA it is possible to use a free response time-signal data. It is appropriate to point out that the correct mathematics background of the Eigensystem Realization Algorithm is very complex. All mathematical processes with precise proofs can be found in [17]. Basis of this method are presented below and the practical steps necessary for successful implementation of the method are shown.

ERA uses the principles of the minimum realization to obtain a state space representation of the structure. The state space representation of the discrete time system can be written as

$$\mathbf{x}(k+1) = \mathbf{A}\mathbf{x}(k) + \mathbf{B}\mathbf{u}(k) \tag{4.33}$$

$$\mathbf{y}(k) = \mathbf{C}\mathbf{x}(k) + \mathbf{D}\mathbf{u}(k) \tag{4.34}$$

where $\mathbf{x}(k)$ marks a state vector (in our case usually $\mathbf{x} = \{\mathbf{x}, \dot{\mathbf{x}}\}^{\mathrm{T}}$), $\mathbf{u}$ is the vector of the system inputs (applied forces, excitation) and $\mathbf{y}(k)$ is the vector of outputs (measured acceleration, displacement or velocity) at the $k$-th time step. $\mathbf{A}$, $\mathbf{B}$, $\mathbf{C}$ and $\mathbf{D}$ are discrete time state space matrices [18].

A realization is the estimation of the system matrices from the response of the structure. There can be found an infinite number of the state space matrices $\mathbf{A}$, $\mathbf{B}$, $\mathbf{C}$ and $\mathbf{D}$ each of different dimensions, but we don't know the dimension of the system because we don't know a number of modes in the measured signal. In the experimental or the operation modal analysis we are not interested in the matrices $\mathbf{B}$ and $\mathbf{D}$ because all modal parameters are located in matrix $\mathbf{A}$ and $\mathbf{C}$. The eigenvalues of $\mathbf{A}$ are complex conjugates poles of the system. From each pair of the poles can be obtain the natural frequency and the damping ratio using (3.30). The mode shapes are related to matrix $\mathbf{C}$.

The Eigensystem Realization Algorithm could be described in a few steps

1. Forming the Hankel matrix[6] with structure

$$\mathbf{H}(k) = \begin{bmatrix} \mathbf{y}(k+1) & \mathbf{y}(k+2) & \cdots & \mathbf{y}(k+m) \\ \mathbf{y}(k+2) & \mathbf{y}(k+3) & \cdots & \mathbf{y}(k+m+1) \\ \vdots & \vdots & \ddots & \vdots \\ \mathbf{y}(k+n) & \mathbf{y}(k+n+1) & \cdots & \mathbf{y}(k+m+n) \end{bmatrix} \tag{4.35}$$

where $n$ is number of rows and $m$ number of columns, however, these values aren't closely specified

2. Singular value decomposition (SVD) of $\mathbf{H}(0)$
In linear algebra and signal processing, singular value decomposition is used quite often ([20],[21]). Three new matrices are found by SVD of $\mathbf{H}(0)$ (Hankel matrix $\mathbf{H}(k)$ at $k = 0$)

$$\mathbf{H}(0) = \mathbf{R}\boldsymbol{\Sigma}\mathbf{S}^{\mathrm{T}} \tag{4.36}$$

where $\mathbf{R}$ and $\mathbf{S}$ are $m$ x $m$ and $n$ x $n$ orthonormal matrices and $\boldsymbol{\Sigma}$ is $m$ x $n$ matrix with non-negative elements on the main diagonal.

3. Decision of the system order, number of poles in the frequency range
Theoretically, under perfect conditions, the matrix $\boldsymbol{\Sigma}$ is singular with the structure

$$\boldsymbol{\Sigma} = \begin{bmatrix} \boldsymbol{\Sigma}_g & \mathbf{0} \\ \mathbf{0} & \mathbf{0} \end{bmatrix} \tag{4.37}$$

where $\boldsymbol{\Sigma}_g$ is a square ($g$ x $g$) diagonal matrix and $g$ is the system order. In reality, due to measured noise, the diagonal elements of $\boldsymbol{\Sigma}$ are non-zero therefore the system order $g$ has to be chosen. The matrices $\boldsymbol{R}$ and $\boldsymbol{S}$ have to be reduce into $\boldsymbol{R}_g$ and $\boldsymbol{S}_g$ by choosing the first $g$ columns of $\boldsymbol{R}$ and $\boldsymbol{S}$.

4. Minimum realization (elimination the smallest singular values)
This procedure leads to minimum order system that represents the structure [18]. It can be shown that the system matrices $\mathbf{A}$ and $\mathbf{C}$ can be computed according to:

$$\mathbf{A} = \boldsymbol{\Sigma}_g^{-1/2}\mathbf{R}_g^{\mathrm{T}}\mathbf{H}(1)\mathbf{S}_g\boldsymbol{\Sigma}_g^{-1/2} \tag{4.38}$$

$$\mathbf{C} = \mathbf{E}_g^{\mathrm{T}}\mathbf{R}_g\boldsymbol{\Sigma}_g^{-1/2} \tag{4.39}$$

where $\mathbf{H}(1)$ is Hankel matrix $\mathbf{H}(k)$ at $k = 1$ and matrix $\mathbf{E} = [\mathbf{I} \quad \mathbf{0}]$ in which $\mathbf{I}$ is identity matrix and $\mathbf{0}$ is zero matrix, both of the appropriated dimensions.

[6] In linear algebra, Hankel matrix is a square matrix with constant skew-diagonals. It is upside-down Toeplitz matrix [19].

5. Eigenvalue solution and modal parameter determination
   The poles of the system, and therefore the natural frequencies and the damping ratios, can be extracted from the state space matrix $\boldsymbol{A}$. The eigenvalues of this matrix are directly the poles of the system. As it was said above, the poles are transformed into the modal parameters by (3.30). The mode shapes are found through expression

$$\boldsymbol{\Phi} = \mathbf{C}\boldsymbol{\kappa} \tag{4.40}$$

   where $\boldsymbol{\kappa}$ are the eigenvectors of matrix $\boldsymbol{A}$. The eigenvectors that are obtained by this method are always complex.

For successful implementation of ERA it needs to be decided about the number of the rows $n$ and the columns $m$ in the Hankel matrix. However, a greater problem is provided by a fact that we don't know the order of the analysed system which means we don't know $g$. Of course, we can guess it, but it is more convenient to plot stabilization chart in order to estimate proper parameters.

## 4.4 Stabilization charts

Stabilization charts (or diagrams) are very useful for a determination of an appropriate system order. Then, the number of the mode shapes is given as a half of the system order. The order of the system is unknown in the beginning of the estimation process and has to be determined because based on it we will calculate the modal properties. Basically, the stabilization diagram shows how modal properties differ with the changing system order. Into this chart we can plot an information about stabilization of the poles. "Stabilization", in this context, means how much values of given the pole differ between each other. According to if we choose to plot this information we can divide stabilization diagrams onto 3 kinds:

1. without stabilization - into this graphs we don't plot the information about the stabilization, we just plot all poles

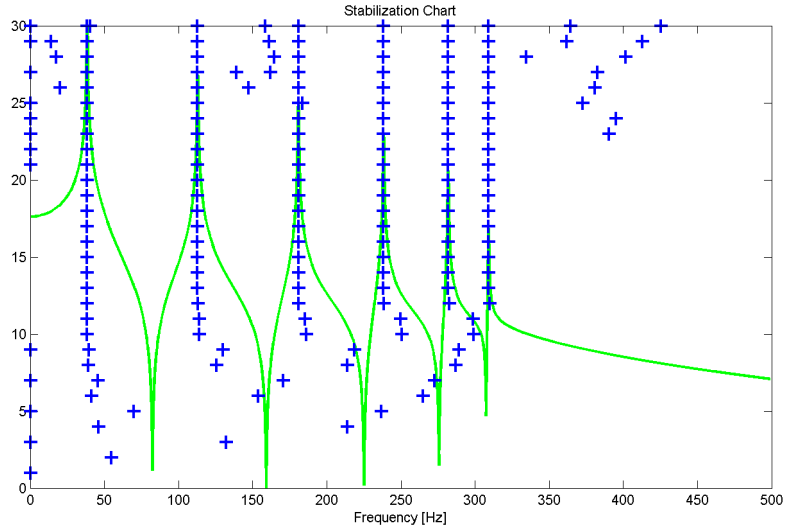


Fig. 4.5: Stabilization diagram without criterion

2. with stabilization - the stabilization criteria can be given for the frequency, the damping or even for the mode shapes
3. filtered stabilization charts - the purpose of this type is just to remove the incorrect poles.

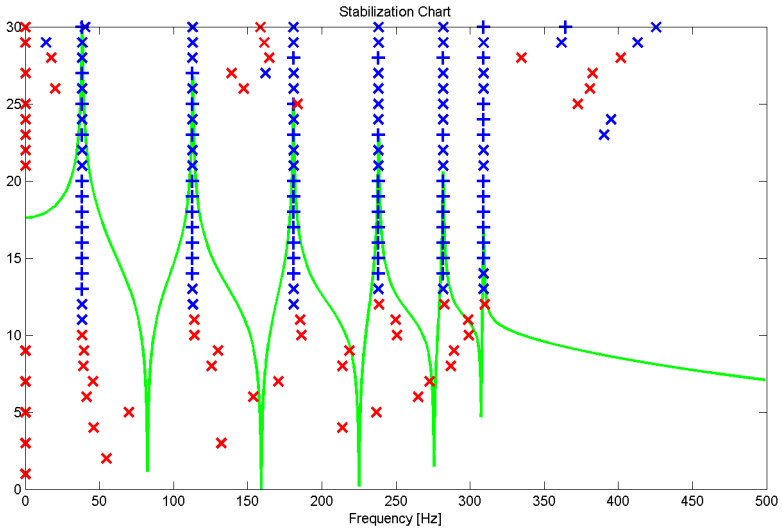


Fig. 4.6: Stabilization diagram with criterion

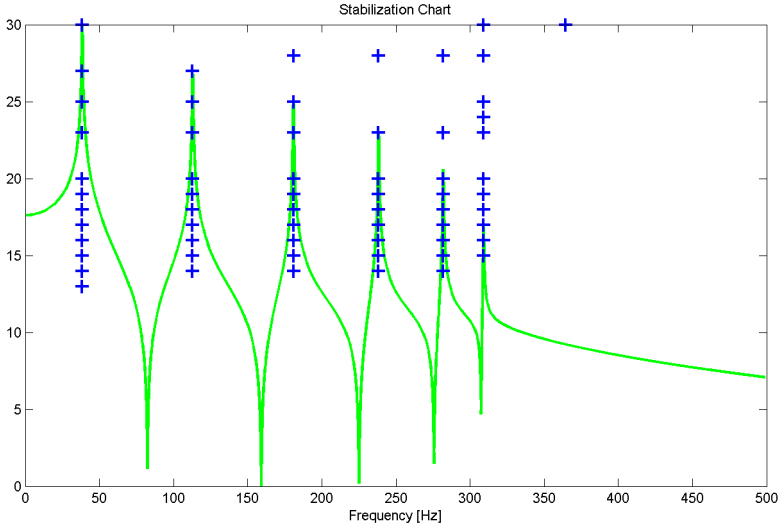


Fig. 4.7: Filtered stabilization diagram

# 5 APPLICATION FOR MODAL PARAMETER ESTIMATION

The main topic of the diploma thesis is focused on a creation of the modal parameter estimation application. Although this application was supposed to be only for the modal parameter estimation process, the extension of the application was made for a complete process of the experimental modal analysis and in a limited way for the operation modal analysis as well.

A description is given for each section of the application. This description cannot be considered as a manual to the application but only as the brief description, however, it should give a good sense what is possible in the application. The application is written in the Matlab.

## 5.1 Overview of the application

A main screen of the application together with its parts description is shown in the Fig. 5.1.

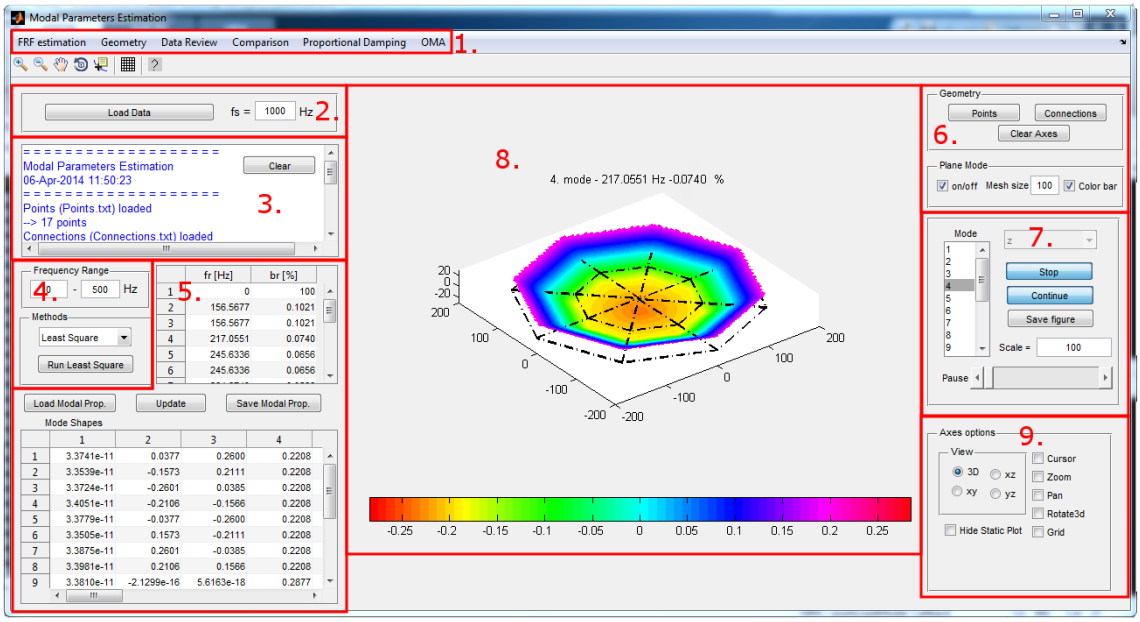


Fig. 5.1: Application overview

**1 Access to the application parts**

It is possible to call all of the rest sections of the application from these menus. Inserted data is transferred to the rest of the application automatically through these buttons.

**2 Loading data**

The data and sampling frequency have to be entered in this part. The data is in the form of .txt-file which can be obtained from external programs or from FRF estimation section of the application. The sampling frequency is provided from the measurement and should be chosen wisely. Nyquest's frequency is the half of the sampling frequency.

**3 Information console**

A small place for giving an information to the user. Everything which has happened in the application is written into this section. Also some errors and possible solutions are given in this window.

**4 Methods selection**

The method is chosen here and the frequency of interest can be specified. Four different methods can be chosen. Their description is located in the further section of this chapter.

**5 Modal properties**

All found or loaded modal properties can be seen there (the found modal properties are those estimated in the application). They can be saved into .txt-file and used in the other software, reports etc. or they can be loaded back into application and used for the post processing techniques such as the comparisons or the animation of the mode shapes.

**6 Geometry loading**

A geometry can be loaded in the section. The geometry files are produced in the geometry module of the application. The files are two or three - "points" represent the measurement points, "connections" symbolize the measured grid and in the case of plane structures, "edges" can be loaded for the better animation of the mode shapes.

**7 Mode shape animation setting**

In this part the mode shape which should be animated is selected. The mode shapes are relative so for better animation they have to be multiplied by scaling constant which can be insert here as well. In addition, the speed of animation is controlled and the picture of the animated mode shape can be captured.

**8 Plot options**

There are some basic animation options such as the view, grid, zoom or cursor which can be used for better identification of the zero displacement in the mode

shape and so on. Also the opportunity of hiding static geometrical shape is included.

## 5.2 Data acquisition and FRF estimation

This environment can be used for the FRF estimation. The theoretical description on the techniques isn't given in this diploma thesis but it can be found in [10],[22] or [23].

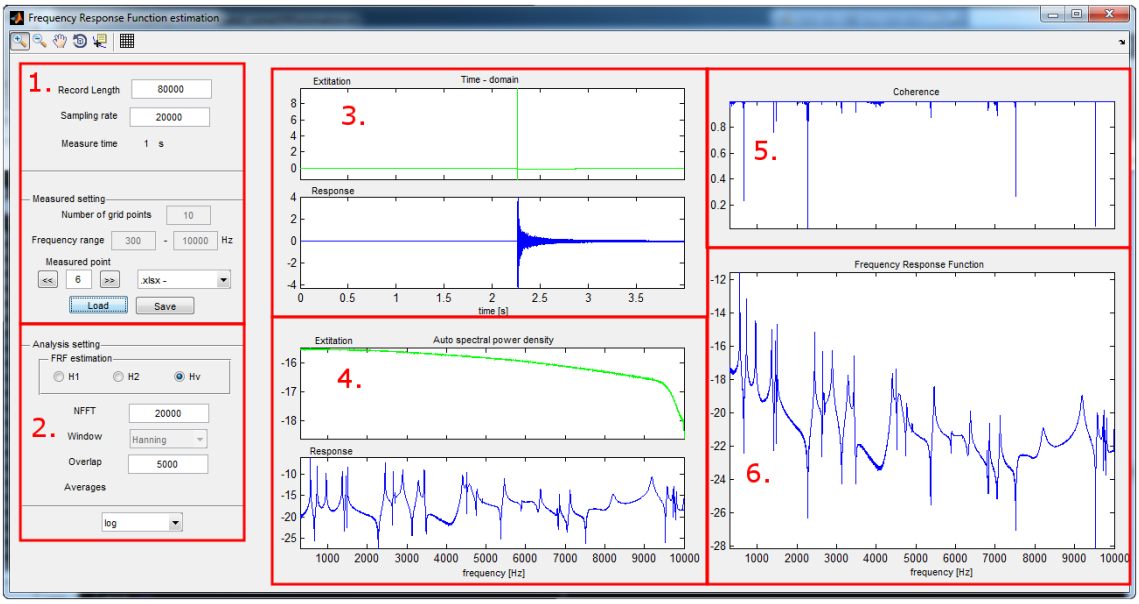


Fig. 5.2: FRF estimation module

**1 Measurement setting**

The setting of the measured signal has to be entered. Besides record length and sampling frequency the information about the measurement grid has to be included, for instance, how many points will be measured and which point is measured. The measured signals can be inserted in different forms - it depends on the measurement device. In any case - the time signal, excitation signal and response signal have to be entered.

**2 Estimation setting**

$H_1$, $H_2$ and $H_v$ estimation techniques can be chosen for the estimation of the frequency response functions. All signal processing techniques commonly used for the spectra estimation are included (windows, averaging, overlap). For an information about these techniques see [13],[23] or [24].

**3 Time-domain plotting**
The entered signals are plotted in these graphs. The first graph (green) is for the excitation signal and the second one for the output signal (blue).

**4 Auto spectral power density**
The auto spectral power densities are plotted in the graphs in this section. Again, the green one stands for the excitation signal and the blue one for the output signal.

**5 Coherence**
A coherence obtained from the FRF estimation process is plotted. The coherence can give us an information about the estimation errors. We can assume about the good level of the excitation and if the frequency response function is enough excited in the frequency range of interest.

**6 Frequency response function**
Frequency response function which is estimated based on the chosen estimation technique is show in the logarithmic magnitude vs. frequency graph. The quality of the estimation has to be appropriate and if it is not, the setting of the parameters should be changed.

## 5.3 Geometry modeling

It is very simple geometry module, but for the experimental modal analysis should be just sufficient. A screen of this "modeller" can be seen in Fig. 5.3.

**1 Points**
"Points" stands for the measured points which are placed on the real structure. The coordinates of the points are entered in the table and can be plotted in the interface. After all points are inserted they have to be saved into .txt-file which is used as an input in the main application.

**2 Connections**
The term of "connection" stands for the experimental grid. This grid doesn't need to be very detailed, but for better visualization of the mode shape, specially, in the "wire animation" it is useful. They have to be saved into .txt-file as well.

**3 Vertices**
In the case of "plane animation" when the coloured shapes are animated the

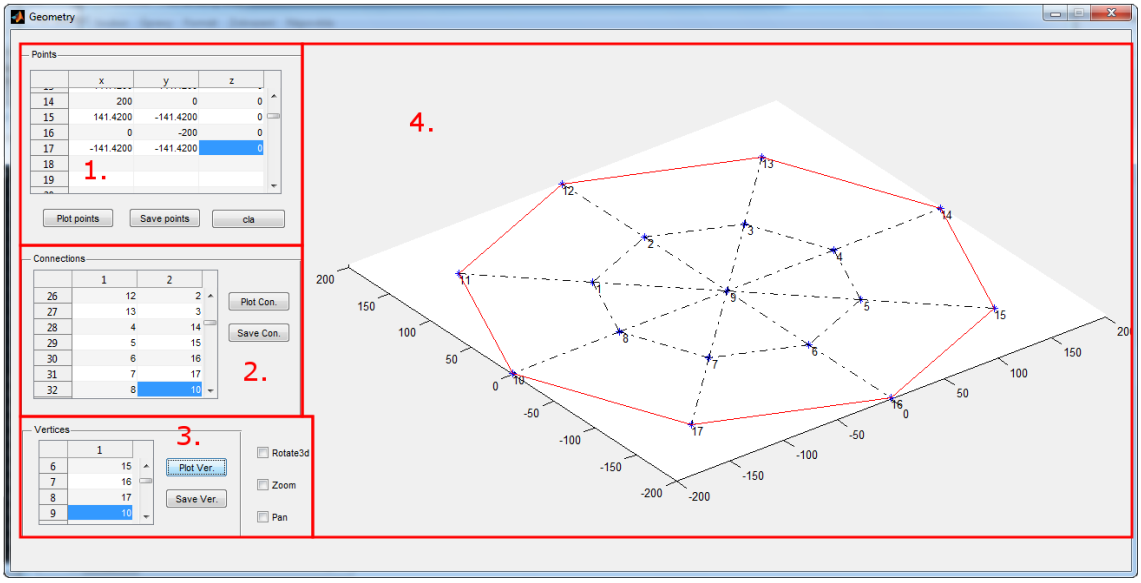


Fig. 5.3: Geometry module

"vertices" have to be entered. These vertices create the edges of the structure and according to them the shape can be approximate into colour maps. The last .txt-file is created based on these vertices.

**4 Visualization**

This is a space for a visualization of the geometry. The connections are black and vertices are red. Basic operations with the graph such as zoom, rotating and so on are possible.

## 5.4 FRF data review

It could seem pointless to have a re-viewer of FRFs when we can see them in the FRF estimation module, but it is very useful for an initial check of data before the modal parameter estimation process itself [1]. The screen of the interface is shown in the Fig. 5.4

**1 Basic information**

A basic information is given such as the measured frequency range and the number of the measured points.

**2 Plot setting**

In the plot setting section, the FRF which should be plotted is chosen. One or more FRFs can be selected. The kind of the visualization has to be chosen

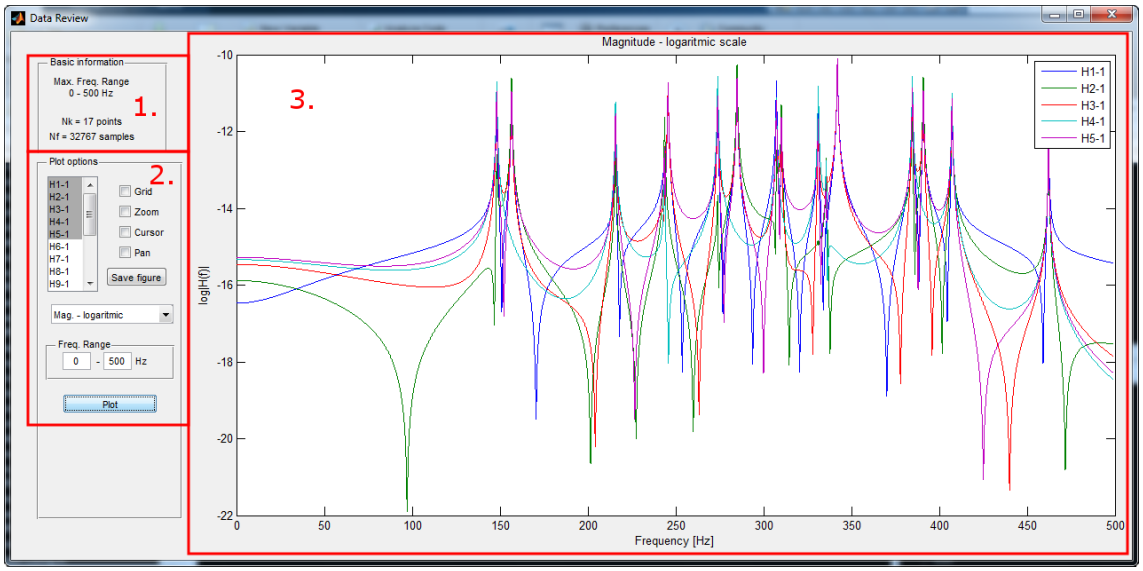


Fig. 5.4: Data review module

together with the displayed frequency range. The plot can be captured into .png using save button.

**3 Plot of FRF**
The selected FRFs are plotted into the axes. Two axes are used in the case of amplitude and phase graphs so these graphs can be compared.

## 5.5 Comparison of modal properties

Techniques of comparison which are described in the section 3.6 are implemented in post processing parts of the application. The interface of the modal properties comparison is shown in the Fig. 5.5.

**1 Loading of the modal properties**
Two sets of the modal properties are loaded through these buttons and their names can be specified in the edit boxes. The names are displayed in the graph titles and on the $x$-axis and $y$-axis.

**2 Frequency comparison**
The comparison of frequencies is made in this part. We can find the table of two sets with their errors. A graphical comparison of frequencies is in the bottom part of the section.

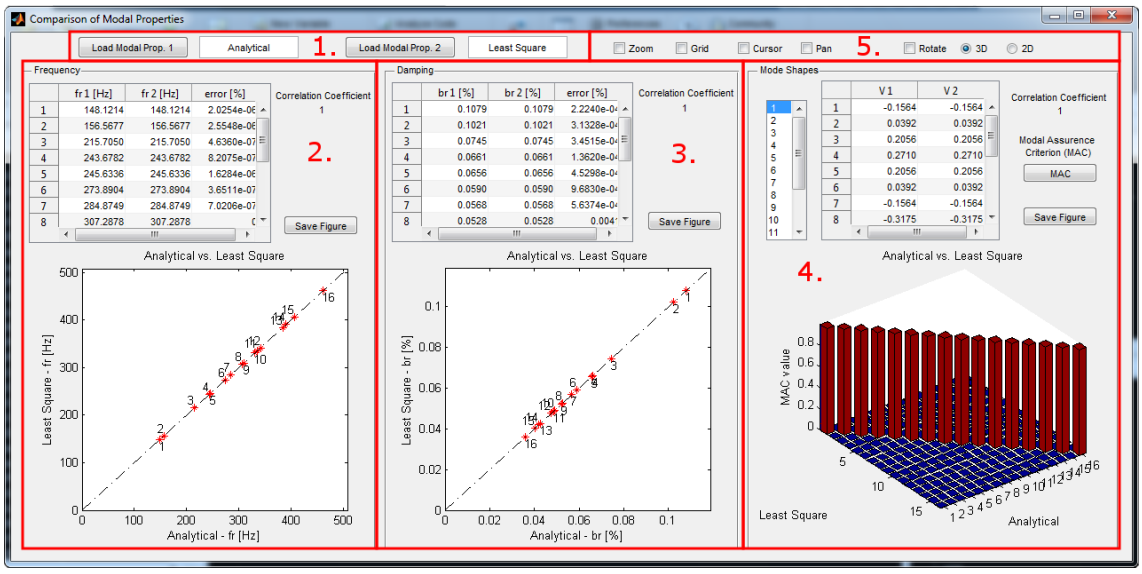


Fig. 5.5: Modal comparison module

**3 Damping comparison**

The structure of this part is made exactly in the same way as the comparison of the natural frequencies.

**4 Mode shapes comparison**

Beside the comparison similar to frequencies and damping the button for calculation of the modal assurance criterion can be found there.

**5 Graphs options**

Graphical options which are in this part such as zoom or rotate create supporting elements of this modal properties comparison module. All pictures and graphs from this comparison can be captured into .png format.

## 5.6 Comparison of frequency response function

This section is useful for the comparison of two sets of the frequency response function. The first one is measured and the second one reconstructed.

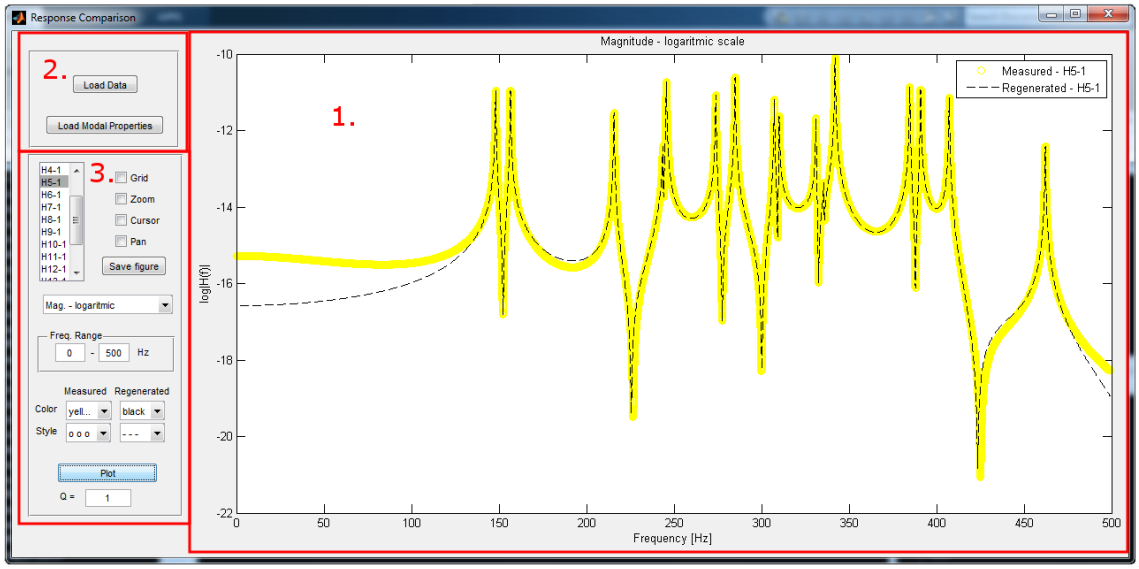


Fig. 5.6: FRF comparison module

**1 Graphical window**

The comparison is made in this axes and legend is added. The contents of this graph can be saved by the save figure button.

**2 Loading of data**

In the loading data section two sets of the data have to be entered. The first one is FRF in the similar form as for the main application. The second set is created by the modal properties from which the regenerated frequency response function is calculated and consequently plotted.

**3 Graphical options**

All plotted frequency response functions are controlled through these graphical options. The plotted FRF can be chosen together with its colour and plotted style. Also we can find different options of the visualization of the selected FRFs.

## 5.7 Proportional damping calculator

One of the main task of EMA is the determination of the damping factors and through that material properties. We added a simple tool for the calculation of the coefficients of the proportion damping model (Fig. 5.7) which can be used in FEM analysis. The calculation is based on [5].

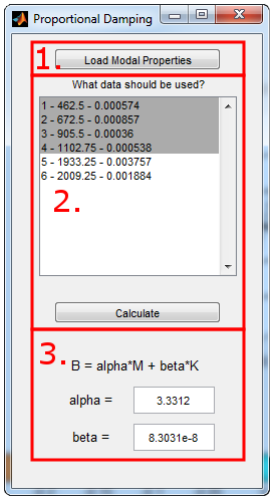


Fig. 5.7: Proportional damping module

**1 Loading**

A loading of .txt-file containing the modal properties is done by a loading button. The structure of the file is the same as in the all application. This file is also produced from the main application by saving the modal properties.

**2 Selection**

In this list the modes which should be used for the calculation can be selected. One, two or more modes can be chosen. The results can be different according to the selected modes.

**3 Results**

The results are shown in these two edit boxes. They should lay in the bound which are given in [5] or in the theoretical part of this thesis.

## 5.8 Animation of mode shapes

The mode shapes are animated directly in the application's main screen. There are two choices, we can animate in a "wire mode" (Fig. 5.8a) or use a "plane mode" for the coloured animation (Fig. 5.8b).


(a) "Wire" animation (b) "Plane" animation

Fig. 5.8: Mode shape animation module

## 5.9 Peak Picking method

Peak Picking method creates a part of the modal parameter estimation application. The method was implemented according to the description given in the section 4.1.1. The Peak Picking interface screen can be seen in the Fig. 5.9.

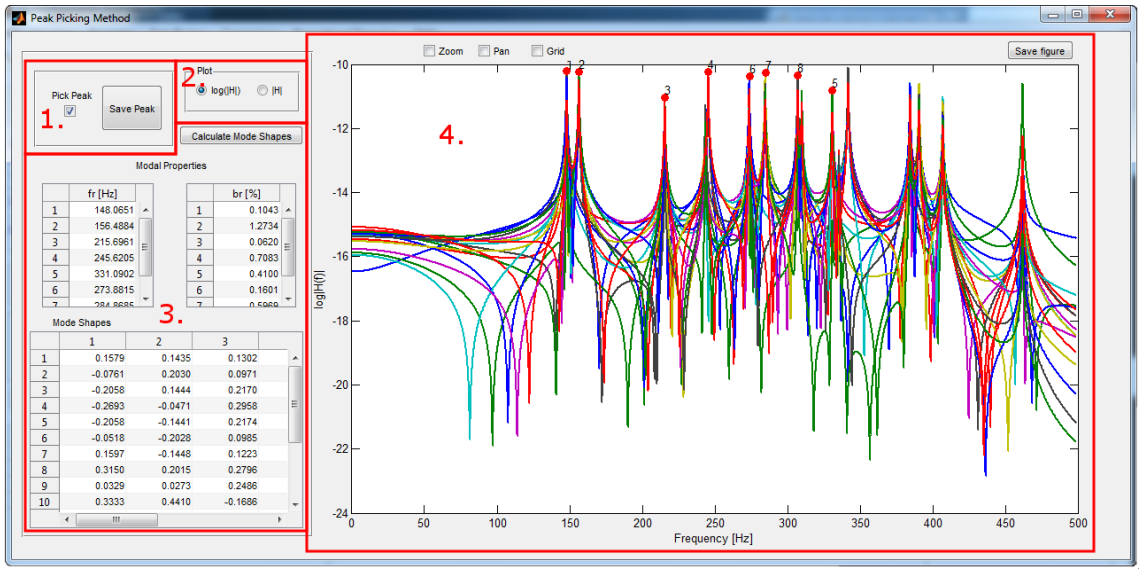


Fig. 5.9: Peak Picking application

**1 Peak Picking**
Peak is identified on the frequency response function and save using "Save Peak" button.

**2 FRF visualization**
This part was made just for a comfort of the user. The FRF can be visualised in the logarithmic or the linear scale on the $y$-axis. This can help in some situations for a successful identification of the peak.

**3 Modal properties**
The identified modal properties are saved into this section and in the end, the modal constants are transferred to the mode shapes using "calculate mode shape" button.

**4 Frequency response function**
Frequency response functions are plotted in this window and the peaks are identified in there. The picture of the peak picking procedure can be taken using save button.

The individual peaks of the FRF has to be identified and saved manually. The rest of procedure is performed automatically. The peaks could be found by means of finding local maximums of the frequency response function, however, it would be tough task in the presence of the noise in the FRF and time requirements for a correct identification of the peaks could be greater than for the peak picking method itself, therefore the manual pick of the peaks is chosen.

## 5.10 Circle Fit method

Circle fit method was implemented into the application according to section 4.1.2. The points which are used for the fitting of the circle have to be picked manually, the rest of the procedure is performed automatically. Beside the modal properties, the application allows studying of a dependent of the damping factor on the frequency so one can check a linear behaviour of the damping.

**1 Points selection**
The points are selected using this "check" button. Number and a "quality" of the selected points can effect the quality of the estimation process and the estimated parameters.

**2 Picture saving**
All graphs in the application can be captured in the .png format by an appropriate button.

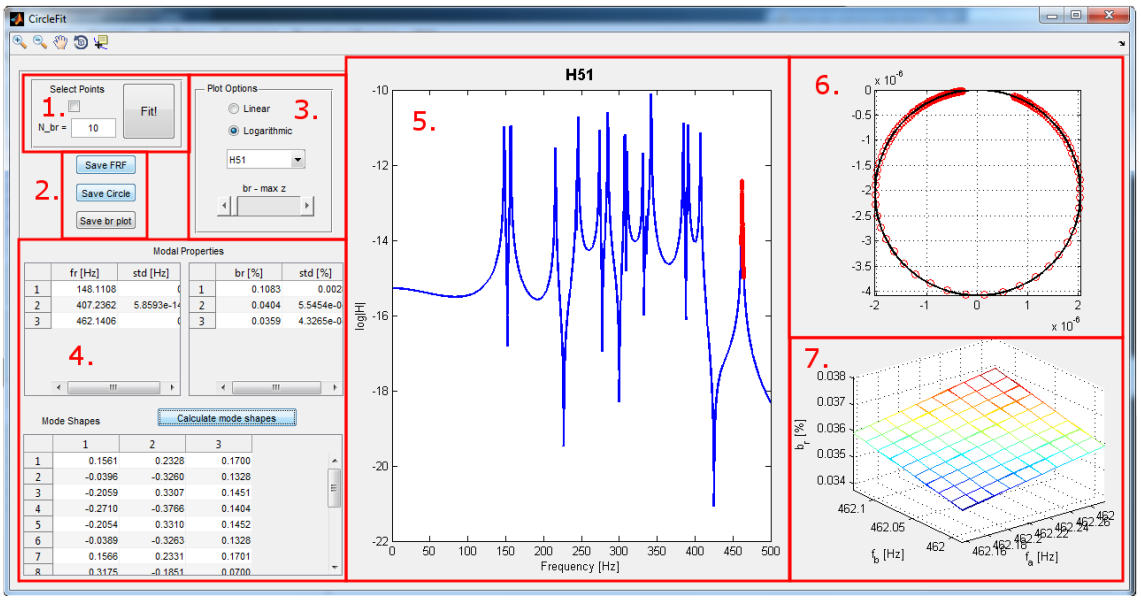


Fig. 5.10: Circle Fit application

**3 Estimation viewer**

We can check the quality of the estimation throughout all frequency response functions using these tools. We can examine the selected points, the damping or the quality of the fitted circle.

**4 Modal properties**

The identified modal properties are written into these tables. The mode shapes can be computed from the modal constant matrix using "calculate mode shape" button.

**5 Frequency response function**

We can see the frequency response functions in this window and also the points around individual peak are selected in this window .

**6 Fitted circle**

We can see the selected points with the fitted circle in this Nyquist plot. We can check the quality of the fit visually.

**7 Damping check**

The dependence of the damping on the frequencies can be seen in this graph. We can assume about a linearity in the damping and about a linearity of the the frequency response functions.

The individual peaks and the points have to be identified from the frequency response function manually. It would be possible to do it using an algorithm but manual picking is more sensible.

## 5.11 Least Square methods

Least Square methods are described in section 4.2.1. As it is oblivious the method can be programmed in many ways, with different robustness of the algorithm, with different fitting core etc. The way which is used in the application is so-called Least Square Complex Exponential method. This method is commonly used, very effective and it provides good results. The detailed discussion about the different ways of a programming of this method is given in [13]. This module includes a stabilization diagram discussed in the section 4.4.

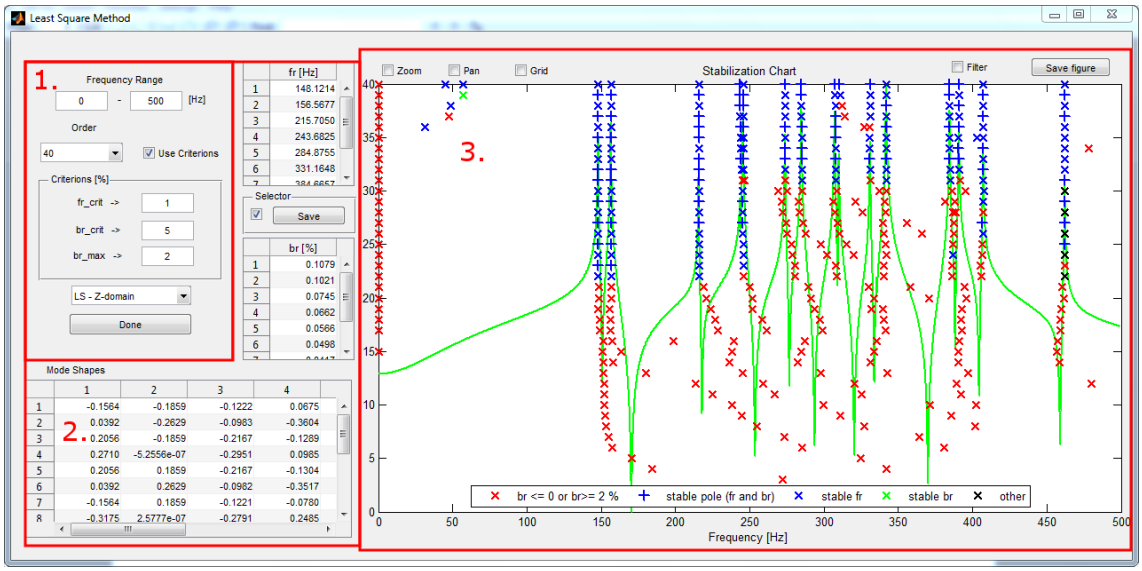


Fig. 5.11: Least Square application

**1 Analysis setting**

A system order and A frequency range of interest have to be chosen. Also, we can choose if we want to produce the stabilization diagram with criterion so it can indicate "convergence" of the the poles. Although all methods are based on the least square solution, the concrete method which is used for the identification of the modal properties can be chosen from pop-up menu.

**2 Modal properties**

The identified modal properties are written into these tables. For saving, the manual pick of the poles is used. It could be done automatically, but manual

pick is more sensible and better for the successful identification, in addition, it gives a possibility to look at the "history" of the estimation.

**3 Stabilization chart**

The stabilization chart produced by the least square method is plotted in this axes. A check box for a creation of a filtered version of the stabilization diagram is included.

## 5.12 Eigensystem Realization Algorithm

Eigensystem Realization Algorithm is programmed according to section 4.3.1 of this thesis. The stabilization diagram is added as well. The raster of the stabilization diagram is created by an auto-correlation spectra of an output signal. The ERA itself runs in the time-domain.

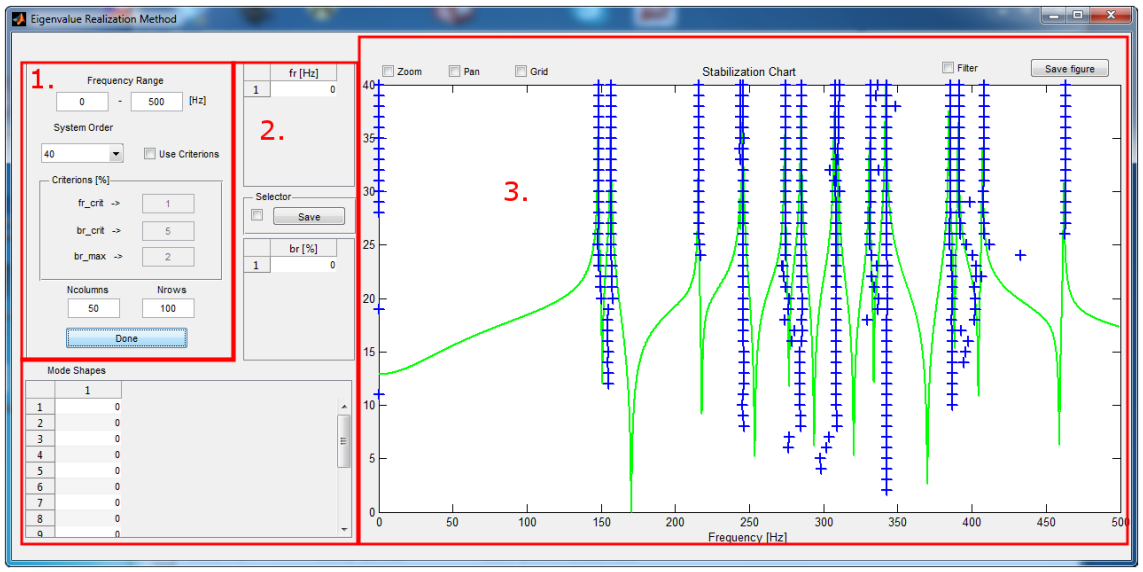


Fig. 5.12: Eigensystem Realization Algorithm application

**1 Analysis setting**

In this analysis setting section it is possible to set the frequency range of interest. Also, a system order has to be chosen. The system order is increasing steadily from 1 to the selected value and poles are drawn into the stabilization chart. Again, we can choose if we want to work with the criterion or not.

**2 Modal properties**

The identified modal properties are written into these table. Mode shapes are identified in the complex form but these mode shape vectors aren't proper

eigenvectors because of its identification wasn't successful due to SISO measurements. ERA is designed for MIMO systems. However, estimation of the natural frequencies and the damping factors is successfully performed.

**3 Stabilization diagram**

A similar stabilization diagram as in case of Least Square method is plotted and again, we can choose if we want to produce the filtered stabilization diagram.

For a successful identification we have to choose the poles from the stabilization diagram. Obtaining of the mode shapes wasn't successful implemented. Nevertheless, the natural frequencies and the damping factor are estimated successfully.

# 6 TEST CASES

When the application was being written we needed to test its functions therefore we made two simulated test cases. The first one is 6 DOF beam from the section 3.4.3. The another one is 15 DOF plane. The application was already used for the experimental modal analysis of the real structures. As an example, EMA of the turbine wheel is described.

## 6.1 Simulated beam

A calculation of the modal properties and FRFs is shown in section 3.4.3. We tried to estimate the modal properties from the calculated FRFs with every method.

### Geometry

To sum up, the 6 DOF beam is fixed on one side and free on the another one. It contents of 6 participles which can move in $z$-direction only. The geometry is shown in Fig. 3.4 and here (Fig. 6.1) as it can be seen in the application.

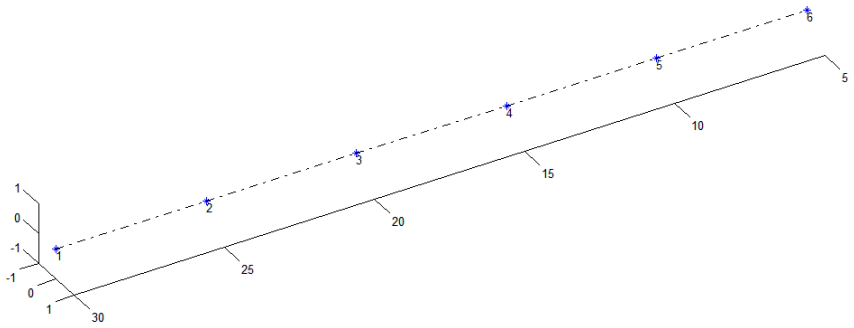


Fig. 6.1: Beam in geometry module

### Response

FRFs are displayed in the Fig. 3.6 and how they are seen in the application (in the FRF review module) is shown in Fig. 6.2.

From these plotted FRFs can be observed that there are not any close coupled modes of the vibration. All peaks can be clearly identified and we can assume that modes don't effect each other. It can be judge based on this assumption that all MPE methods provide suitable results.

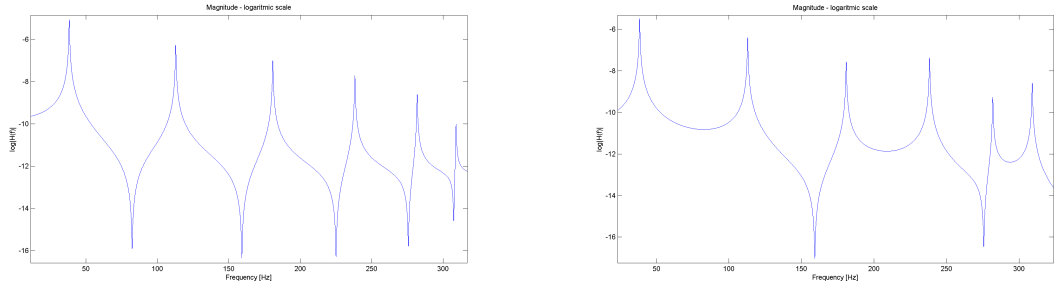


(a) FRF 11 - logarithmic scale

(b) FRF 41 - logarithmic scale

Fig. 6.2: Beam FRFs

### Peak Picking estimation

The first method we performed was PP. Using the manual pick of the peaks we were able to identified all 6 modes. The scheme of this picking is displayed in the Fig. 6.3.

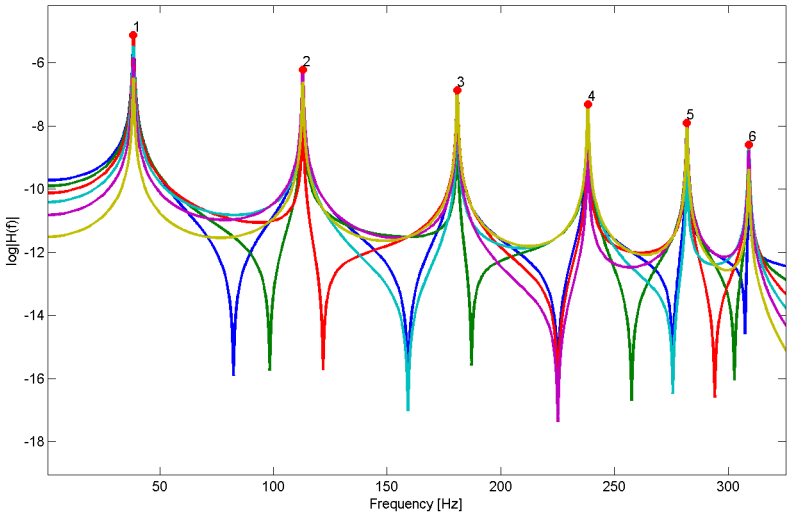


Fig. 6.3: Peak Picking of beam

### Circle Fit method estimation

Since we calculated FRFs with a great number of the points we had a lot of points to selected for the fitting of a circle onto them. Again, it was possible to identified all 6 modes of the vibration. The scheme of the chosen points, the fitter circle and the damping dependence on the frequency are displayed in the Fig. 6.4.

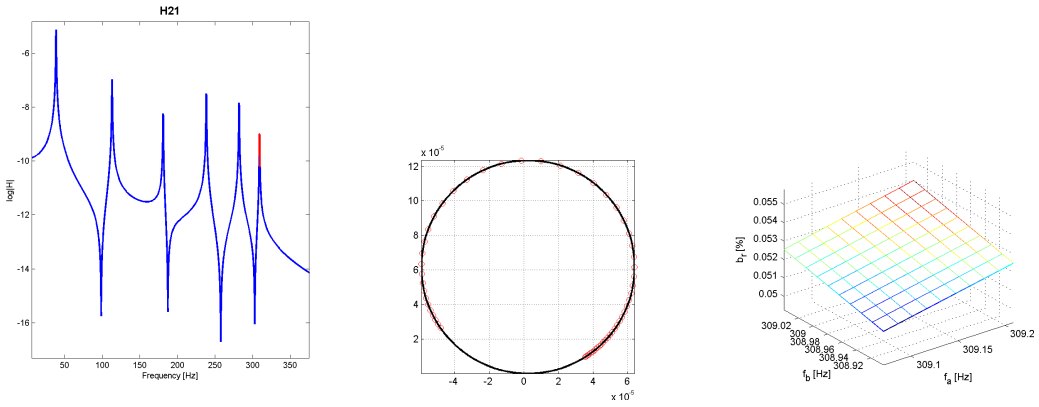


(a) Points selection (b) Fitted circle (c) Damping

Fig. 6.4: Circle Fit of beam

### Least Square method estimation

Least Square estimation was perform as well. The stabilization diagram can be seen in the Fig. 6.5.

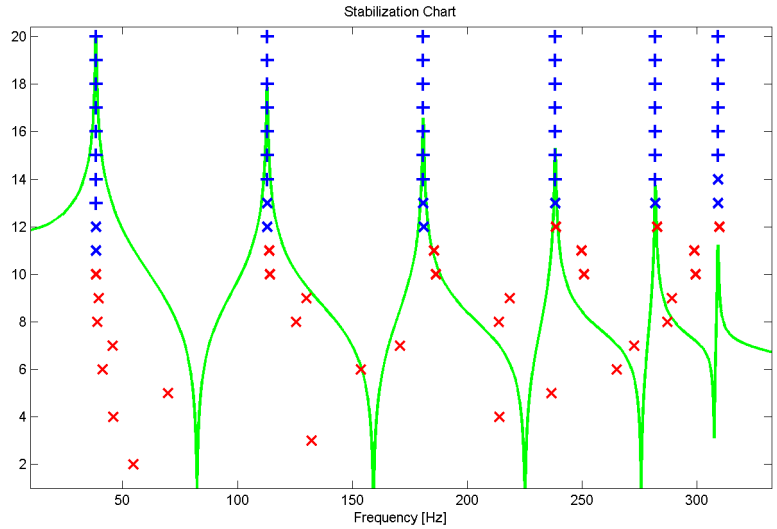


Fig. 6.5: Least Square stabilization diagram of beam

We can observed that there is not problem with the identification on the modes. All modes were identified on the system order number 12, which is exactly as it should be.

### Eigensystem Realization Algorithm

ERA was successful in the identification of the all modes as well. The stabilization diagram is seen in the Fig. 6.6.

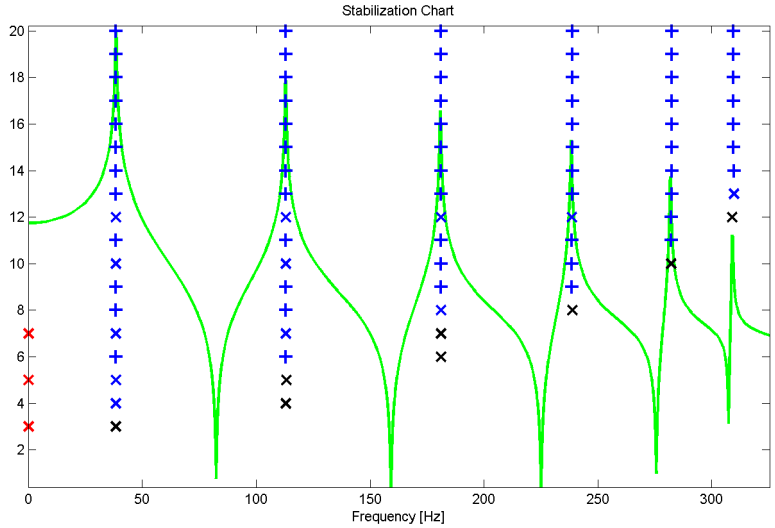


Fig. 6.6: ERA stabilization diagram of beam

A convergence of the modes is faster than in the case of Least Square method. But in general, it can be more difficult to set the ERA properly.

### Results of estimations

The natural frequencies and the damping factors are summarized in the table B.1 in the appendix.

From the table, it can be seen that all frequencies and almost all damping factors were estimated successfully. The maximum error in the damping factor is almost 20% in the case of the Peak Picking method. The comparison of damping factors using graphical way is shown in the Fig. B.1. Moreover, since the main goal of the experimental modal analysis is to determinate the proportional damping model's coefficients these coefficients have been computed and their comparison is given in the table 6.1. From this table we can see that although the differences in the damping factors aren't huge they can make differences in the proportional damping model coefficients but these differences aren't very significant.

The mode shapes were successfully estimated by all methods with exception of ERA. The comparison of the mode shapes is done in appendix where are plotted

| Method | $\alpha$ | $\beta$ |
|---|---|---|
| Analytical | 2.0000 | $1.0000*10^{-8}$ |
| Peak Picking | 1.9729 | $1.1627*10^{-7}$ |
| Circle Fit | 2.0018 | $1.1150*10^{-8}$ |
| Least Square | 1.9999 | $1.0280*10^{-8}$ |
| ERA | 2.0039 | $9.9882*10^{-9}$ |

Tab. 6.1: Beam - proportional damping coefficients

the first 3 mode shapes. Modal assurance criterion is calculated and it is plotted in the Fig. B.2. From both form of presentation we can see that mode shapes obtained by different methods correspond very well.

## 6.2 Simulated plane

The objective of this simulated test case was a creation of the case with close coupled modes where the estimation would be a bigger problem than in case of 6 DOF beam.

### Geometry

The plane have 15 DOF. It is modelled to be fixed on two side. The other two edges are free. The geometry from the "geometry module" is displayed in the Fig. 6.7.

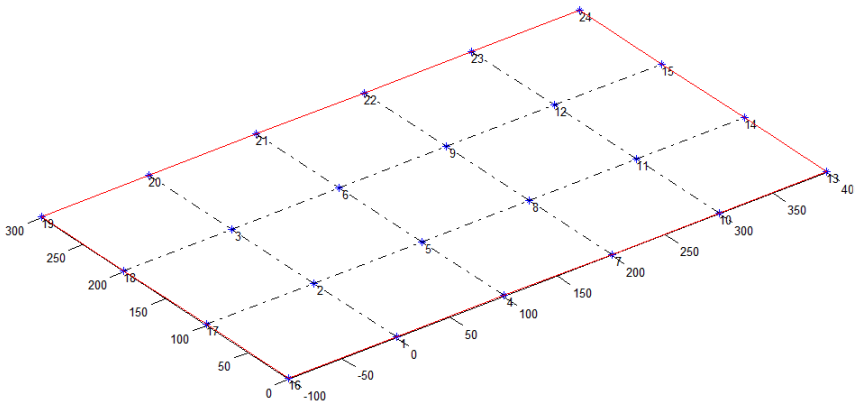


Fig. 6.7: Plane in geometry module

### Response

Response model and modal properties were computed in the exactly same way as for the 6 DOF beam. The Matlab code (appendices A.1 and A.2) for this is the same as for the 6 DOF beam, just with bigger matrices as an input. A few of FRF is shown in the Fig. 6.8.

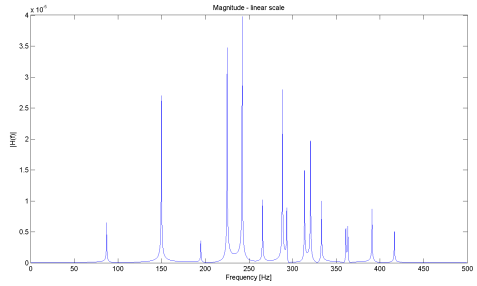


(a) FRF 21 - linear scale

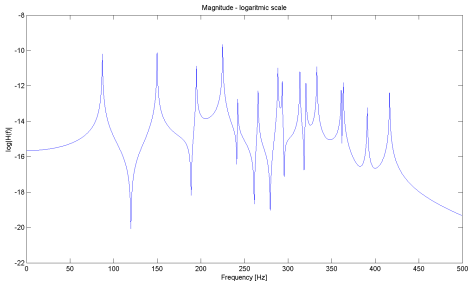


(b) FRF 41 - logarithmic scale

Fig. 6.8: Plane FRFs

From this figure we can see that an area of the close coupled modes of the vibration is presented in the frequency range and therefore we can assume that estimation shouldn't be so straightforward as in the case of the beam. Mainly, the SDOF methods shouldn't work with so good performance.

### Peak Picking estimation

Peak Picking was performed on the response of the plane and using the manual pick of peaks we were able to find all 15 peaks in the frequency range. The scheme of the peak picking is given in the Fig. 6.9.

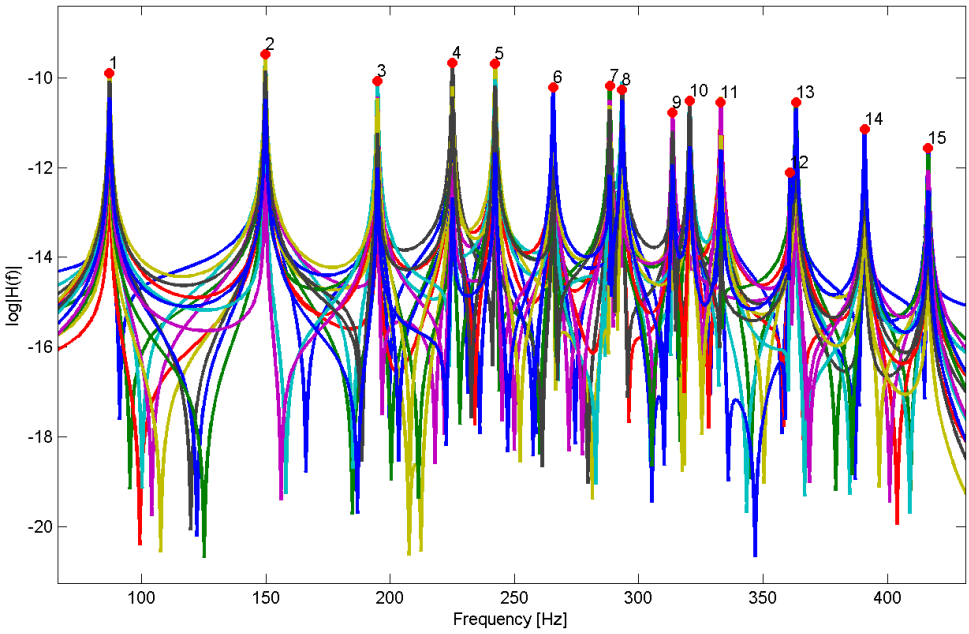


Fig. 6.9: Peak Picking of plane

The picking of the peaks in the close coupled modes area was complicated and one had to decide on what frequency the peak should have been defined.

### Circle Fit method estimation

Similar as in case of the beam we had a lots of points in the frequency spectra so we could pick a lot of them for fitting a circle. The scheme of the circle fit is given in the Fig. 6.10.

And again, the identification of the close coupled mode wasn't so easy and also the results aren't so accurate.

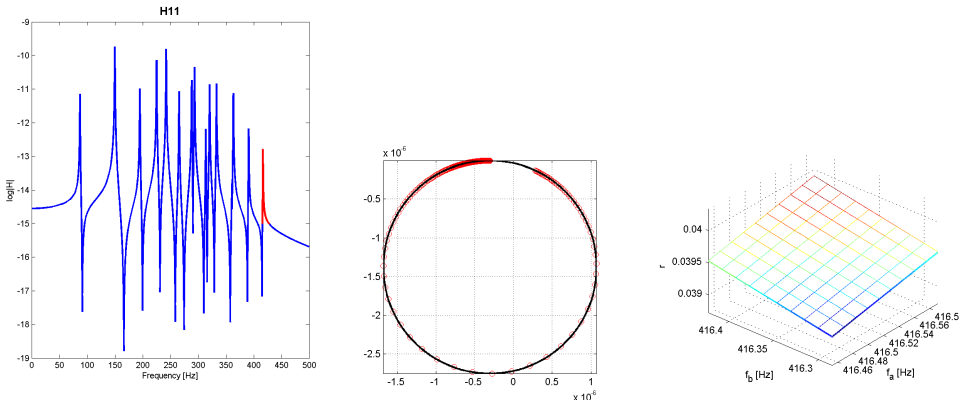


(a) Points selection (b) Fitted circle (c) Damping

Fig. 6.10: Circle Fit of plane

### Least Square method estimation

Least Square method was successful in the case of plane as well. A stabilization diagram is seen in the Fig. 6.11. From the stabilization diagram can be observed

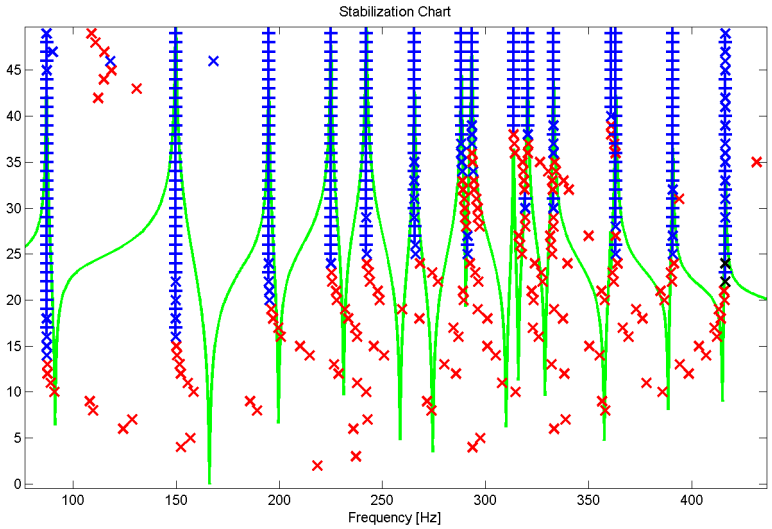


Fig. 6.11: Least Square stabilization diagram of plane

that identification of the close coupled modes takes more iterations and a system order had to be increased appropriately.

### Eigensystem Realization Algorithm

ERA was successful in an identification of all modes. A stabilization chart is plotted in the Fig. 6.12.

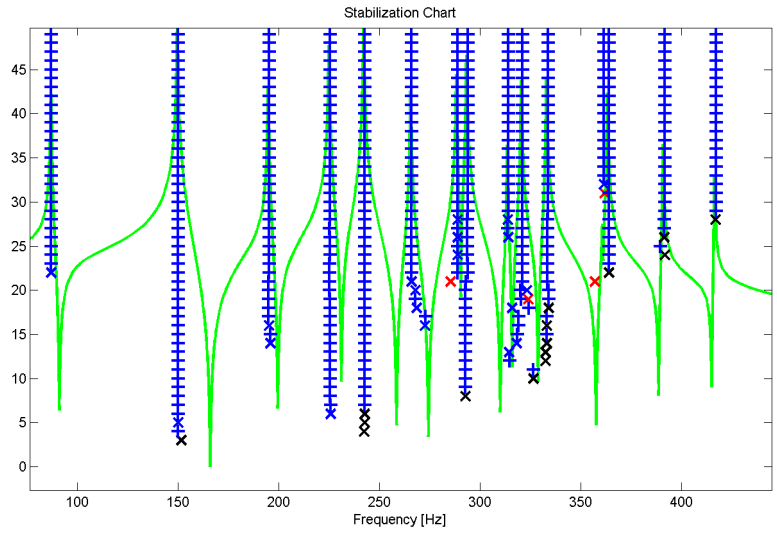


Fig. 6.12: ERA stabilization diagram of plane

The stabilization diagram appears more cleaner then in the case of Least Square method.

### Results of estimations

The natural frequencies and the damping factors are summarized in the table C.1 in the appendix.

From the table we can see that not all damping factors correspond very well therefore we made a comparison by the means of graphical method as it is described in the section 3.6. The graphs are displayed in the Fig. C.1. From this figure we can see that there is trend in the damping factor estimated by the Peak Picking and the Circle Fit method which proves the theory that we cannot rely on these methods in the case of the close coupled modes. Coefficients of the proportional viscous damping modal were calculated and they are written into table 6.2. The difference between Peak Picking and the rest of the methods is significant, but we have to keep in mind that for the calculation of these coefficients we used all damping factors which we estimated. The results would be better if we don't include the damping factors from the coupled modes.

| Method | $\alpha$ | $\beta$ |
|---|---|---|
| Analytical | 2.0000 | $1.0000*10^{-8}$ |
| Peak Picking | 1.0888 | $1.2349*10^{-6}$ |
| Circle Fit | 1.9870 | $2.6060*10^{-8}$ |
| Least Square | 2.0003 | $9.8404*10^{-9}$ |
| ERA | 2.0039 | $9.9799*10^{-9}$ |

Tab. 6.2: Plane - proportional damping coefficients

Mode shapes were estimated as well, but not all so successfully, especially in case of the coupled modes. Their comparison is done by means of modal assurance criterion displayed in the Fig. C.2. From the modal assurance criterion it can be seen that some modes estimated by Peak Picking method aren't estimated so properly as in the case of the rest methods. The selected mode shapes are also plotted in the appendix C.

## 6.3 Turbine wheel

Beam and Plane were simulated cases in which we knew the system properties exactly. But the modal parameter estimation methods are primary used for the experimental modal analysis where the response model is measured. Therefore we performed the experiment on the wheel from turbine and compared the results with those obtained by finite element method. This experiment was done as a part of Marek Pekar's diploma thesis [25]. More details about an experimental setting and a measurement itself can be found in this thesis and references therein.

### Geometry

Geometry of the wheel is shown in the Fig. 6.13. The geometry was made based on the 3D scan of the wheel.

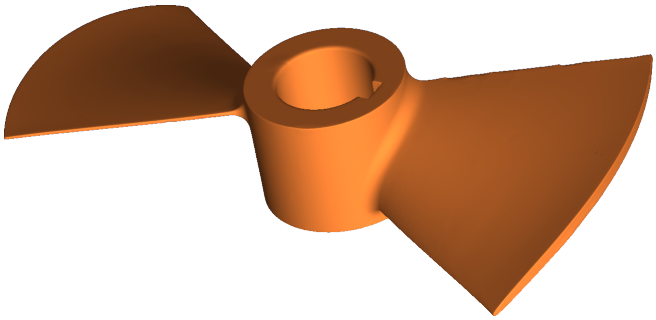

Fig. 6.13: Turbine wheel in Ansys

In the figure 6.14 we can see how we covered the wheel with experimental points in which we performed the measurement of the response.

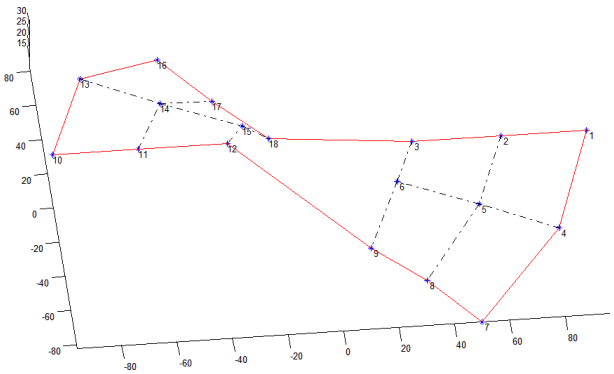

Fig. 6.14: Turbine wheel in geometry module

The density of the points on the wheel can, of course, effect the results of the analysis, but since we were looking for lower modes the density is just satisfied for us.

### Response

The response was measured by means of the impact hammer testing and the frequency response functions were calculated in the FRF estimation module of the application. The example of FRF is displayed in the Fig. 6.15

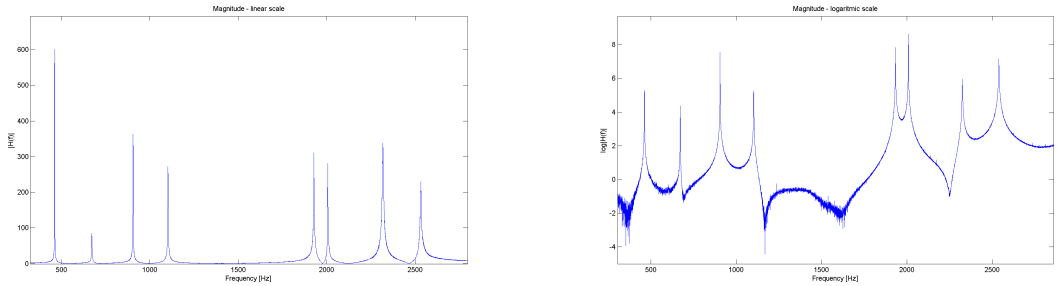


(a) FRF 11 - linear scale

(b) FRF 11 - logarithmic scale

Fig. 6.15: Turbine wheel FRFs

Even from this figure it is seen that the frequency response function aren't so good as in case of the calculated response model. They are effected by the noise and the measurement inaccuracies and therefore we cannot expect that the process of estimation will be so smooth as in the case of the simulated examples.

### Peak Picking estimation

Firstly, peak picking was used and we were able to identified 8 modes in the frequency range up to 3000 Hz. The picture captured from the peak picking application is shown in the Fig. 6.16.

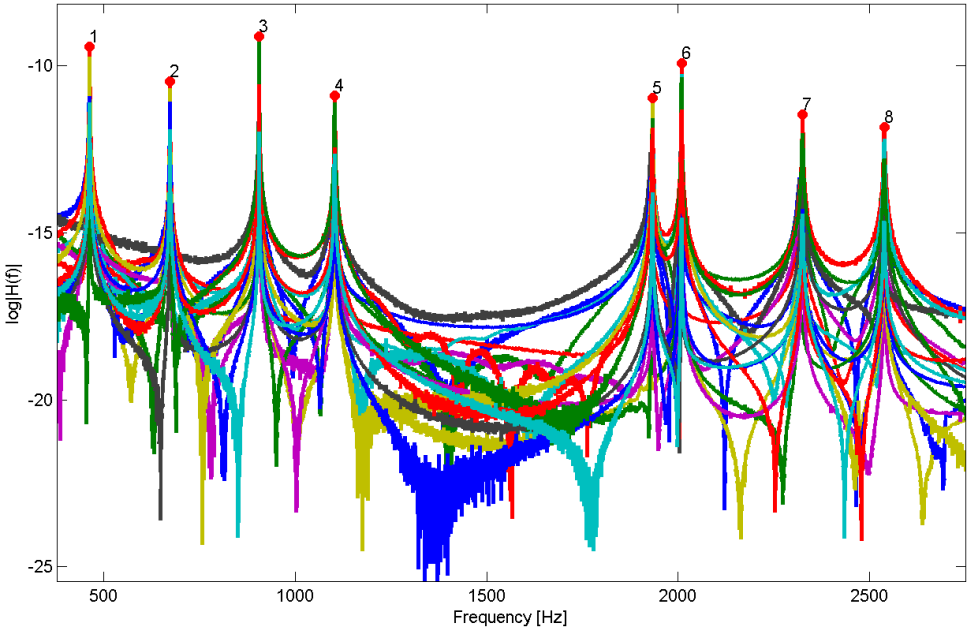


Fig. 6.16: Peak Picking of turbine wheel

The accuracy of the natural frequencies and the damping factors is effected by the resolution of the FRF so we can only estimate them with the given accuracy and we cannot expect them to be "100% accurate".

### Circle Fit method estimation

In the case of the Circle Fit method we can have some difficulty to select appropriate points for fitting a circle because of the resolution of the frequency spectra. Also due to the resolution the estimation of the damping factors cannot be done along so much points, but just a few points have to be used. The scheme of the Circle Fit method can be seen in the Fig. 6.17.

The circle fit method results are very effected by the selection of the points for fitting.

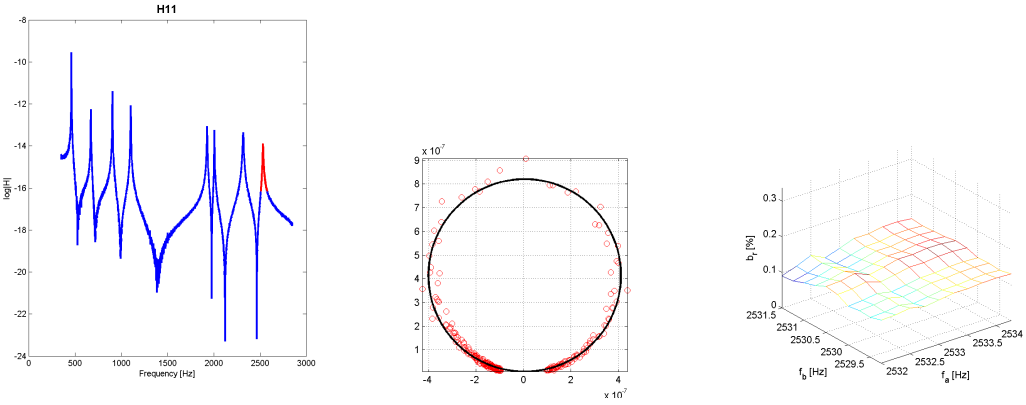


(a) Points selection (b) Fitted circle (c) Damping

Fig. 6.17: Circle Fit of turbine wheel

### Least Square method estimation

Least Square method identification was performed on the wheel as well and again, the stabilization diagrams can be seen in the Fig. 6.18.

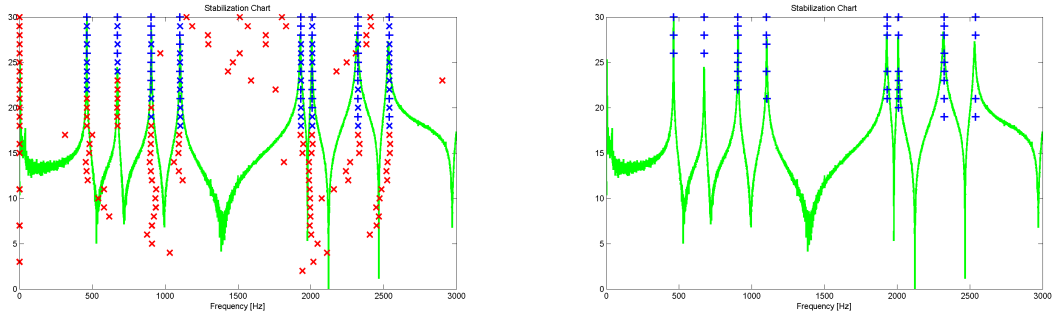


(a) with criteria (b) filtered

Fig. 6.18: Least Square stabilization diagram of turbine wheel

It can be easy observed that the stabilization diagram of Least Square method for the wheel is much more complicated than in the case of simulated structures.

### Eigensystem Realization Algorithm

Eigensystem Realization Algorithm was able to identified all mode as well. The stabilization diagrams can be seen in the Fig. 6.19.

ERA produces much cleaner algorithm than Least Square method. On the other hand, the setting of the method itself is more complicated ([18] or [26]) and we needed more runs of the algorithm to set it properly.

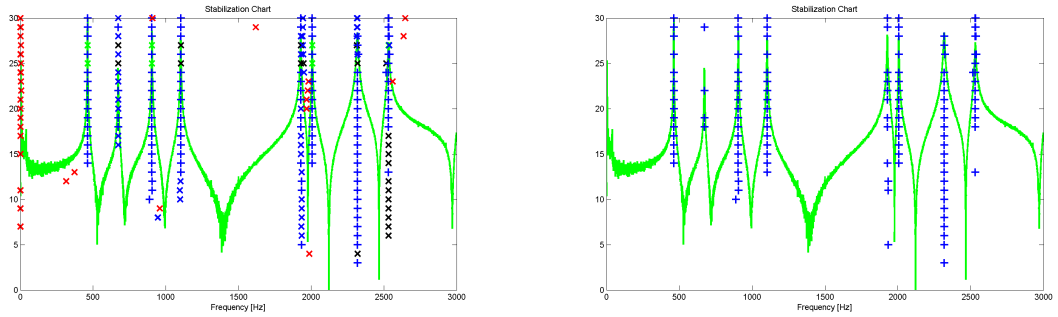


(a) with criteria (b) filtered

Fig. 6.19: ERA stabilization diagram of turbine wheel

### Results of estimations

Results of the estimations and from FEM are summarized in the table D.1 in the appendix.

From the table we can see that even frequencies and also damping factors are varied quite a lot. The graphical comparison is made and shown in the Fig. D.1. All natural frequencies lie on the one side on the straight line so it indicates that error are systematic. In this case the material properties used for FEM solution should be probably adjust.

A comparison of the damping factors by graphical way isn't done because we don't know a predicted set of the damping factor. Nevertheless, the coefficients of the proportional damping model were computed and they are written in the table 6.3. We can see that coefficients from the different set of the estimated modal properties

| Method | $\alpha$ | $\beta$ |
|---|---|---|
| Peak Picking | 3.3182 | $8.3031*10^{-8}$ |
| Circle Fit | 3.7886 | $7.5241*10^{-8}$ |
| Least Square | 1.0236 | $3.6369*10^{-8}$ |
| ERA | 2.9974 | $1.5417*10^{-7}$ |

Tab. 6.3: Turbine wheel - proportional damping coefficients

are different. On the other hand, coefficients from all set lie in the common bound so we cannot say which set is wrong.

Mode shapes were estimated by Peak Picking, Least Square method and Circle Fit method. The mode shapes are plotted in the appendix and the MAC is given in the Fig. D.2. Although the figures of the mode shapes look quite the same the MAC indicates otherwise. In the case of Least Square method the MAC is slightly worse

than in the case of SDOF methods. This, however, isn't error of the estimation process, but the error which rose from the quality of the measured data.

# 7 CONCLUSION

## 7.1 Conclusion

The application for the experimental modal analysis is the output and the main result of this diploma thesis. The modal properties (natural frequencies, damping factors, mode shapes) can be estimated by four methods - Peak Picking, Circle Fit method, Least Square methods and Eigensystem Realization Algorithm. Beside the modal parameter estimation process itself, several more techniques such as FRF estimation, comparison of the response models, modal properties etc. are implemented in the application. The application was already used for the experimental modal analysis on simulated test cases and also on real structures. Three cases are described in the thesis and the comparison of the methods is shown on them.

In the second chapter of this thesis, the three aims were declared.

1. Present a background of the theoretical and the experimental modal analysis. This is done in the third chapter. First of all, the overview of the modal testing is given then the theory of single-degree-of-freedom and multi-degree-of-freedom system is presented. In the next part the theory connected to frequency response function is shown and finally, the possible methods of comparison of the modal parameters or frequency response function are summarized.

2. Describe the chosen modal parameter estimation methods.
   This is done in the fourth chapter. The modal parameter estimation methods are divided and four of them are described in the details - Peak Picking method, Circle Fit method, Least Square method and Eigensystem Realization Algorithm. In the last part of the chapter the stabilization diagrams which are commonly used for the better identification of the system order are presented.

3. Implement the chosen MPE methods into an application. The input of the application will be created by FRFs and the output will be natural frequencies, damping factors and mode shapes.
   This particular goal was addressed too by the creation of the application which is capable to estimate the modal properties by the four described methods and even more is possible such as comparisons, frequency response function estimation and others. The application, with a small help, is enclosed to this diploma thesis. The brief description of the application is also given in the fifth chapter.

From the author's point of view, all the objectives have been successfully achieved.

## 7.2 Future work

This diploma thesis is focused on the experimental modal analysis, but there can be found more general experiments and measurement activities in the structural dynamics. So possibilities how to expand the application are many, to name a few:

- Improving interface of the application
  This is not the matter of the dynamics or modal testing but still, user-friendly environment and good image of the application can be very useful. There are a lot of details which could be done better or more effective in the application from the programmer's point of view.

- Operation modal analysis
  The application could be expressed into more complex application which could handle the operation modal analysis. This possibility already exists in the application, but it is very limited by the quality and the form of the input signal.

- More modal parameter estimation techniques
  There are plenty of the methods which weren't mentioned in the thesis but which can be effective for modal parameter estimation. The implementation of the new method would be easy because the application is written in the way that we can simply "add" new interface for the new method and this will not effect the rest of the application.

- Non-linear measurements
  The experimental modal analysis assumes that all elements of the measured structures are linear or at least, linear for small amplitudes of the displacement. However, very few real structures are truly linear and moreover non-linearity can have a lot of different forms. Next logical step would be to implement some methods for non-linear identification, but as a matter of fact this is not a easy task. Although there are some methods for specific non-linear system identification they are not generally effective. An experimental identification of the non-linear system is one of the main research interest in the structure dynamics in the recent years [27].

# BIBLIOGRAPHY


[1] D. J. Ewins. *Modal Testing: Theory and Practice*. Research Studies Press LTD., England, 1986.

[2] S. Miláček. *Modální analýza mechanických kmitů*. České Vysoké Učení Technické v Praze, 1992.

[3] P. Avitabile. *Mechanical Vibrations - Overview of Experimental Modal Analysis*, 2001. University of Massachusstts Lowel, Mechanical Engineering Department.

[4] C. Kratochvíl and J. Slavík. *Mechanika těles - Dynamika*. Akademické nakladatelství CERM, Brno, July 2007.

[5] E. Malenovský. *Studijní opory z předmětu Počítačové metody mechaniky v dynamice*, February 2007. Brno University of Technology, Institude of Solid Mechanics, Mechatronics and Biomechanics.

[6] J. Woodhouse. Linear damping models for structural vibration. *Journal of Sound and Vibration*, 215:547–569, 1998.

[7] A. Srikantha Phani and J. Woodhouse. Viscous damping identification in linear vibration. *Journal of Sound and Vibration*, 303:475–500, 2007.

[8] S. Adhikari. Damping modelling using generalized proportional damping. *Journal of Sound and Vibration*, 293:156–170, 2006.

[9] E. Parloo. *Application of frequency-domain system identification techniques in the field of operational modal analysis*. PhD thesis, Vrije Universiteit Brussel, May 2003.

[10] P. Verboven. *Frequency-domain system identification for modal analysis*. PhD thesis, Vrije universiteit Brussel, May 2002.

[11] P. Avitabile. Experimental modal analysis - a simple non-mathematical overview. *Sound and Vibration magazine*, 35:20–31, 2001.

[12] A. Bilošová. *Experimentální modální analýza*. Technická universita Ostrava, Ostrava, 2011.

[13] B. Cauberghe. *Applied frequency-domain system identification in the field of experimental and operational modal analysis*. PhD thesis, Vrije universiteit Brussel, May 2004.

[14] V. Ondra and P. Lošák. Comparison of modal parameter estimation techniques for experimental modal analysis. In *20th International Conference Engineering Mechanics*, 2014.

[15] D. Umbach and K. N. Jones. A few methods for fitting circle to data. *Transactions on instrumentation and measurement*, XX:1–5, 2000.

[16] C. Rusu. Classical geometrical approcah to circle fitting - review and new developments. *Journal of Electronic Imaging*, 12:179–193, 2003.

[17] J.N. Juang and R.S. Pappa. An eigensystem realization algorithm for modal parameter identification and modal reduction. *Journal of Guidance, Control and Dynamics*, 8:620–627, 1985.

[18] J.M. Caicedo. Practical guidelines for the natural excitation technique (next) and the eigensystem realization algorithm (era) for modal identification using ambient vibration. *Experimental Techniques*, 35:52–52, 2012.

[19] Bi-Qiang Mu and Han-Fu Chen. Hankel matrices for system identification. *Journal of Mathematical Analysis and Applications*, 409:494–508, 2014.

[20] P. Orlowski. Selected problems of frequency analysis for time varying, discrete-time system using singular value decomposition and dicrete fourier transform. *Journal of Sound and Vibration*, 278:903–921, 2004.

[21] A. G. Akritas and G. I. Malaschonok. Applications of singular-value decomposition (svd). *Mathematics and Computers in Simulation*, 67:15–31, 2004.

[22] A. W. Phillips and R. J. Allemang. An overview of mimo-frf excitation/averaging/processing techniques. *Journal of Sound and Vibration*, 262:651–675, 2003.

[23] Zhu Mao and Michael Todd. Statistical modeling of frequency response function estimation for uncertainty quantification. *Mechanical Systems and Signal Processing*, 38:333–345, 2013.

[24] P. Verboven and P. Guillaume. A comparison of frequency-domain transfer function model estimator formulations for structural dynamics modelling. *Journal of Sound and Vibration*, 279:755–798, 2005.

[25] M. Pekar. *Modální analýza lopatek oběžného kola vírové turbíny*. Master's thesis, Brno University of Technology, Institude of Solid Mechanics, Mechatronics and Biomechanics, June 2014. Supervised by: Pert Lošák Ph.D.

[26] F.S.V. Bazán. Eigensystem realization algorithm (era): reformulation and system pole petrurbation analysis. *Journal of Sound and Vibration*, 274:433–444, 2004.

[27] G. Kerschen, K. Worden, A. F. Valakis, and Golinval J. C. Past, present and future of nonlinear system identification in structural dynamics. *Mechanical Systems and Signal Processing*, 20:505–592, 2006.

# LIST OF ABBREVIATIONS

| | |
|---|---|
| SISO | Single Input and Single Output system |
| MIMO | Multi Input and Multi Output system |
| SI | International System of Units |
| DOF | Degree of Freedom |
| SDOF | Single-Degree-of-Freedom |
| MDOF | Multi-Degree-of-Freedom |
| FEM | Finite Element Method |
| MAC | Modal Assurance Criterion |
| MSF | Modal Scale Factor |
| MSCC | Mode Shape Correlation Coefficient |
| FRF | Frequency Response Function |
| EMA | Experimental Modal Analysis |
| OMA | Operation Modal Analysis |
| IRF | Impulse Response Function |
| MPE | Modal Parameter Estimation |
| FEA | Finite Element Analysis |
| ERA | Eigenvalue Realization Algorithm |
| PP | Peak Picking method |
| LSCE | Least Square Complex Exponential |

# LIST OF SYMBOLS AND PHYSICAL CONSTANTS

| Symbol | Unit | Description |
|---|---|---|
| ${}_rA_{jk}$ | – | modal constant |
| $\boldsymbol{A}$ | – | state space matrix |
| $\mathbf{A}(\omega)$ | – | accelerance, inertance |
| $\boldsymbol{A}^{-1}(\omega)$ | – | apparent mass |
| $b$ | $N/ms$ | viscous damper constant |
| $\mathbf{B}$ | $N/ms$ | damping matrix |
| $\boldsymbol{B}$ | – | state space matrix |
| $b_r$ | $\%, -$ | damping factor of $r$-th mode |
| $\boldsymbol{C}$ | – | state space matrix |
| $d(\omega)$ | – | denominator of transfer function |
| $\boldsymbol{D}$ | – | state space matrix |
| e | – | Euler's constant |
| $e$ | – | index for experimental set of the modal properties |
| $E_k$ | $J$ | kinetic energy |
| $E_p$ | $J$ | potential energy |
| $f$ | $Hz$,$s^{-1}$ | frequency |
| $f_r$ | $Hz$ | natural frequency of $r$-th mode |
| $f(t)$ | $N$ | time-varying force |
| $H_k(\omega_f)$ | – | measured transfer function |
| $\hat{H}_k(\Omega_f, \Theta)$ | – | theoretical transfer function |
| $i$ | – | imaginary unit |
| $\boldsymbol{J}$ | – | Jacobian matrix |
| $k$ | $N/m$ | stiffness |
| $\mathbf{K}$ | $N/m$ | stiffness matrix |
| $\bar{\mathbf{K}}$ | – | "stiffness" matrix in state space |
| $n$ | – | number of degree of freedom |
| $N_f$ | – | number of measured frequencies |
| $N_k$ | – | number of measured FRF |
| $N_k(\omega)$ | – | numerator of transfer function |
| $m$ | $kg$ | mass |
| $p$ | – | index for predicted set of the modal properties |
| $\mathbf{M}$ | $kg$ | mass matrix |
| $\bar{\mathbf{M}}$ | – | "mass" matrix in state space |
| $\boldsymbol{R}_k$ | – | Toeplitz matrix (in Least Square method) |

| | | |
|---|---|---|
| $s$ | $-$ | complex variable |
| $\boldsymbol{S}_k$ | $-$ | Toeplitz matrix (in Least Square method) |
| $t$ | $s$ | time |
| $T$ | $s$ | period of vibration |
| $T_s$ | $s$ | sampling period |
| $\boldsymbol{T}_k$ | $-$ | Toeplitz matrix (in Least Square method) |
| $\mathbf{u}(k)$ | $-$ | vector of system's inputs in state space |
| $x(t)$ | $m$ | time-varying displacement |
| $\mathbf{x}$ | $m$ | time-independent vector of amplitudes |
| $\dot{x}(t)$ | $ms^{-1}$ | time-varying velocity |
| $\ddot{x}(t)$ | $ms^{-2}$ | time-varying acceleration |
| $\mathbf{x}(t)$ | $m$ | time-varying vector of displacement |
| $\dot{\mathbf{x}}(t)$ | $ms^{-1}$ | time-varying vector of velocity |
| $\ddot{\mathbf{x}}(t)$ | $ms^{-2}$ | time-varying vector of acceleration |
| $\mathbf{y}(k)$ | $-$ | vector of system's outputs in state space |
| $\mathbf{Y}(\omega)$ | $-$ | mobility |
| $\boldsymbol{Y}^{-1}(\omega)$ | $-$ | mechanical impedance |
| | | |
| $\alpha$ | $-$ | proportional damping model constant |
| $\alpha(\omega)$ | $-$ | receptance of SDOF system |
| $\boldsymbol{\alpha}(\omega)$ | $-$ | receptance, dynamic flexibility |
| $\boldsymbol{\alpha}^{-1}(\omega)$ | $-$ | dynamic stiffness |
| $\beta$ | $-$ | proportional damping model constant |
| $\boldsymbol{\phi}$ | $-$ | mass-normalized mode shape vector |
| $\boldsymbol{\Phi}$ | $-$ | modal matrix with mass-normalized modes |
| $\lambda_r$ | $-$ | $r$-th mode of the system $\lambda_r = -\lambda_r^{\mathrm{re}} + \mathrm{i}\lambda_r^{\mathrm{im}}$ |
| $\boldsymbol{\Lambda}$ | $-$ | spectral matrix |
| $\boldsymbol{\psi}$ | $-$ | unscaled mode shape vector |
| $\boldsymbol{\Psi}$ | $-$ | modal matrix with unscaled modes |
| $\omega$ | $rad/s$ | angular frequency $\omega = 2\pi f$ |
| $\omega_0$ | $rad/s$ | angular natural frequency of SDOF system |
| $\omega_a$ | $rad/s$ | frequencies before resonance (in Peak Picking method) |
| $\omega_b$ | $rad/s$ | frequencies after resonance (in Peak Picking method) |
| $\omega_r$ | $rad/s$ | angular natural frequency of $r$-th mode $\omega_r = 2\pi f_r$ |
| $\Delta\omega$ | $rad/s$ | half-band difference of frequencies (in Peak Picking method) |
| $\Omega_j(\omega)$ | $-$ | polynomial basic function (in Least Square method) |
| $\zeta_r$ | $\%, -$ | damping factor |

# LIST OF APPENDICES

# A MATLAB SCRIPTS

## A.1 Modal analysis for 6 DOF system

This script performs modal analysis for the structure from section 3.4.3.

```
clear all            % clear all variables from workspace
close all            % close all figures
clc                  % clear command window

%% structure parameters
n = 6;               % number of DOF
m = 1;               % mass [kg]
k = 1e6;             % stiffness [N/m]
alpha = 2;           % damping constant
beta = 1e-8;         % damping constant

%% assembling of system's matrices
M = m*eye(n);                                        % mass matrix
K = diag(2*ones(1,n)) - diag(ones(1,n-1),-1)...
    - diag(ones(1,n-1),1); K(n,n) = 1; K = k*K;      % stiffness matrix
B = alpha*M + beta*K;                                % damping matrix

%% matrices in the state space
Ms = [zeros(n) M; M B];
Ks = [-M zeros(n);zeros(n) K];

%% eigenvalue problem and its solution
[Phi,Lambda] = eig(-inv(Ms)*Ks); % calculation of spectral
     % and modal matrix, eigenvectors are scaled to
     % unity modal vector lenght

%% cutting out the conjugate pairs from spectral and modal matrix
%  this is needed due to state space
Lambda = Lambda([1:2:2*n],[1:2:2*n]);
lambda = diag(Lambda);            % complex frequency in vector
Phi = real(Phi([1:n],[1:2:2*n])); % mode shapes are real,
                                  % their imag. part = 0

%% sorting modal matrix into increasing order
[lambda,index] = sort(lambda);    % increasing sorting
Lambda = diag(lambda);            % sorted spectral matrix
Phi = Phi(:,index);               % sorted modal matrix

%% extraction of modal properties from the spectral matrix
fr = imag(lambda)/(2*pi);         % natural frequency [Hz]
br = -real(lambda)./abs(lambda);  % damping factor [-]
```

## A.2 Harmonic analysis for 6 DOF system

This script performs harmonic analysis for the structure from section 3.4.3. It establishes with previous script (modal analysis of the structure).

```
samples = 32768;           % total count of sample frequencies
omega = linspace(0,2*pi*500,samples); % frequency vector [rad/s]
j = 1;                     % driving point index

%% size definition
alpha_complet = zeros(n,n,samples); % complet FRF matrix
alpha_dir = zeros(n,samples);  % FRF obtained by direct inverse
alpha_mode = zeros(n,samples); % FRF based on mode superposition

%% direct inversion of the system matrix
tic               % start of time measure for direct inverse method
for f = 1:samples % inversion at each frequency
    alpha_complet(:,:,f) = inv(K + 1i*omega(f)*B - (omega(f)^2)*M);
end

for k = 1:n   % selection of the first row from FRF matrix
    alpha_dir(k,:) = alpha_complet(k,j,:);
end
toc           % end of time measure for direct inverse method

%% mode superposition method
tic        % start of time measure for mode superposition
omega_r = 2*pi*fr;   % vector of natural frequencies
for k = 1:n       % index of point
    for r = 1:n   % sum along natural frequencies
        alpha_mode(k,:) =   alpha_mode(k,:) + ...
        Phi(j,r)*Phi(k,r)./(omega_r(r)^2 - omega.^2 + ...
        1i*2*br(r)*omega_r(r)*omega);
    end
end
toc      % end of time measure for mode superposition
```

# B SIMULATED TEST CASE - BEAM

## B.1 Comparison of modal properties

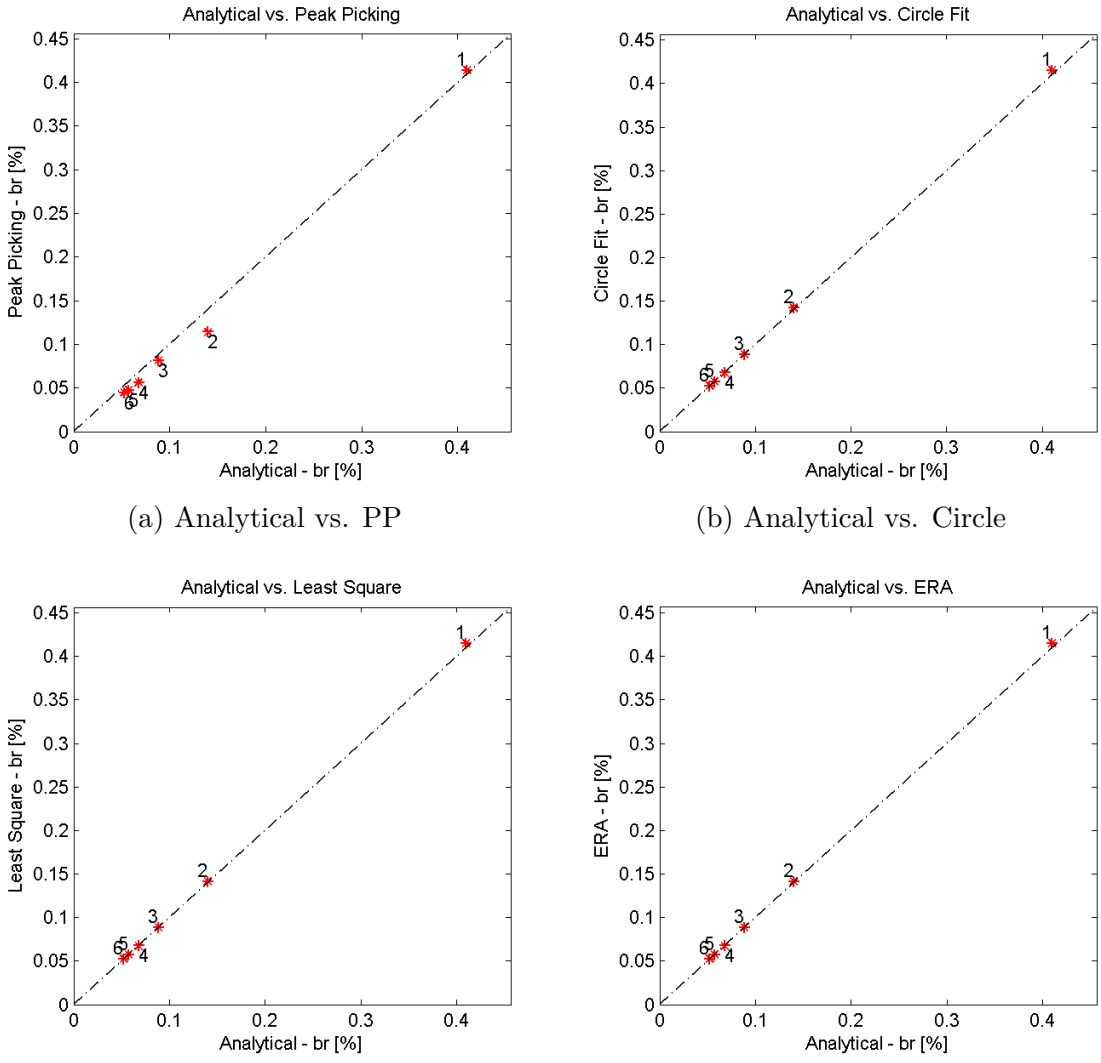


(a) Analytical vs. PP

(b) Analytical vs. Circle

(c) Analytical vs. LSCE

(d) Analytical vs. ERA

Fig. B.1: Graphical comparison of beam's damping factors

| | Analytical | | PP | | Circle fit | | LSCE | | ERA | |
|---|---|---|---|---|---|---|---|---|---|---|
| $r$ | $f_r$ [Hz] | $b_r$ [%] | $f_r$ (er. [%]) | $b_r$ (er. [%]) | $f_r$ (er. [%]) | $b_r$ (er. [%]) | $f_r$ (er. [%]) | $b_r$ (er. [%]) | $f_r$ (er. [%]) | $b_r$ (er. [%]) |
| 1 | 38.37 | 0.41 | 38.36 (0.02) | 0.40 (0.95) | 38.36 (0.02) | 0.41 (1.27) | 38.37 (0.01) | 0.41 (1.19) | 38.44 (0.19) | 0.41 (1.20) |
| 2 | 112.87 | 0.14 | 112.88 (0.01) | 0.13 (18.43) | 112.86 (0.01) | 0.14 (1.5) | 112.87 (0.01) | 0.14 (1) | 113.09 (0.19) | 0.14 (0.97) |
| 3 | 180.82 | 0.09 | 180.83 (0.01) | 0.08 (7.99) | 180.81 (0.01) | 0.09 (0.34) | 180.82 (0) | 0.09 (0.12) | 181.17 (0.19) | 0.09 (0.1) |
| 4 | 238.26 | 0.07 | 238.27 (0.01) | 0.06 (17.40) | 238.25 (0.01) | 0.07 (0.15) | 238.26 (0) | 0.07 (0.44) | 238.72 (0.19) | 0.07 (0.37) |
| 5 | 281.85 | 0.06 | 281.85 (0) | 0.05 (17.11) | 281.85 (0) | 0.06 (0.17) | 281.85 (0) | 0.06 (0.17) | 282.40 (0.19) | 0.06 (0.09) |
| 6 | 309.06 | 0.05 | 309.06 (0) | 0.04 (14.88) | 309.06 (0) | 0.05 (0.19) | 309.06 (0) | 0.05 (0.19) | 309.67 (0.19) | 0.05 (0.13) |

Tab. B.1: Beam - results

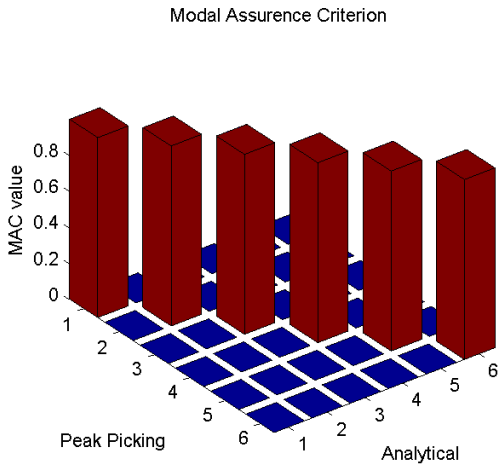


(a) Analytical vs. PP

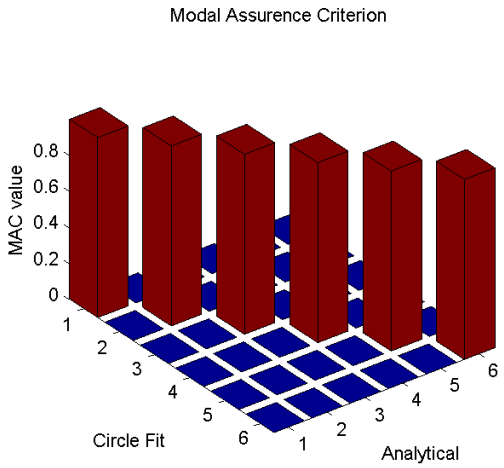


(b) Analytical vs. Circle

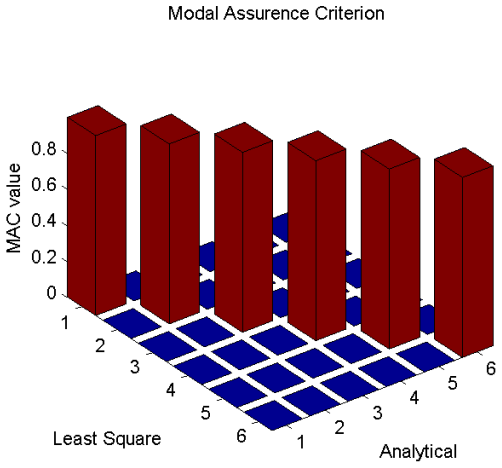


(c) Analytical vs. LSCE

Fig. B.2: MAC comparison - beam

## B.2 Mode shapes

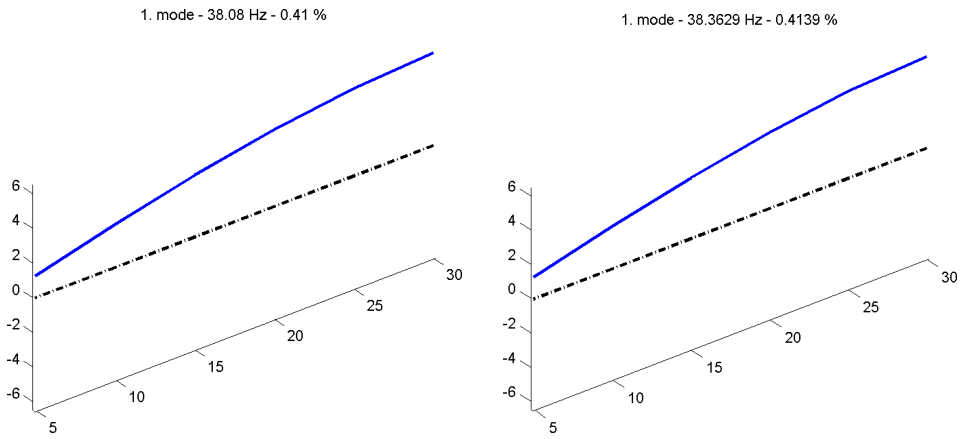


(a) Analytical (b) Pick-picking

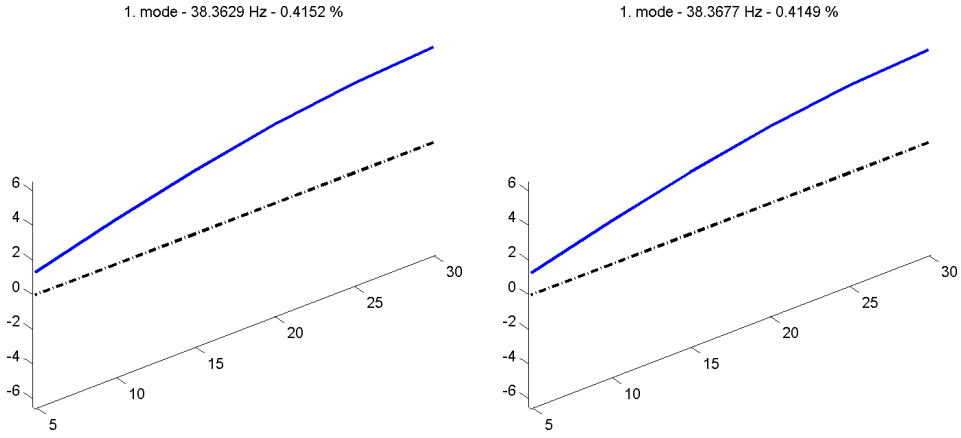


(c) Circle fit (d) Least square

Fig. B.3: Beam - first mode shape

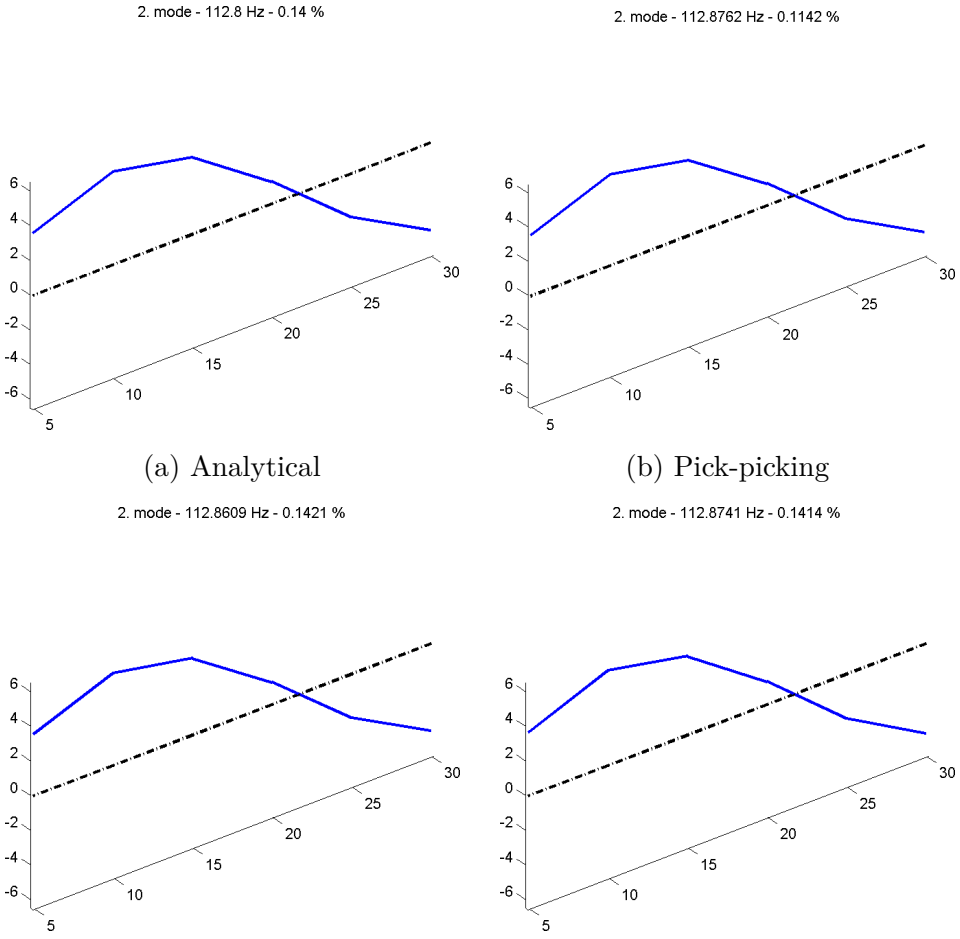


(a) Analytical

(b) Pick-picking

(c) Circle fit

(d) Least square

Fig. B.4: Beam - second mode shape

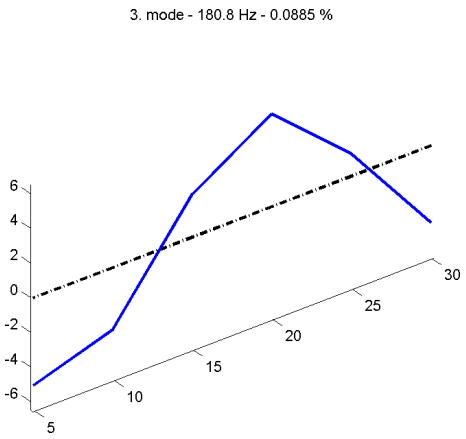


(a) Analytical

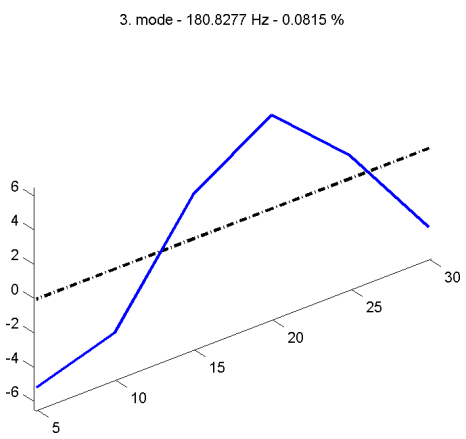


(b) Pick-picking

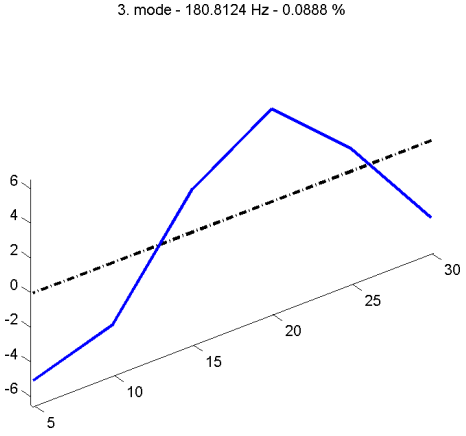


(c) Circle fit

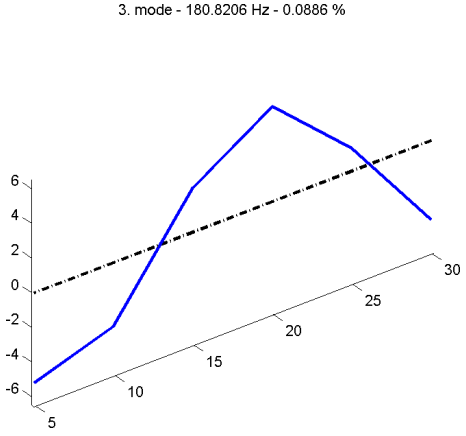


(d) Least square

Fig. B.5: Beam - third mode shape

# C SIMULATED TEST CASE - PLANE

## C.1 Comparison of modal properties

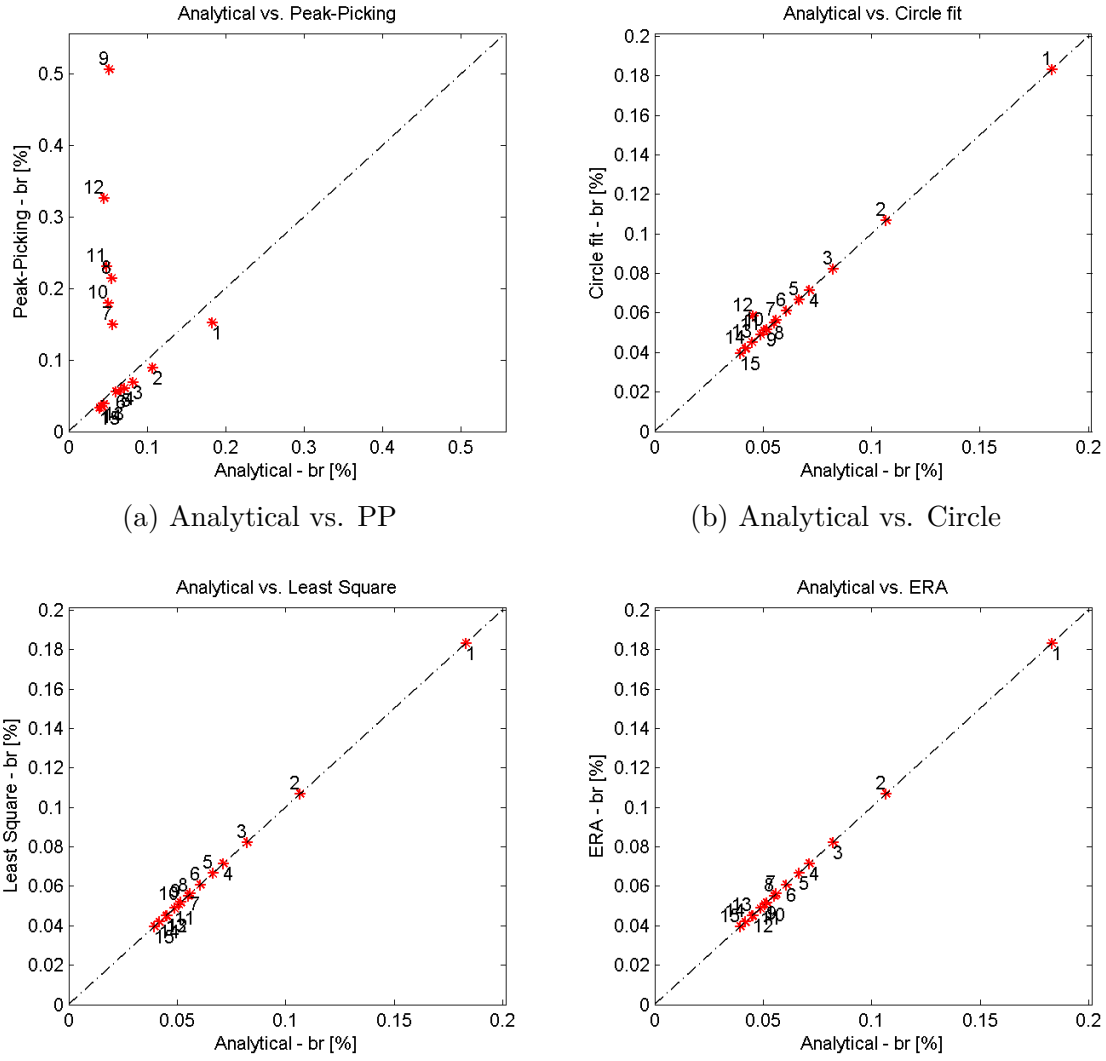


(a) Analytical vs. PP

(b) Analytical vs. Circle

(c) Analytical vs. LSCE

(d) Analytical vs. ERA

Fig. C.1: Graphical comparison of plane's damping factors

| | Analytical | | PP | | Circle fit | | LSCE | | ERA | |
|---|---|---|---|---|---|---|---|---|---|---|
| $r$ | $f_r$ [Hz] | $b_r$ [%] | $f_r$ (er. [%]) | $b_r$ (er. [%]) | $f_r$ (er. [%]) | $b_r$ (er. [%]) | $f_r$ (er. [%]) | $b_r$ (er. [%]) | $f_r$ (er. [%]) | $b_r$ (er. [%]) |
| 1 | 87.04 | 0.18 | 87.04 (0) | 0.15 (16.77) | 87.04 (0) | 0.18 (0.05) | 87.04 (0) | 0.18 (0.01) | 87.21 (0.19) | 0.18 (0) |
| 2 | 149.75 | 0.11 | 149.74 (0) | 0.09 (16.81) | 149.74 (0) | 0.10 (0.04) | 149.74 (0) | 0.11 (0.04) | 150.04 (0.19) | 0.11 (0) |
| 3 | 194.86 | 0.08 | 194.85 (0) | 0.07 (16.39) | 194.85 (0) | 0.08 (0.02) | 194.85 (0) | 0.08 (0.01) | 195.24 (0.19) | 0.08 (0) |
| 4 | 225.01 | 0.07 | 225.00 (0) | 0.06 (14.89) | 225.00 (0) | 0.07 (0.06) | 225.00 (0) | 0.07 (0.06) | 225.45 (0.19) | 0.07 (0) |
| 5 | 242.20 | 0.07 | 242.23 (0.01) | 0.06 (13.34) | 242.20 (0) | 0.06 (0.19) | 242.21 (0) | 0.06 (0.04) | 242.68 (0.19) | 0.06 (0) |
| 6 | 265.54 | 0.06 | 265.55 (0) | 0.06 (8.17) | 265.53 (0) | 0.06 (0.38) | 265.54 (0) | 0.06 (0.05) | 266.06 (0.19) | 0.06 (0) |
| 7 | 288.30 | 0.06 | 288.30 (0) | 0.15 (166.79) | 288.28 (0) | 0.05 (0.65) | 288.29 (0) | 0.06 (0.02) | 288.86 (0.19) | 0.06 (0) |
| 8 | 293.31 | 0.06 | 293.32 (0) | 0.21 (288.35) | 293.31 (0) | 0.05 (0.51) | 293.32 (0) | 0.05 (0.03) | 293.88 (0.19) | 0.06 (0) |
| 9 | 313.57 | 0.05 | 313.57 (0) | 0.51 (878.74) | 313.57 (0) | 0.05 (0.46) | 313.57 (0) | 0.05 (0.12) | 314.18 (0.19) | 0.05 (0) |
| 10 | 320.49 | 0.05 | 320.48 (0) | 0.18 (253.48) | 320.99 (0) | 0.05 (0.66) | 320.48 (0) | 0.05 (0.06) | 321.11 (0.19) | 0.05 (0) |
| 11 | 333.01 | 0.05 | 333.01 (0) | 0.23 (373.79) | 332.99 (0) | 0.05 (0.33) | 333.00 (0) | 0.05 (0.08) | 333.66 (0.19) | 0.05 (0) |
| 12 | 360.84 | 0.05 | 360.86 (0.01) | 0.33 (622.35) | 360.82 (0) | 0.06 (29.5) | 360.83 (0) | 0.04 (0.09) | 361.54 (0.19) | 0.05 (0) |
| 13 | 363.24 | 0.04 | 363.24 (0) | 0.04 (14.80) | 363.23 (0) | 0.05 (0.31) | 363.23 (0) | 0.04 (0.12) | 363.95 (0.19) | 0.04 (0) |
| 14 | 390.83 | 0.04 | 390.83 (0) | 0.04 (16.56) | 390.83 (0) | 0.04 (0.12) | 390.83 (0) | 0.04 (0.12) | 391.59 (0.19) | 0.04 (0) |
| 15 | 416.44 | 0.04 | 416.44 (0) | 0.03 (16.26) | 416.44 (0) | 0.04 (0.06) | 416.44 (0) | 0.04 (0.07) | 417.25 (0.19) | 0.04 (0) |

Tab. C.1: Plane - results

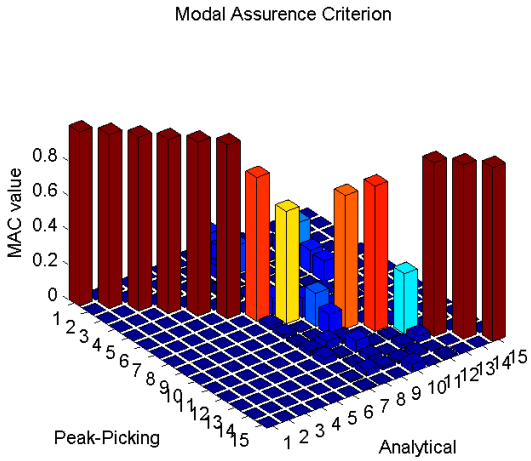


(a) Analytical vs. PP

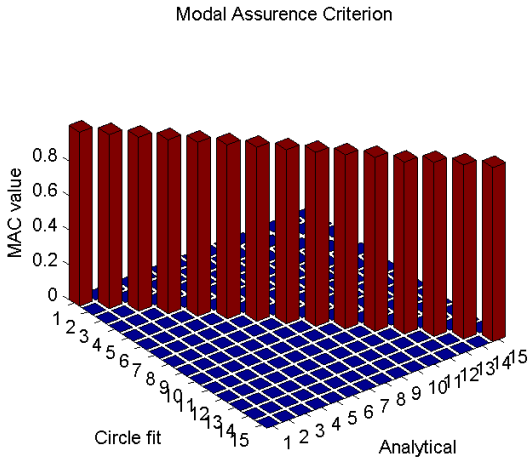


(b) Analytical vs. Circle

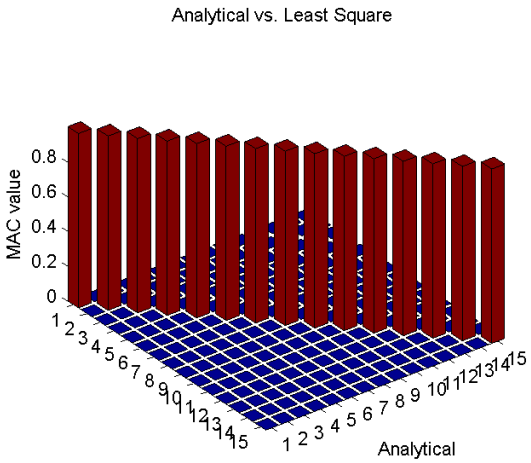


(c) Analytical vs. LSCE

Fig. C.2: MAC comparison - plane

## C.2 Mode shapes

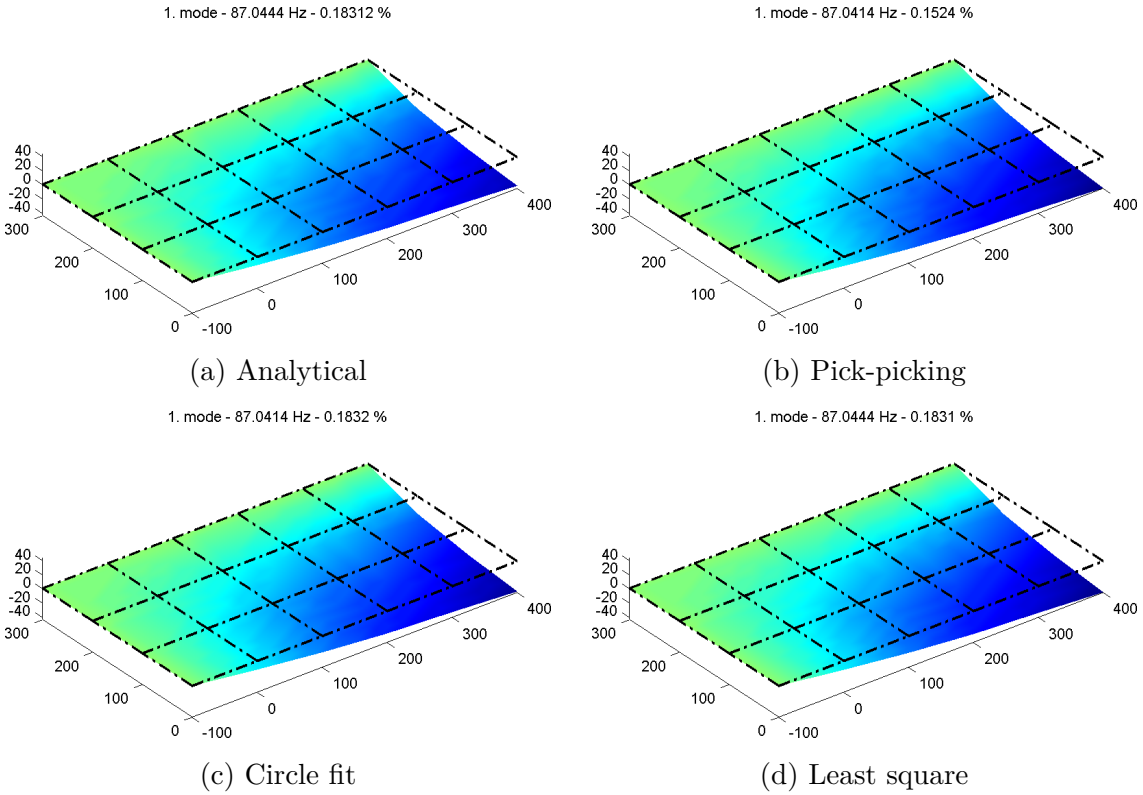


(a) Analytical

(b) Pick-picking

(c) Circle fit

(d) Least square

Fig. C.3: Plane - first mode shape

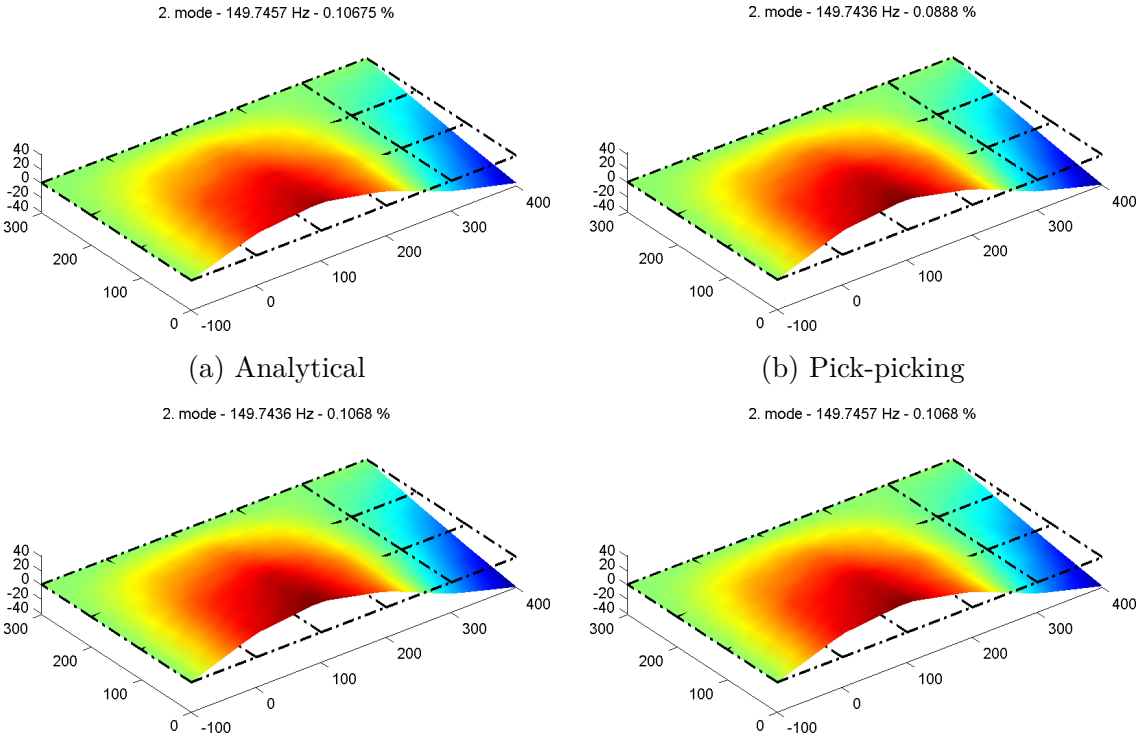


(a) Analytical

(b) Pick-picking

(c) Circle fit

(d) Least square

Fig. C.4: Plane - second mode shape

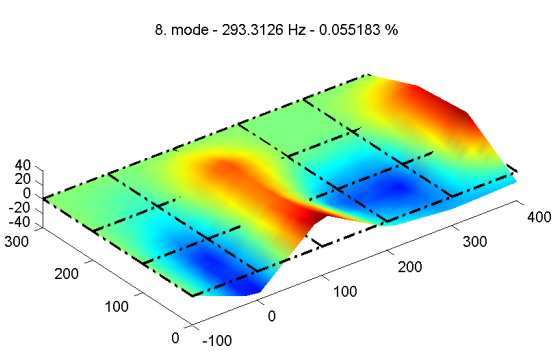


(a) Analytical

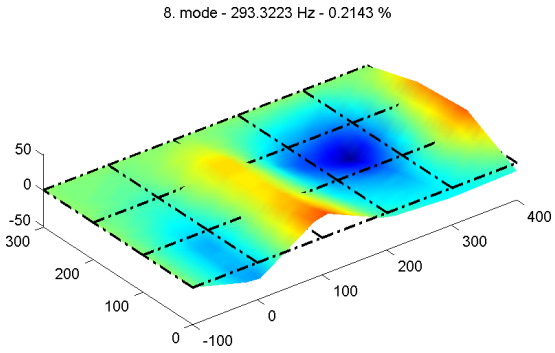


(b) Pick-picking

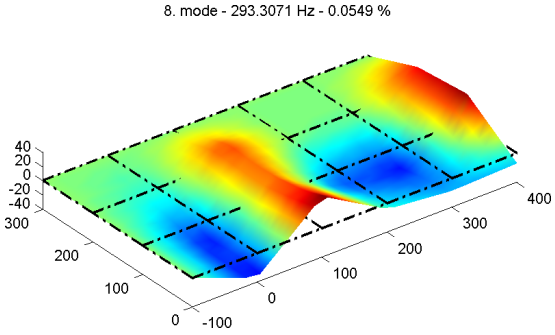


(c) Circle fit

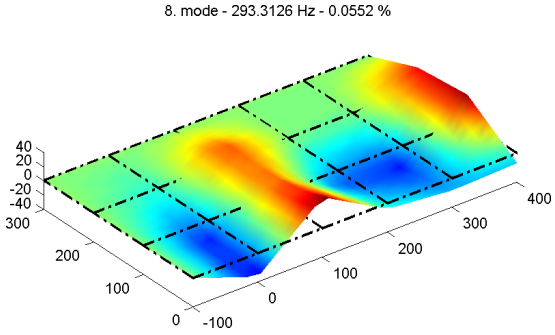


(d) Least square

Fig. C.5: Plane - eighth mode shape

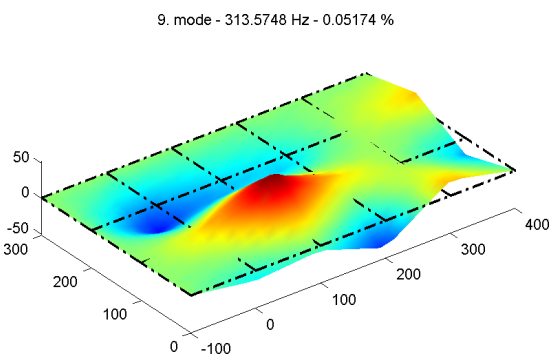


(a) Analytical

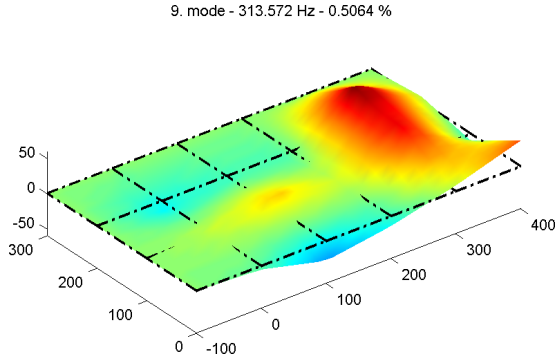


(b) Pick-picking

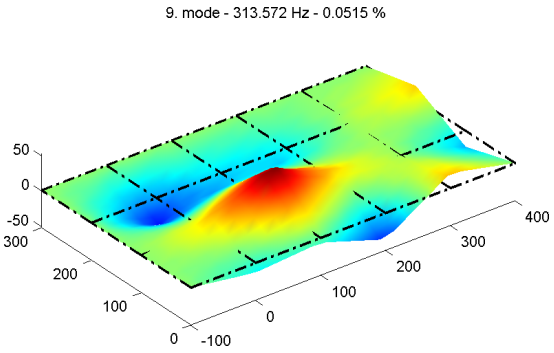


(c) Circle fit

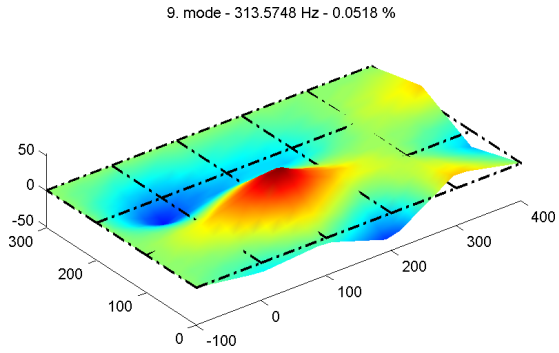


(d) Least square

Fig. C.6: Plane - nineth mode shape

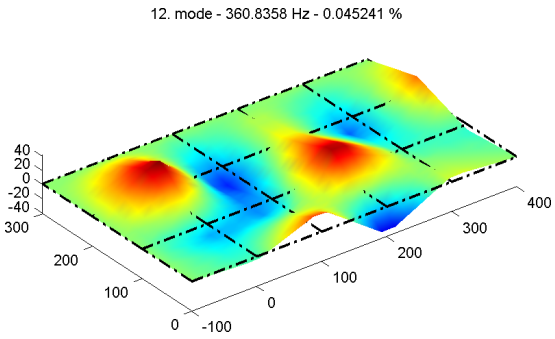


(a) Analytical

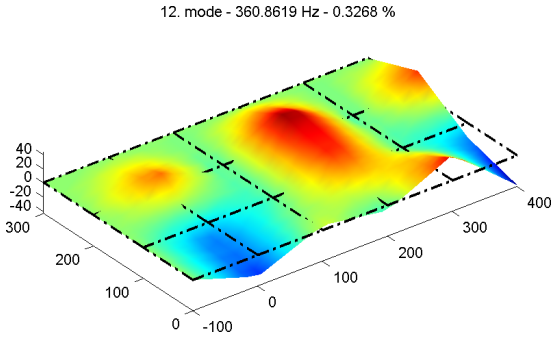


(b) Pick-picking

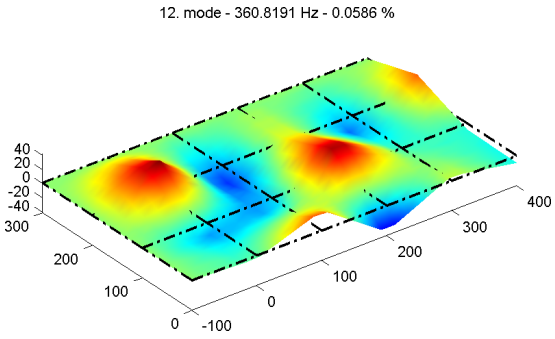


(c) Circle fit

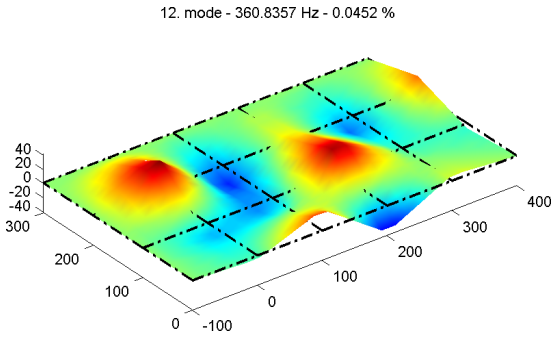


(d) Least square

Fig. C.7: Plane - twelfth mode shape

# D CASE STUDY - TURBINE WHEEL

## D.1 Comparison of modal properties

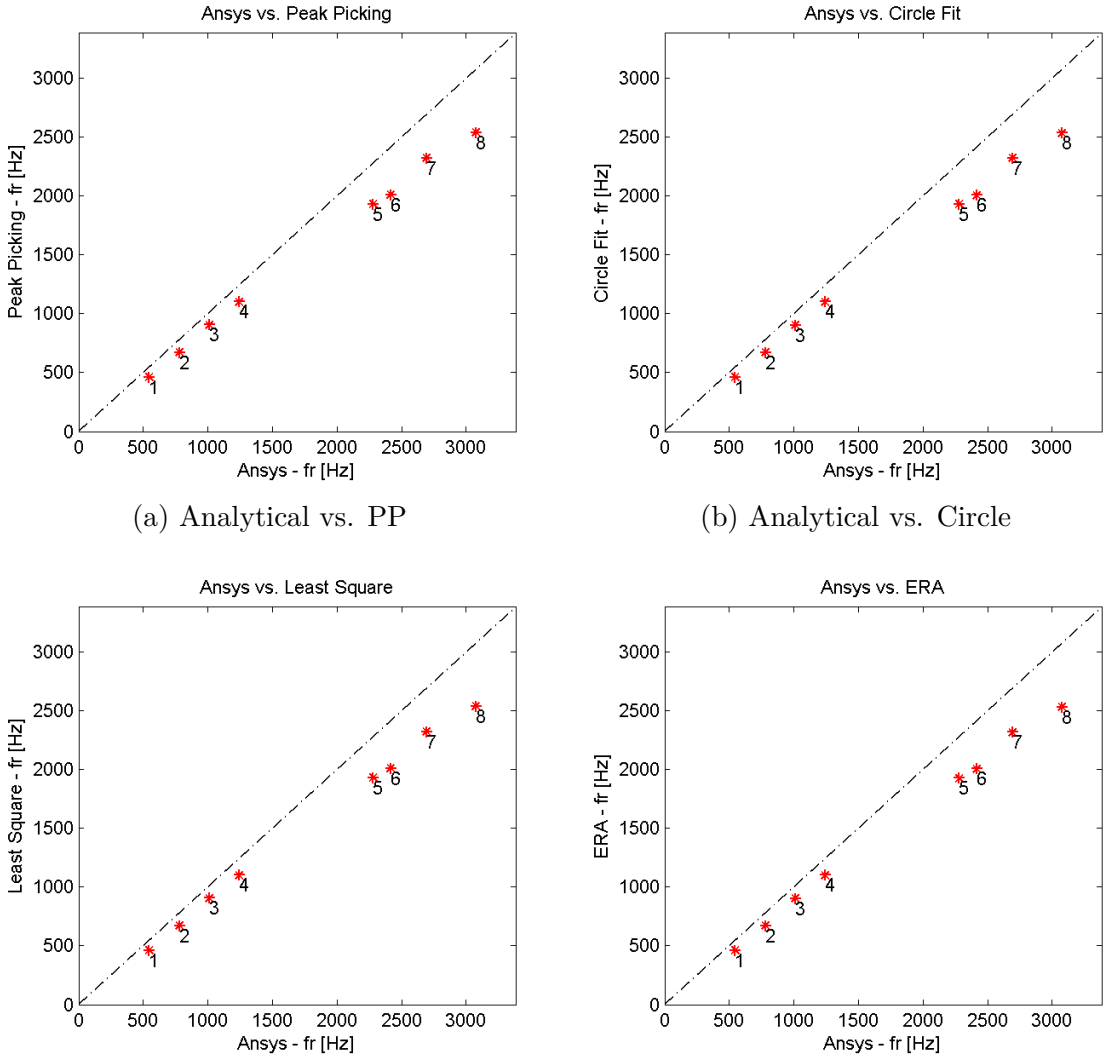


(a) Analytical vs. PP

(b) Analytical vs. Circle

(c) Analytical vs. LSCE

(d) Analytical vs. ERA

Fig. D.1: Comparison for natural frequencies - turbine wheel

| | Ansys | | PP | | Circle fit | | LSCE | | ERA | |
|---|---|---|---|---|---|---|---|---|---|---|
| $r$ | $f_r$ [Hz] | $b_r$ | $f_r$ (er. [%]) | $b_r$ | $f_r$ (er. [%]) | $b_r$ | $f_r$ (er. [%]) | $b_r$ | $f_r$ (er. [%]) | $b_r$ |
| 1 | 544.07 | – | 462.5 (14.99) | 0.06 | 462.18 (15.05) | 0.05 | 462.33 (15.02) | 0.03 | 462.27 (15.03) | 0.03 |
| 2 | 779.96 | – | 672.5 (13.77) | 0.08 | 672.05 (13.84) | 0.1 | 672.46 (13.78) | 0.02 | 672.55 (13.77) | 0.12 |
| 3 | 1010.20 | – | 905.5 (10.36) | 0.04 | 905.22 (10.39) | 0.04 | 905.46 (10.36) | 0.004 | 905.29 (10.38) | 0.05 |
| 4 | 1241.40 | – | 1102.75 (11.17) | 0.05 | 1102.43 (11.19) | 0.07 | 1102.89 (11.16) | 0.02 | 1102.96 (11.15) | 0.07 |
| 5 | 2281.20 | – | 1933.25 (15.26) | 0.37 | 1930.38 (15.37) | 0.04 | 1932.22 (15.29) | 0.02 | 1928.59 (15.46) | 0.10 |
| 6 | 2414.40 | – | 2009.25 (16.78) | 0.19 | 2007.61 (16.84) | 0.03 | 2009.14 (16.79) | 0.004 | 2007.20 (16.86) | 0.05 |
| 7 | 2690.60 | – | 2325.0 (13.59) | 0.24 | 2321.63 (13.71) | 0.1 | 2323.68 (13.64) | 0.04 | 2318.51 (13.83) | 0.15 |
| 8 | 3075.10 | – | 2539.0 (17.43) | 0.27 | 2535.47 (17.55) | 0.08 | 2538.56 (17.45) | 0.04 | 2532.51 (17.64) | 0.14 |

Tab. D.1: Turbine wheel - results

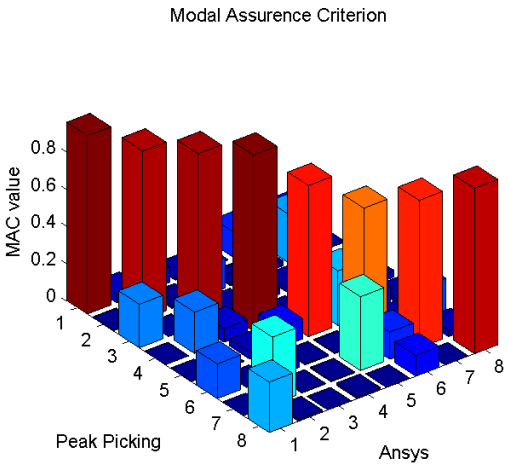


(a) Analytical vs. PP

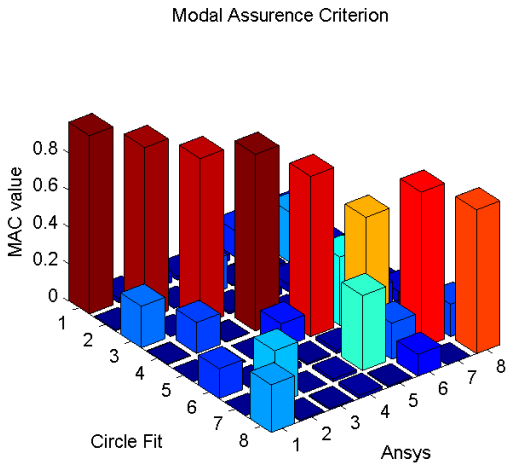


(b) Analytical vs. Circle

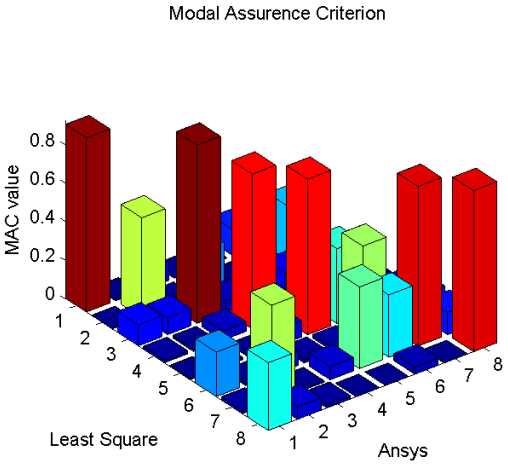


(c) Analytical vs. LSCE

Fig. D.2: MAC comparison - turbine wheel

## D.2 Mode shapes

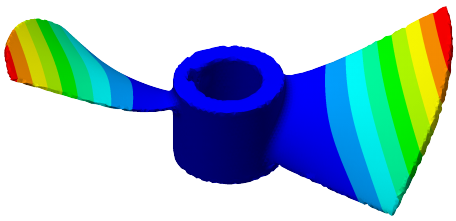

(a) FEM - Ansys

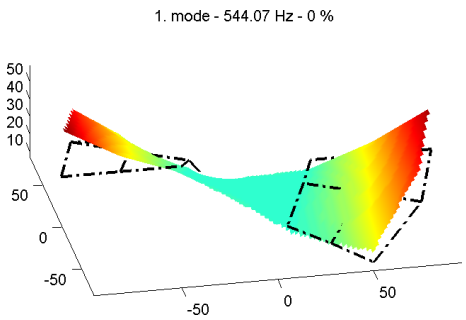


(b) FEM - Application

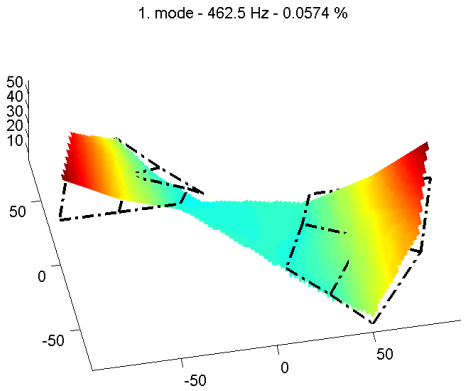


(c) Pick-picking

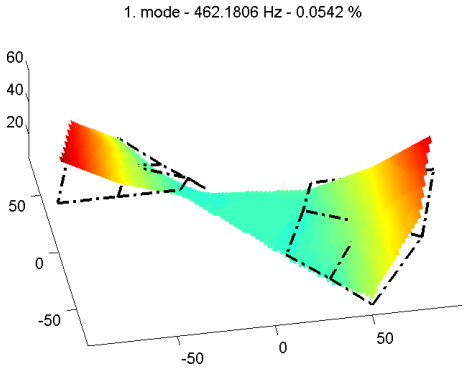


(d) Circle fit

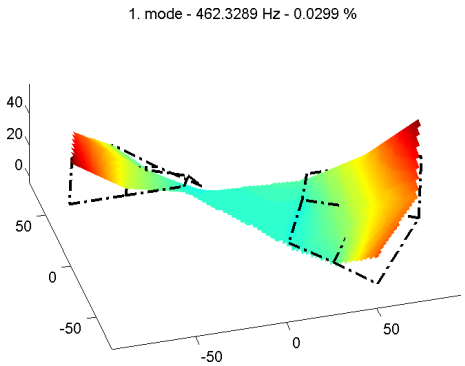


(e) Least square

Fig. D.3: Turbine wheel - first mode shape

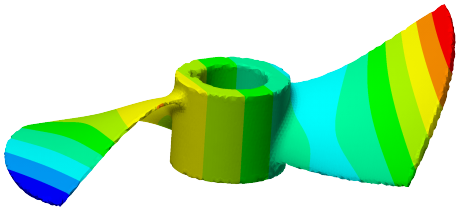

(a) FEM - Ansys

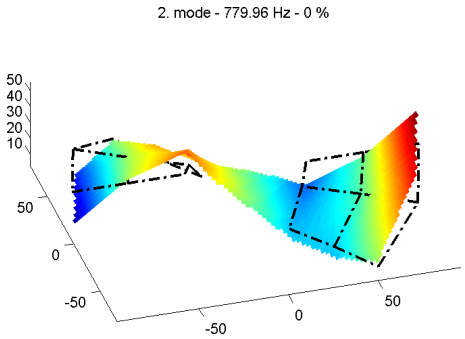


(b) FEM - Application

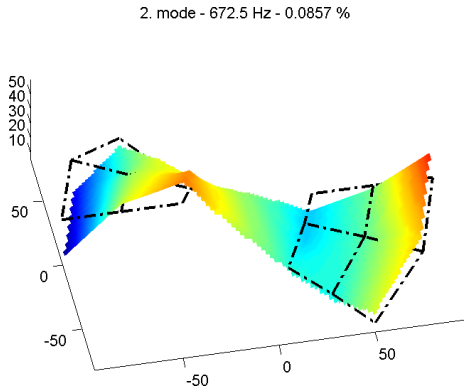


(c) Pick-picking

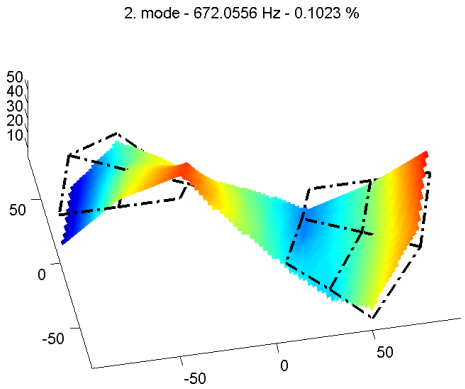


(d) Circle fit

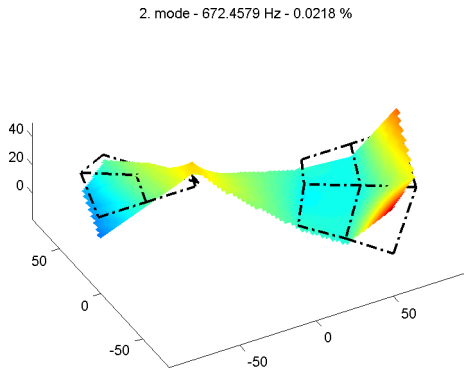


(e) Least square

Fig. D.4: Turbine wheel - second mode shape

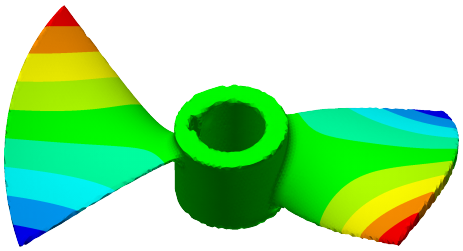

(a) FEM - Ansys

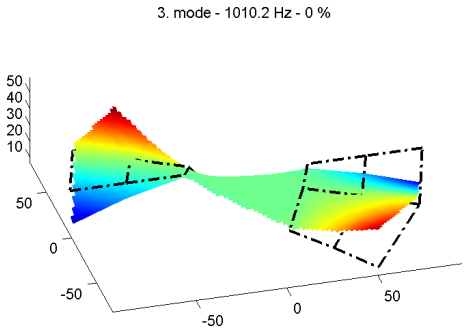


(b) FEM - Application

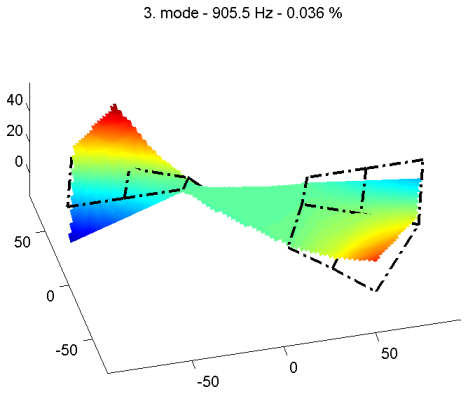


(c) Pick-picking

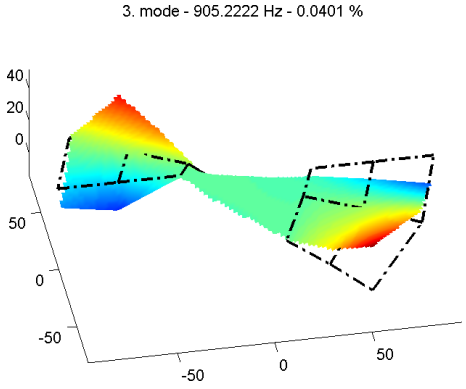


(d) Circle fit

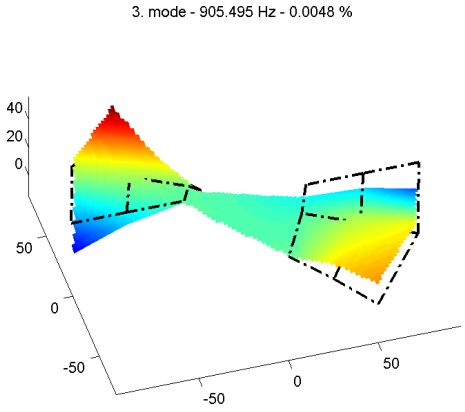


(e) Least square

Fig. D.5: Turbine wheel - third mode shape

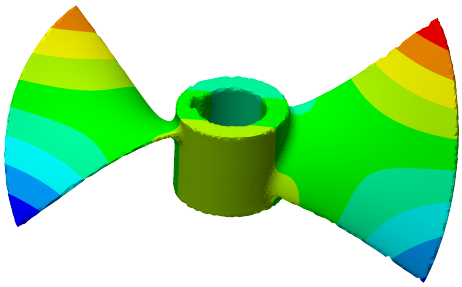

(a) FEM - Ansys

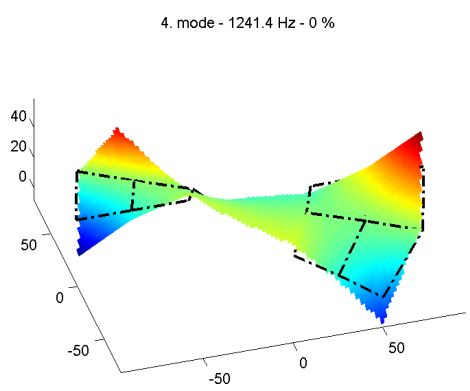


(b) FEM - Application

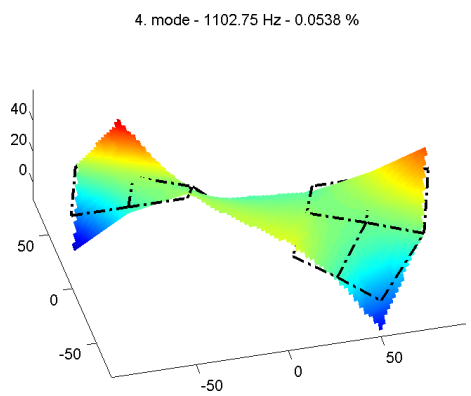


(c) Pick-picking

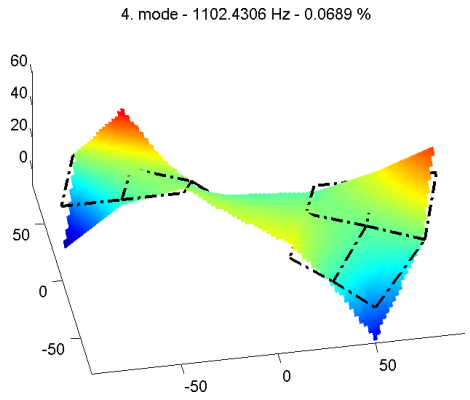


(d) Circle fit

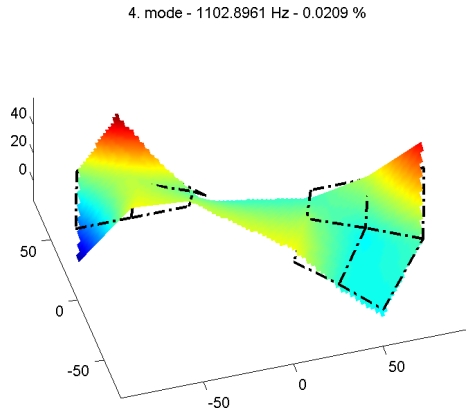


(e) Least square

Fig. D.6: Turbine wheel - forth mode shape

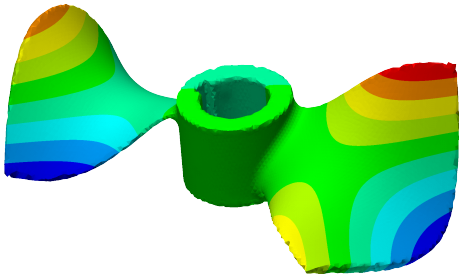

(a) FEM - Ansys

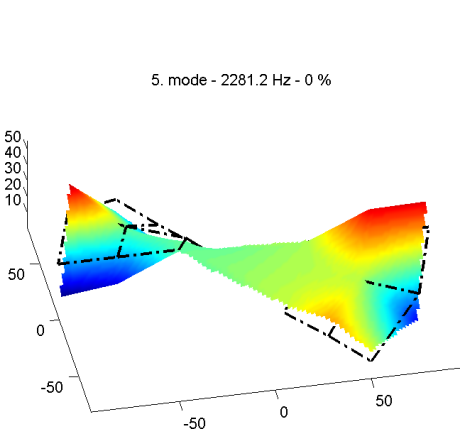


(b) FEM - Application

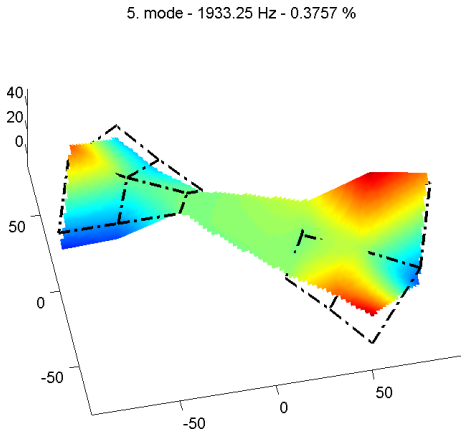


(c) Pick-picking

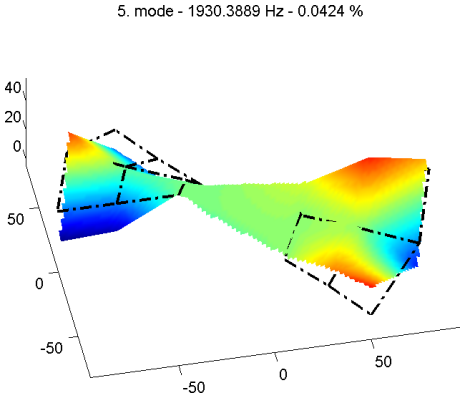


(d) Circle fit

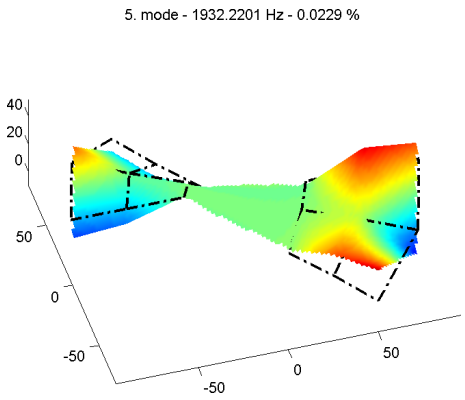


(e) Least square

Fig. D.7: Turbine wheel - fifth mode shape

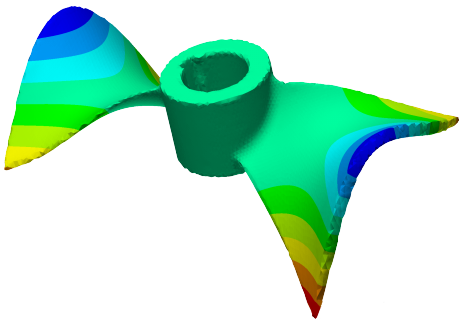

(a) FEM - Ansys

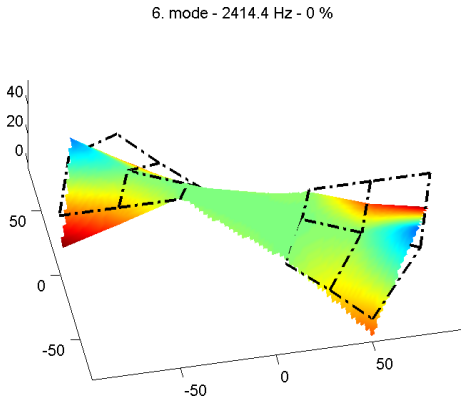


(b) FEM - Application

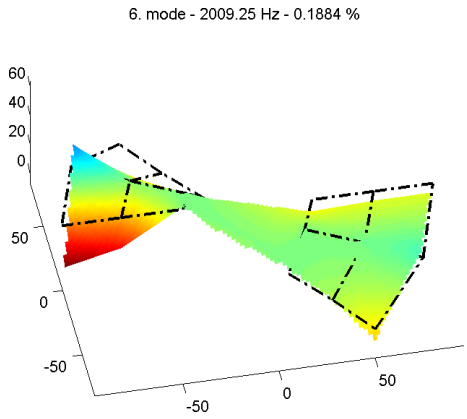


(c) Pick-picking

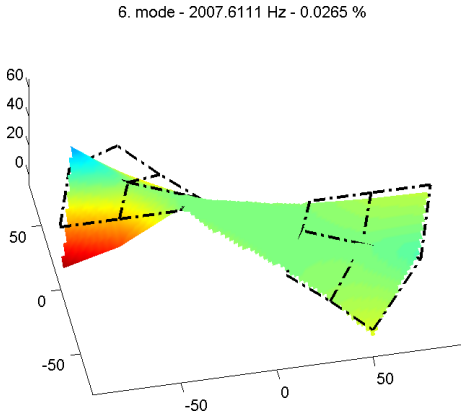


(d) Circle fit

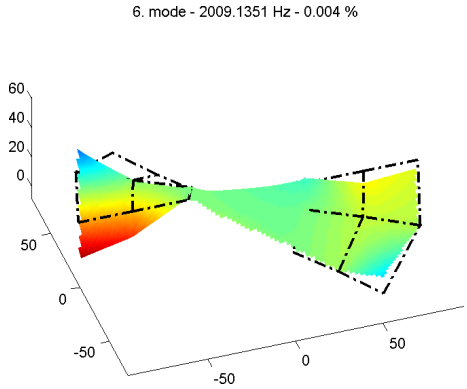


(e) Least square

Fig. D.8: Turbine wheel - sixth mode shape

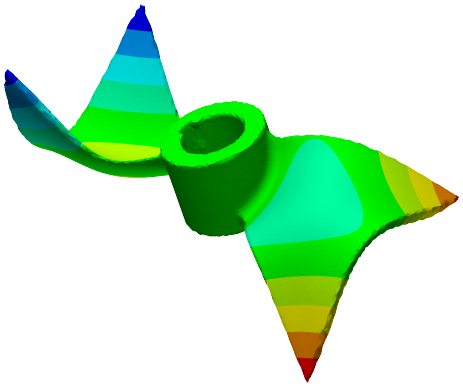

(a) FEM - Ansys

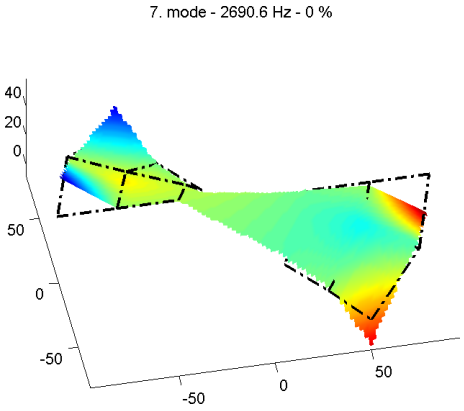


(b) FEM - Application

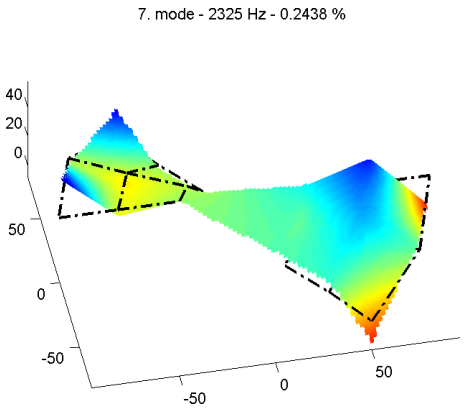


(c) Pick-picking

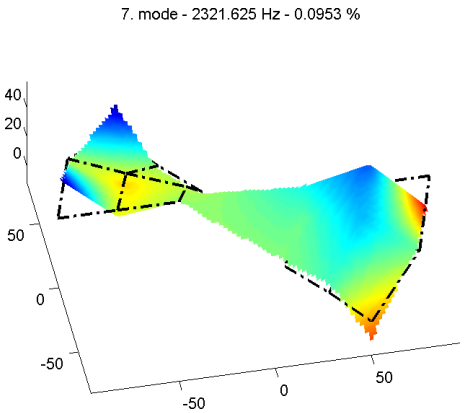


(d) Circle fit

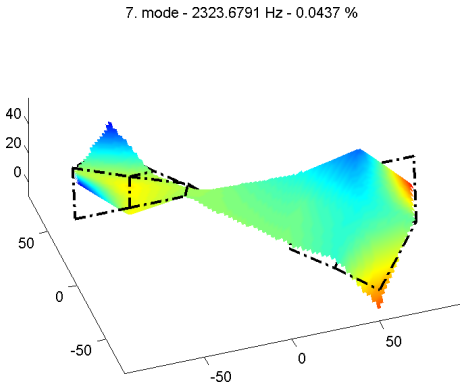


(e) Least square

Fig. D.9: Turbine wheel - seventh mode shape

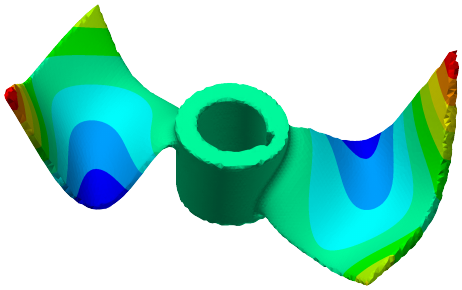

(a) FEM - Ansys

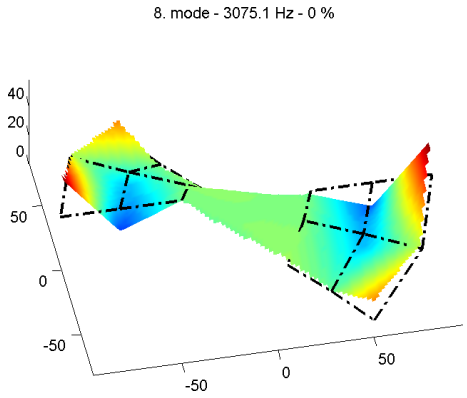


(b) FEM - Application

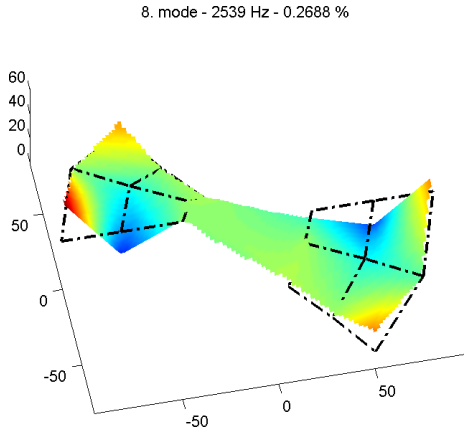


(c) Pick-picking

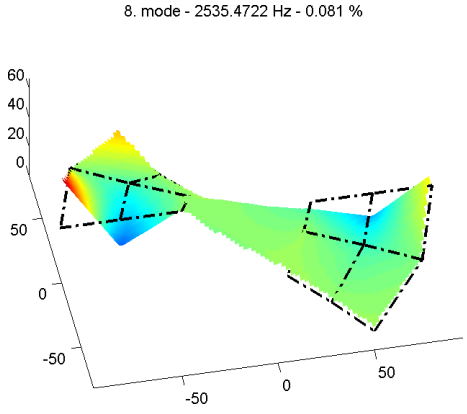


(d) Circle fit

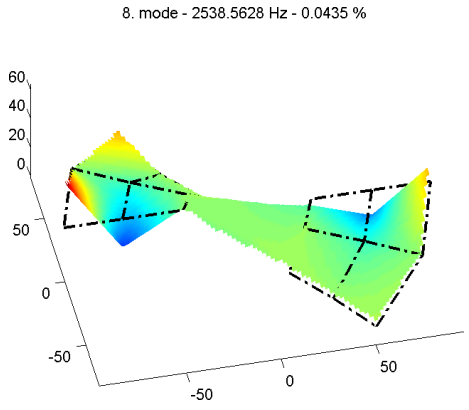


(e) Least square

Fig. D.10: Turbine wheel - eighth mode shape